12-2012

Molecular Processes in Astrophysics: Calculations of H + H2 Excitation, De-Excitation, and Cooling

Matthew Kelley
University of Nevada, Las Vegas

MOLECULAR PROCESSES IN ASTROPHYSICS: CALCULATIONS OF $H + H_2$ EXCITATION, DE-EXCITATION, AND COOLING

by

Matthew Thomas Kelley

Bachelor of Science
Marquette University
2007

A thesis submitted in partial fulfillment
of the requirements for the

Doctor of Philosophy in Astronomy

Department of Physics and Astronomy
College of Sciences
The Graduate College

University of Nevada, Las Vegas
December 2012

UNLV
UNIVERSITY OF NEVADA LAS VEGAS

THE GRADUATE COLLEGE

We recommend the dissertation prepared under our supervision by

Matthew Kelley

entitled

Molecular Processes in Astrophysics: Calculations of H + H_2 Excitation, De-Excitation, and Cooling

be accepted in partial fulfillment of the requirements for the degree of

Doctor of Philosophy in Astronomy
Department of Physics and Astronomy

Stephen Lepp, Ph.D., Committee Chair

Kentaro Nagamine, Ph.D., Committee Member

Bing Zhang, Ph.D., Committee Member

Balakrishnan Naduvalath, Ph.D., Graduate College Representative

Tom Piechota, Ph.D., Interim Vice President for Research &
Dean of the Graduate College

December 2012

ABSTRACT

MOLECULAR PROCESSES IN ASTROPHYSICS: CALCULATIONS OF $H + H_2$ EXCITATION, DE-EXCITATION, AND COOLING

by

Matthew Thomas Kelley

Dr. Stephen Lepp, Examination Committee Chair
Professor of Physics
University of Nevada, Las Vegas

The implications of $H + H_2$ cooling in astrophysics is important to several applications. One of the most significant and pure applications is its role in cooling in the early universe. Other applications would include molecular dynamics in nebulae and their collapse into stars and astrophysical shocks. Shortly after the big bang, the universe was a hot primordial gas of photons, electrons, and nuclei among other ingredients. By far the most dominant nuclei in the early universe was hydrogen. In fact, in the early universe the matter density was 90 percent hydrogen and only 10 percent helium with small amounts of lithium and deuterium. In order for structure to form in the universe, this primordial gas must form atoms and cool. One of the significant cooling mechanisms is the collision of neutral atomic hydrogen with a neutral diatomic hydrogen molecule. This work performs calculations to determine collisional cooling rates of hydrogen using two potential surfaces.

ACKNOWLEDGMENTS

First I would like to thank my advisor Dr. Stephen Lepp who provided technical support as well as the tools to help me fund my education. Mr. Douglas Benton who ignited my interest in physics in high school. Dr. Christopher Stockdale who has been a mentor for many years. As well as my committee members Dr. Bing Zhang, Dr. Kentaro Nagamine, and Dr. Balakrishnan Naduvalath. Also my friend Dr. Tae Song Lee who kept me focused and guided me through graduate school.

I would also like to acknowledge my family. My mother Connie Schauer and father Thomas Kelley. My brothers and sisters Tiffany, Marc, Kerly, Ryan, and Chris. And finally my grandparents Jean and Bruce Knowlton, as well as Robert and May Kelley whom both recently passed away.

Acknowledged Funding and Support Agencies: NVSGC

TABLE OF CONTENTS

LIST OF TABLES

LIST OF FIGURES

CHAPTER 1

THE ENVIRONMENT OF THE EARLY UNIVERSE

The formation of nuclei occured approximately 3 minutes after the big bang in a process known as nucleosynthesis. At this time, a very limited variety of nuclei were actually able to form. These nuclei were hydrogen, helium, deuterium (which, for the purposes of this discussion, will be assigned the atomic symbol D), and lithium; also present were photons, free electrons, and neutrinos. It's important to note that because of the high photon energy density at this epoch, all these nuclei were ionized. there were enough energetic photons to cause any atoms formed to be immediately reionized. The electron scattering cross section is large enough the universe was optically thick to photons.

Hubble (1929) showed that the universe is expanding. Because of the expansion in the early universe, both the matter temperature and photon energy density decreased. The ionisation fraction is defined by equation 1.1 where n is the number density of electrons, e, protons, p, and hydrogen, H.

$$x = \frac{n_e}{n_p + n_H} \tag{1.1}$$

The gas is overall neutral therefore $n_e = n_p$. Neutral hydrogen atoms begin to form when the photons in the universe no longer have enough energy keep the H^+ (protons) ionized. One would assume that this would occur when the temperature is less than the temperature of the binding energy, $T_H = 1.6 \times 10^5$K, but this would be incorrect because the number of photons greatly outnumbers the number of baryons allowing the tail of the distribution of photon energies to ionize a non trivial amount of hydrogen at the ionization energy of 13.6 eV. Hydrogen recombination may be approximated by the saha equation, equation 1.2 where k_B

is the Boltzmann constant, m_e is the mass of an electron, and T is temperature.

$$\frac{x^2}{1-x} = \frac{1}{n_p + n_H}(\frac{m_e k_B T}{2\pi\hbar^2})^{\frac{3}{2}} e^{-\frac{B_H}{k_B T}} \tag{1.2}$$

In this work , recombination will be defined as when the ionization fraction is less than 0.5. This is when most of the hydrogen in the universe was neutral. In this equation time is defined by temperature. Temperature is written in terms of redshift z and the $z = 0$ cosmic microwave background (CMB) temperature $T_{0r} = 2.73$K (equation 1.3). The CMB will be discussed later in this chapter.

$$T = T_{0r}(1+z) \tag{1.3}$$

Due to the expasion of the universe, objects in the universe are moving away from each other. This causes the wavelength of the light emitted by distant objects to get longer (become more red). This relationship was first observed by Hubble (1929). He proposed equation 1.4 where v is velocity of recession, $H_0 \sim 70$ km s^{-1} Mpc^{-1}) is Hubble's constant (Hubble actually measured it to be approximately 200 km s^{-1} Mpc^{-1}), and D is the distance to the object. H_0 has been measured using surveys of atomic spectra from galaxies of known distance though some uncertainty still exists.

$$v = H_0 D \tag{1.4}$$

Cosmic time can then be calculated from equation 1.5 where Ω_0 is the density ratio. For the purposes of this discussion the value of Ω_0 is insignificant.

$$t(z) = \frac{2}{3H_0\Omega_0^{1/2}(1+z)^{3/2}} \tag{1.5}$$

Using these equations, the fractional ionization drops below $.5$ when T $\sim 3200-3800$K depending on the choice of value of the density ratio and Hubble's constant. This corresponds to a t(z) of about $300,000 \rightarrow 400,000$ years after the big bang. At this point, the universe is now optically thin because photons are not being absorbed and scattered with as much frequency. This is known as the last scattering surface. These photons escaped the primordial gas and are observed today in the form of the CMB first detected in 1964 by Penzias & Wilson (1965) and Wilson & Penzias (1965). Missions such as WMAP have been specifically designed to map the CMB which provides insight into the big bang, dark matter, and the early universe.

The composition of the early universe is a problem currently under consideration (eg. Gay et al. 2011). Most studies agree that the only atoms that existed in the early universe were hydrogen, helium, deuterium, and lithium (Lepp et al. 1998), however there have been some studies that make a case for heavier elements created during the big bang in trace quantities (eg. Puy et al. 2007). There is general agreement that the matter density was 90 percent hydrogen, 10 percent helium, and trace amounts of deuterium and Lithium. Smith (1993) reports a mass abundance of $\mathrm{M_{He}/M_H} = 0.21 - 0.24$, $\mathrm{M_D/M_H} = 1.8 \times 10^{-5}$, and $\mathrm{M_{Li}/M_H} = 1.1 \times 10^{-10}$. Either way one calculates abundances, hydrogen is the most abundant so it is reasonable to persume that it will have a significant impact on cooling.

A logical question to ask at this point is "why does cooling matter?" The matter in the universe at the time of recombination was an atomic gas with small abundances of molecules. In order for structure to form, this gas must collapse in an

expanding universe. This collapse is generally believed to have occurred due to the gravity of dark matter. However, thermodynamics states that under an adiabatic collapse, as volume decreases, pressure increases where temperature remains constant. This very quickly halts collapse preventing the formation of galaxies and stars. In order for a full collapse to occur, the collapse must be non-adiabatic; energy must leave the gas. This occurs via collisional cooling, a very significant amount of which is atomic hydrogen colliding with diatomic hydrogen molecules.

The formation of H_2 in the early universe is an area of interest particularly since in the local ISM, molecular hydrogen is believed to predominantly form on the surface of grains. This is due to the fact that in the ISM, direct formation of H_2 in open space from ordinary chemical processes is too inefficient to explain the abundances observed. Cazaux et al. (2005) provides a very good overview of these processes. However, dust in the early universe was non existent due to the absense of heavy nuclei needed for its formation. Also, since dust is generally formed by mechanisms such as supernova explosions, it was not present until after the first star formation. As a result, H_2 was formed directly in the primordial gas. Some of these reactions are described by Galli & Palla (1998), referred to as GP98, and are presented in table 1. Also presented in the table are a list of reactions involving heavier elements that may have occured in the early universe, assuming of course heavy nuclei were present, from Vonlanthen et al. (2009), refered to as V09 in the table. The reactions in V09 are most likely insignificant contributors to the H_2 abundance due to the extremely low predicted abunances of heavy elements in the early universe but may be of interest in environments such as supernovae.

The main collision partners with H_2 in the early universe are H, D, electrons, HD, and other H_2 molecules. There is some evidence that LiH cooling may be significant in terms of structure formation. For a discussion of LiH in the early

Table 1 H_2 formation reactions without grains

reaction	reference
$H^- + H \rightarrow H_2 + e^-$	GP98
$H_2^+ + H \rightarrow H_2 + H^+$	GP98
$H_3^+ + H \rightarrow H_2^+ + H_2$	GP98
$H_3^+ + e^- \rightarrow H_2 + H$	GP98
$HD + H \rightarrow H_2 + D$	GP98
$HD + H^+ \rightarrow H_2 + D^+$	GP98
$HD + H_3^+ \rightarrow H_2 + H_2D^+$	GP98
$H_2D^+ + e^- \rightarrow H_2 + D$	GP98
$LiH + H \rightarrow Li + H_2$	GP98
$LiH + H^+ \rightarrow Li^+ + H_2$	GP98
$LiH^+ + H \rightarrow Li^+ + H_2$	GP98
$H_2^+ + CH+ \rightarrow CH^+ + H_2$	V09
$CH^+ + H \rightarrow C^+ + H_2$	V09
$H + CH_2^+ \rightarrow CH^+ + H_2$	V09
$He^+ + CH_2 \rightarrow C^+ + He + H_2$	V09
$H_2^+ + CH_2 \rightarrow CH_2^+ + H_2$	V09
$CH_2^+ + e^- \rightarrow C + H_2$	V09
$H + CH \rightarrow C + H_2$	V09
$H_3^+ + C \rightarrow CH^+ + H_2$	V09
$H + CH_2 \rightarrow CH + H_2$	V09
$H^+ + CH_2 \rightarrow CH^+ + H_2$	V09
$H_3^+ + CH \rightarrow CH_2^+ + H_2$	V09
$H_2^+ + OH \rightarrow OH^+ + H_2$	V09
$H + H_2O \rightarrow OH + H_2$	V09
$OH^+ + H \rightarrow O^+ + H_2$	V09
$H_2^+ + H_2O \rightarrow H_2O^+ + H_2$	V09
$H + OH \rightarrow O + H_2$	V09
$H_3^+ + O \rightarrow OH^+ + H_2$	V09
$H_2O^+ + e^- \rightarrow O + H_2$	V09
$H_3^+ + OH \rightarrow H_2O^+ + H_2$	V09

universe, refer to Bougleux & Galli (1997). The reactions listed in table 1 are only reactions that create H_2, not listed are the dozens of reactions that consume H_2 while creating other molecules. While studying the cooling of H_2 can be both interesting and advantageous, it by no means sums up the imortance of molecular hydrogen in the early universe.

The calculation conducted here is an idealized calculation designed to determine density and temperature dependent cooling rates for diatomic molecular hydrogen in an atomic hydrogen bath. This calculation includes two potential surfaces assuming steady state. The steady state approximation is common in these types of calculations.

CHAPTER 2

BKMP2 AND MIELKE POTENTIAL SURFACES

In literature, the $H + H_2$ potential surface is generally referred to as the H_3 surface. The history of reseach developing the H_3 surface is quite extensive and can be traced back to at least the 1930's (eg. Eyring & Polanyi 1931). This reaction has been heavily studied for several reasons. First, because it is the simplest atomic-molecular reaction that only requires understanding of 1 atomic surface. Next, it was used to develop theories of tunneling (Marshall et al. 1969). Also it has been used as a probe into the effects of isotopes because each atom can be substituted by either dueterium or tritium (Truhlar et al. 1976). It has also been used as a means of studying various approximations such as the adiabatic approximation, the Born-Oppenheimer approximation, and a wide range of semi-classical approximations (Liu 1973). More recently it has been studied for its applications in astrophysics.

Modern potential surfaces really began with the LSTH potential surface (Liu 1973, Sieghbahn & Liu 1978, and Truhlar & Horowitz 1978). This potential surface was considered to be the most accurate semi-classical attempt to model the potential surface to date. It was also used as a test of the configuration interaction method that would be used for more complicated systems. Since then, several surfaces have been presented that were at least partially based on the LSTH surface. These include the double many-body expansion (DMBE) (Varandas et al. 1987), BKMP (Boothroyd et al. 1991), BKMP2 (Boothroyd et al. 1996), and Mielke (Mielke et al. 2002) potentials. The calculation presented here involved only the BKMP2 and Mielke potentials.

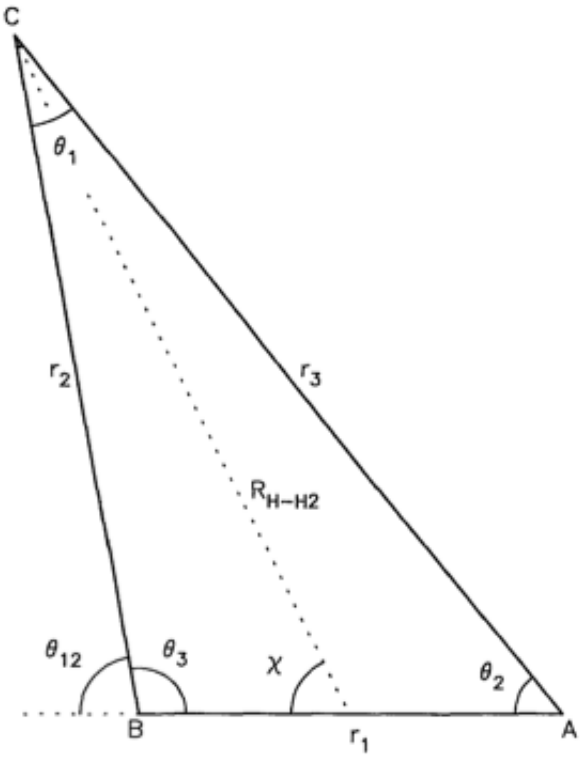

Figure 1 The geometry parameters of the BKMP H_3 potential surface (Boothroyd et al. 1996)

H_3 GEOMETRY AND HAMILTONIANS

The H_3 potential can be modeled geometrically as a molecule of 3 hydrogen atoms with dynamic relative coordinates. Figure 1 is a visual representation of the H_3 system for three hydrogen atoms labeled A, B, and C. In this diagram r_i is the distance between the molecules, θ_i are the interior angles opposite r_i, $\theta_{1,2}$ is the angle between C and $-\infty$ on the horizontal axis in a right handed coordinate system with B at the vertex, R_{H-H_2} is the distance from C to a point positioned at $\frac{1}{2}\ \overline{AB}$, and χ is the angle between C and B with the vertex at $\frac{1}{2}\overline{AB}$. Atoms A and B represent the H_2 molecule.

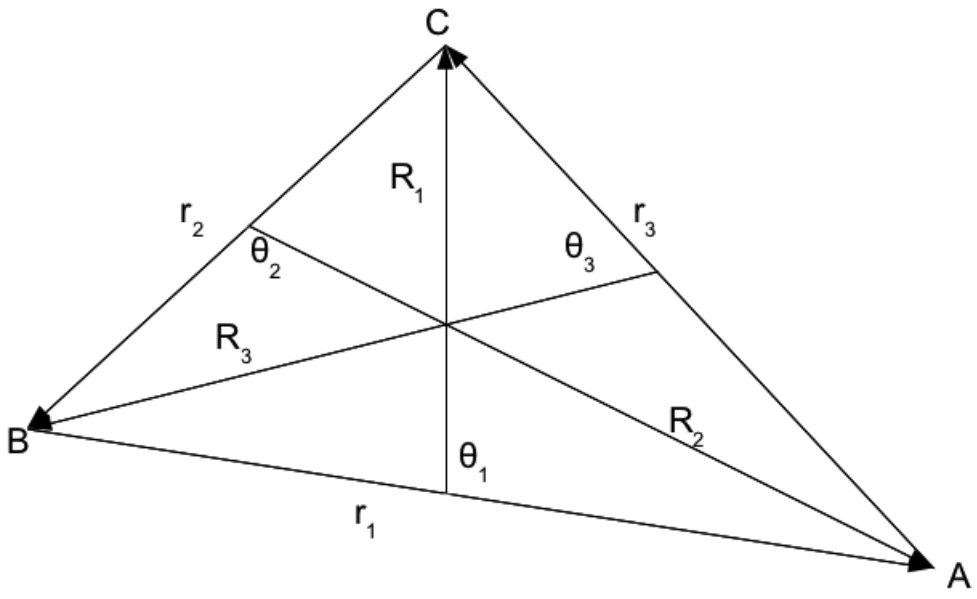

Figure 2 The Jacobi representation of the geometry of H_3

The polar coordinate system depicted in figure 1 is useful due to its simplicity. However, another common coordinate system used are Jacobi coordinates. These are often used when calculating the Hamiltonian of the system because the Hamiltonian of the nuclei can be expressed in terms of the hyperradius, ρ (equation 2.2) and the coefficient μ (equation 2.1) with units of mass. This is a center of mass reference frame. Figure 2 shows the Jacobi coordinate system of H_3 based off the system used by Tolstikhin & Nakamura (1998). In this coordinate system, θ_i is the angle between r_i and the opposite atom as shown in the figure. Equations 2.1 and 2.2 show that ρ is related to the moment of inertia perpendicular to the plane of the triangle through the center of the triangle $I_\perp = \mu\rho^2$.

$$\mu = \left(\frac{m_A m_B m_C}{m_A + m_B + m_C}\right)^{\frac{1}{2}} \tag{2.1}$$

$$\rho = \left(\frac{m_A r_2^2 + m_B r_3^2 + m_C r_1^2}{\mu}\right)^{1/2} \tag{2.2}$$

The general form of the time independent Schrödinger equation is written as equation 2.3. In this equation T is the kinetic energy, V is the potential energy, E is the total energy and Ψ is the wave function.

$$(T + V)\Psi = E\Psi \tag{2.3}$$

The kinetic energy of a system of particles is presented in equation 2.4.

$$T = -\frac{\hbar^2}{2\sum_{i=A}^{C} m_i} \bigtriangledown^2 \tag{2.4}$$

In polar coordinates the Schrödinger equation then becomes equation 2.5.

$$E\Psi = (-\frac{\hbar^2}{\sum_{i=A}^{C} 2m_{P,i}} + V(R_\alpha, \omega_\alpha))\Psi \tag{2.5}$$

In terms of the center of mass system from Tolstikhin (1998) gives equation 2.6. Λ is the Smith's grand angular momentum operator (Smith 1960) and $H_{surface}$ is the surface Hamiltonian where $V(R_\alpha, \omega_\alpha)$ is the surface potential.

$$E\Psi = (-\frac{\hbar^2}{2\mu}\frac{1}{\rho^5}\frac{\partial}{\partial\rho}\rho^5\frac{\partial}{\partial\rho} + \frac{\Lambda^2}{2\mu\rho^2} + V(R_\alpha, \omega_\alpha))\Psi \tag{2.6}$$

GENERAL POTENTIAL SURFACE FORM

The BKMP2 potential has the general form of equation 2.7 and the Mielke potential has the form of equation 2.8 and 2.9. In equation 2.7, dropping the (r_1, r_2, r_3), V_{London} is the London potential (equations 2.10, 2.11, and 2.12)(London 1929), V_{asym} is the asymetric geometry term (non-zero for all asymetric geometries), V_{bend} is the bent geometry term (non-zero for all bent geometries), and the C's are the compact

geometry terms (non-zero for their respective compact geometries) where C_{all} is non-zero for all compact geometries. In equations 2.8 and 2.9, V_A are the single atom energies, V_{AB} are the two-body energies which are calculated for both long and short range interactions, and V_{ABC} are the three body energies; each with a functional form of equation 2.9. V_{3C} is the three-center correction term designed to account for the center of mass coordinate system. Both equations maintain the notation from their respective papers.

$$\begin{aligned} V_{total}(r_1, r_2, r_3) = \quad & V_{London}(r_1, r_2, r_3) + V_{asym}(r_1, r_2, r_3) + V_{bend}(r_1, r_2, r_3) \\ & + C_{all}(r_1, r_2, r_3) + C_{asym}(r_1, r_2, r_3) + C_{bend}(r_1, r_2, r_3) \end{aligned} \tag{2.7}$$

$$V_{ABC} = \sum V_A^{(1)} + \sum V_{AB}^{(2)} + \sum V_{ABC}^{(3)} \tag{2.8}$$

$$V = V_{London} + V_{3C} \tag{2.9}$$

$$V_{London}(r_1, r_2, r_3) = \sum_{i=1}^{3} Q(R_i) \pm (\epsilon^2 + \frac{1}{2} \sum_{i>j} [J(R_i) - J(R_j)]^2)^{1/2} \tag{2.10}$$

$$Q(R_i) = \frac{1}{2}[V_{sing}(R_i) + V_{trip}(R_i)] \tag{2.11}$$

$$J(R_i) = \frac{1}{2}[V_{sing}(R_i) - V_{trip}(R_i)] \tag{2.12}$$

The London potential was the first significant attempt to model collisions between atoms and molecules. Though quite inaccurate, it has been used as a starting point for more modern techniques. In equations 2.11 and 2.12, V_{sing} and V_{trip} are the H_2 singlet and triplet diatomic potentials. The $\pm$ indicate electronic gound state (-) and excited states (+). Since only the Mielke potential considers excited states it uses the $\pm$ where the BKMP2 potential uses only the -. Each of these individual correction terms are expressed as formidable system of parameters causing both of these potentials to have a significant number of fit parameters. For example, the

BKMP2 has a total 129 parameters that the system is fit to for various molecular configurations. As a result it is not prudent to go into anymore detail on the functions themselves. However, it is informative to take note of the two techniques used to derive these potentials.

CONFIGURATION INTERACTION METHOD

Consider the H_3 molecule with 3 electrons, one centered on each hydrogen nuclei. The Born-Oppenheimer approximation allows us to consider the electrons independently of the kinetic energy of the nuclei to calculate the wavefunction. This is made possible by the following assumptions. (1) There is little momentum transfer between the electrons and nuclei. (2) Since the forces between them is similar due to having the same but opposite charges, their momentums must be similar. (3) Since the electrons are much smaller and have the same momentum as the nuclei, they have much greater velocites. (4) The electrons are able to relax to the ground state around relatively stationary nuclei. Therefore, the wavefunction of the H_3 molecule can be considered as a function of its equlibrium electronic and nuclear wavefunctions in terms of the nucleus positions. This principle is applied to an H_3 system using the configuration interaction method. This method was used for the BKMP2 potential, the Mielke potential used the very similar multi reference configuration interaction method which allowed the consideration of excited states.

Each of the electrons can be expressed in terms of a spin orbital $\chi_{\mathrm{i}}(\mathrm{r}_{\mathrm{i}})$ for i $= 1, 2, 3$ where r_{i} are the positions of each of the electrons with respect to their nucleus. The number of spin orbitals considered varies depending on the author's desired accuracy. Liu (1973) used Slater-type orbitals (equation 2.13) normalized and fit for N and ζ. n is the principle quantum number. In order to satisfy the

requirement that the wavefunction needs to be anti-symmetric, the particles must also be indistinguishable. Each electron should be interchangeable with any other electron. The anti-symmetric wavefunctions can be expressed as a linear combination of all possible Slater determinants (equation 2.14) which satisfies the Pauli exclusion principle (equation 2.15). k_i are calculated using the Clebsch Gordan coefficients.

$$\chi(r_i) = Nr^{n-1}e^{-\zeta r_i} \tag{2.13}$$

$$\phi(r_1, r_2, r_3) = \frac{1}{\sqrt{3!}} \begin{vmatrix} \chi_1(r_1) & \chi_2(r_1) & \chi_3(r_1) \\ \chi_1(r_2) & \chi_2(r_2) & \chi_3(r_2) \\ \chi_1(r_3) & \chi_2(r_3) & \chi_3(r_3) \end{vmatrix} \tag{2.14}$$

$$\psi_j = \sum k_i \phi_i \tag{2.15}$$

Next by solving equation 2.16, the eigenstates of the sytem can be calculated where **H** is the Hamiltonian matrix (equation 2.17). The first term is usually the result of the Hartree-Fock method. This gives the eigenvectors of the system. These can be defined as equation 2.18 where $i, j = 1 \rightarrow k$, x is the number of electrons and k is the total number of basis functions. The elements of H_{ij} can be calculated using Slater's rules written in terms of their appropriate integrals.

$$\mathbf{H}|\Psi> = E|\Psi> \tag{2.16}$$

$$H_{ij} = <\psi_i|H|\psi_j> \tag{2.17}$$

$$\begin{aligned} |\Psi_j> &= \sum_{i=1}^{k} c_{ij}|\psi_i> \\ \mathrm{k} &= \frac{l!}{x!(l-x)!} \end{aligned} \tag{2.18}$$

The eigenvectors of **H** can now be written as a sum of all the one, two, and

three electron orbitals to get the wave function (equation 2.19). There are several algorithms available that use the configuration interaction method to fit the wave-functions and hamiltonians through iterative techniques that produce a solution that converge to a calcualted ab initio energy for a given geometry.

$$|\Psi >= \sum_{i=1}^{I} c_i |\Psi_i > \tag{2.19}$$

CLASSICAL SCATTERING THEORY

Consider again the H_3 system with three atoms A,B,C. Also consider a coordinate system to describe the configuration of the system consisting of three dimensions, $\sum_{\mathrm{i=1}}^{3} \sum_{\mathrm{k=A}}^{\mathrm{C}} x_{i,k}$. The Hamiltonian of such a system can be written as equation 2.20 where $\mathrm{V(x_i)}$ is the potential.

$$\mathrm{H} = \sum_{\mathrm{k=A}}^{\mathrm{C}} \frac{1}{2\mathrm{m_k}} \sum_{\mathrm{i=1}}^{3} \mathrm{x_i} + \mathrm{V(x_i)} \tag{2.20}$$

One can then write Hamilton's equations as equation 2.21 where p is the particle momentum.

$$\begin{aligned} -\frac{\partial \mathrm{H}}{\partial \mathrm{x_{i,k}}} &= \frac{\mathrm{dp_{i,k}}}{\mathrm{dt}} \\ \frac{\partial \mathrm{H}}{\partial \mathrm{p_{i,k}}} &= \frac{\mathrm{dx_{i,k}}}{\mathrm{dt}} \end{aligned} \tag{2.21}$$

More specifically, the velocity between the particles, which macroscopically corresponds to temperature, can be obtained using equation 2.22.

$$\mathrm{dp} = -\frac{\partial \mathrm{v}}{\partial \mathrm{x_i}} \mathrm{dt} \tag{2.22}$$

Now, assuming atom A to be the collider, the molecule consisting of atoms B and C can be placed on the plane x,y. This molecule will be in an initial ro-vibrational state $E_{v_i j_i}$. Using conservation of momentum, one can determine the energy transferred between the molecule and collider given the coordinates of the collider relative to the molecule. If this energy is above the energy of a molecular energy level, the molecule will then transfer to that energy level. The reaction probability can thus be written as a function of the velocity $V_{A\rightarrow BC}$ j_i, v_i, and b. By considering this initial set of conditions and evaluating the results from a range of configurations (Monte Carlo calculation), the number of trajectories that yield a reaction can be determined. This allows one to calculate the probability of a transition, equation 2.23. Chapter 4 discusses how these trajectories are used to calculate the collision rate coefficients.

$$P_i(V_{A\rightarrow BC}, j_i, v_i) = \frac{N_{v_i f j_f}}{N_{v_i j_i}} \tag{2.23}$$

CHAPTER 3

COOLING

COLLISIONAL COOLING: A SAMPLE CASE

Diatomic molecules store energy in the form of rotation and vibration. Clearly in order for cooling to occur, a transition from an excited energy level to a lower energy level must occur and a photon must be released. The energy of a harmonic oscillator and rigid rotator is expressed as equation 3.1. Keep in mind that this is only a sample case, in reality the H_2 molecule loses its harmonic oscillator properties after the first couple dozen energy levels. This property will be discussed in more detail later. In equation 3.1, $E_{\nu,J}$ is the energy, ω is the vibrational frequency (1.32×10^{14} Hz for H_2), B is the characteristic rotational energy (7.56×10^{-3} eV for H_2), J is the rotational quantum number, and v is the vibrational quantum number.

$$E_{\nu,J} = \omega(\nu + \frac{1}{2}) + BJ(J+1) \tag{3.1}$$

A molecule can transition to a higher energy state through two mechanisms, absorption of a photon or collisions with another molecule/atom. It can transition to a lower energy state via stimulated emission from a photon, de-excitation from collisions with another molecule/atom, and sponatneous emission. This calculation makes the assumption that stimulated emission and absoption are negligible. Also not considered is dissociative tunneling which does not result in a state transition but rather destruction of the molecule all together. Consider a steady state gas composed of an imaginary H_2 molecule with 3 energy levels and a gas temperature of T $= 5000$ K (figure 3).

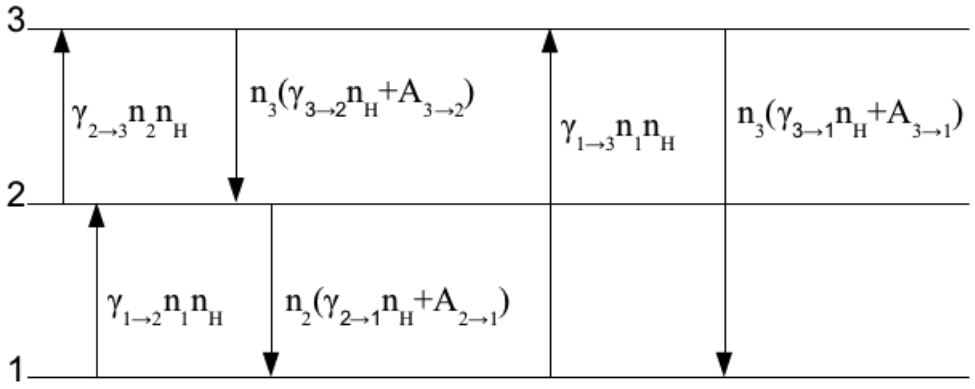

Figure 3 Energy level diagram of an imaginary, 3 level molecule

The imaginary gas consists of molecules in one of these three energy levels in a bath of hydrogen with density n_H. The population density (molecules per cm^{-3}) of each energy level, N_i, is constant if the gas is in steady state. In order to calculate the cooling of this gas, the steady state densities need to be calculated. Consider the definitions in equation 3.2. These definitions allow the final cooling to be expressed independent of the gas density.

$$\begin{aligned} N_{H_2} &= \sum_{i=1}^{3} N_i \\ n_i &= \frac{N_i}{N_{H_2}} \end{aligned} \tag{3.2}$$

As stated before, molecules can transition from one energy level to another through collisions and spontaneous emission. $\gamma_{i\to f}$ is the collisional rate coefficient and $A_{i\to f}$ is the Einstein coefficient for spontaneneous emission. Note that $A_{i\to f}$ is only relavant for $i > f$. From figure 3 equations 3.3 through 3.5 can be written.

$$\frac{dn_1}{dt} = n_2(\gamma_{2\to1}n_H + A_{2\to1}) + n_3(\gamma_{3\to1}n_H + A_{3\to1}) - n_H n_1(\gamma_{1\to2} + \gamma_{1\to3}) \tag{3.3}$$

$$\frac{dn_2}{dt} = \gamma_{1\to2}n_1 n_H + n_3(\gamma_{3\to2}n_H + A_{3\to2}) - n_2[(\gamma_{2\to1}n_H + \gamma_{2\to3}) + A_{2\to1}] \tag{3.4}$$

$$\frac{dn_3}{dt} = n_H(\gamma_{1\to3}n_1 + \gamma_{2\to3}n_2) - n_3[n_H(\gamma_{3\to1} + \gamma_{3\to2}) + A_{3\to1} + A_{3\to2}] \tag{3.5}$$

These equations can be written in matrix form (equation 3.6).

$$\begin{bmatrix} \frac{dn_1}{dt} \\ \frac{dn_2}{dt} \\ \frac{dn_3}{dt} \end{bmatrix} =$$

$$\begin{bmatrix} -(\gamma_{1\to2} + \gamma_{1\to3})n_H & \gamma_{2\to1}n_H + A_{2\to1} & \gamma_{3\to1}n_H + A_{3\to1} \\ \gamma_{1\to2}n_H & -n_H(\gamma_{2\to1} - \gamma_{2\to3}) + A_{2\to1} & \gamma_{3\to2}n_H + A_{3\to2} \\ \gamma_{1\to3}n_H & \gamma_{2\to3}n_H & -n_H(\gamma_{3\to1} + \gamma_{3\to2}) - A_{3\to1} - A_{3\to2} \end{bmatrix} \begin{bmatrix} n_1 \\ n_2 \\ n_3 \end{bmatrix} \tag{3.6}$$

Equation 3.6 can be re-written in the form of equation 3.7.

$$\frac{d\mathbf{n}}{dt} = \mathbf{M} \cdot \mathbf{n} \tag{3.7}$$

The steady state solution is the solution of $\mathbf{n}$ when $\frac{\mathrm{d}\mathbf{n}}{\mathrm{dt}} = 0$. Now the cooling, Λ, of this three state system can be calculated via equation 3.8. Note that only the spontaneous emission produces radiation. Again, it is assumed that all photons

escape the gas. The energy of the escaping photons is the cooling.

$$\frac{\Lambda}{n_{H_2}} = \sum_{i=1}^{3} \sum_{f=0:Ef<Ei}^{i-1} (E_i - Ef) A_{i \to f} n_i \tag{3.8}$$

This section is a simplified example of the calculation conducted in this work. The calculation of the cooling of H_2 from collisions with atomic hydrogen involve 301 energy levels (31 rotational levels and 15 vibrational levels). The proceeding sections describe in detail the calculation of $H+H_2$ cooling performed in this work.

ENERGY LEVEL DENSITY

As demonstrated in the previous section, the first thing that needed to be done was to calculate the populations of the energy levels. The 301 bound energy levels calculated were numbered from lowest energy to highest energy 1 to 301. Figure 4 shows the 301 energy levels from lowest to highest energy level numbered 1 to 301 for both the idealized harmonic oscillator and the actual levels of H_2. The numerical values of the H_2 levels are presented in table 12. Notice the divergence at higher index number between the harmonic oscillator energy levels and the actual H_2 levels.

Following figure 3, the 301 energy levels were expressed as a series of equations describing the population-depopulation rates as the derivative of the level population density with time consisting of both excitation and de-excitation collision coefficients (chapter 4) as well as the Einstein coefficients (chapter 5) divided by the total molecular hydrogen density. These equations are expressed as a 301×301 matrix, **M**, of coefficients similar to equation 3.6. The unknown level populations are expressed as a 301 term vector as are the population-depopulation rates. Again

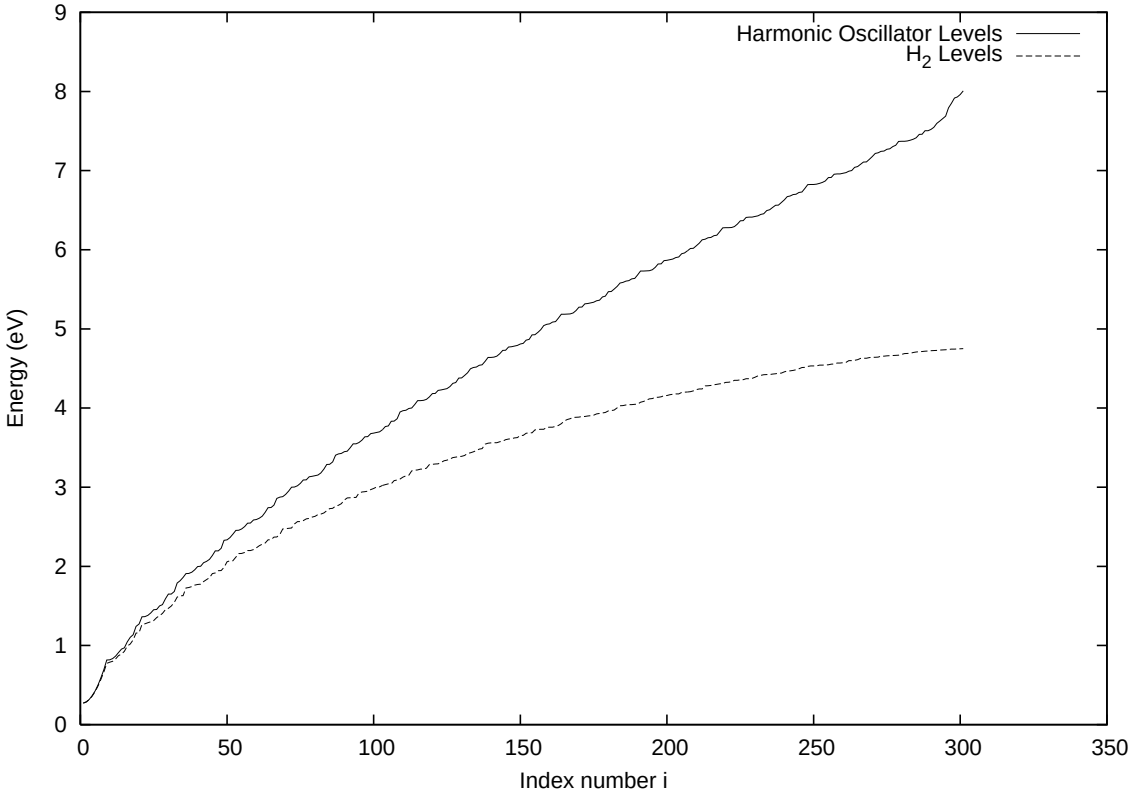

Figure 4 Energy levels of H_2 and the harmonic oscillator with their assigned level numbers

A_{ij} are the Einstein coefficients for spontaneous emission . The steady state solution for the energy level populations can then be solved for by solving for **n** in equation 3.9. In reality the quantities solved for were N_i/N_{H_2} but here the term energy level populations will be used to imply this.

$$0 = \mathbf{M} \cdot \mathbf{n} \tag{3.9}$$

This equation has two solutions, the first is the trivial solution that would result in a vector **n** of all zeros. In order to remedy this, the condition in equation 3.10 is applied.

$$\sum_{i=1}^{301} n_i = 1 \tag{3.10}$$

There are two techniques that were found useful to solve this problem; backward differentiation (BDF) and singular value decomposition (SVD). Press et al. (2007) provides C++ and Fortran versions of an SVD subroutine as part of the software that accompanies their publication. It is very user friendly and can be simply copied directly into a larger program. This was very effective in most instances; however, from time to time, particularly in densely populated matrices it would struggle to converge. But it did prove useful as a check with the BDF solution. An alternative to the Press et al. (2007) subroutine is the Octave SVD subroutine. It is utilized in a subroutine in the final version available in the appendix CD. Octave (Eaton 2009) is an open source command line mathematical software package very similar to Matlab. As an alternative to the SVD solution, it was used to conduct a

Figure 5 Level Densities T $= 1000$K, $\mathrm{n_H} = 1\mathrm{cm}^{-3}$

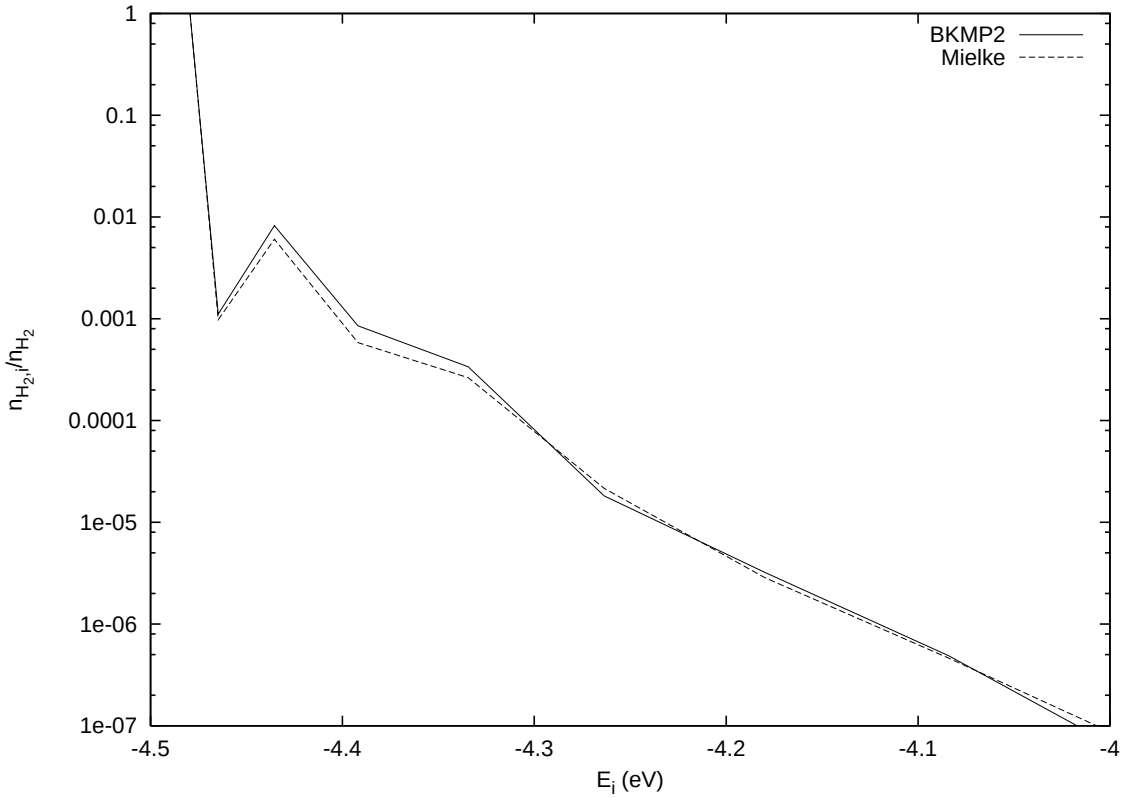

backward differentiation to get the values of the energy level populations.

The levels populations are plotted for $T = 1000$ and 10000K in figures 5 through 8. Notice that both increased temperature, and increased hydrogen density causes the higher energy levels (Appendix C) to become more densely populated. As these two quantities are increased, considerations such as dissociation, unbound levels should be included.

Figure 6 Level Densities T $= 1000$K, $\mathrm{n_H} = 1E4\mathrm{cm}^{-3}$

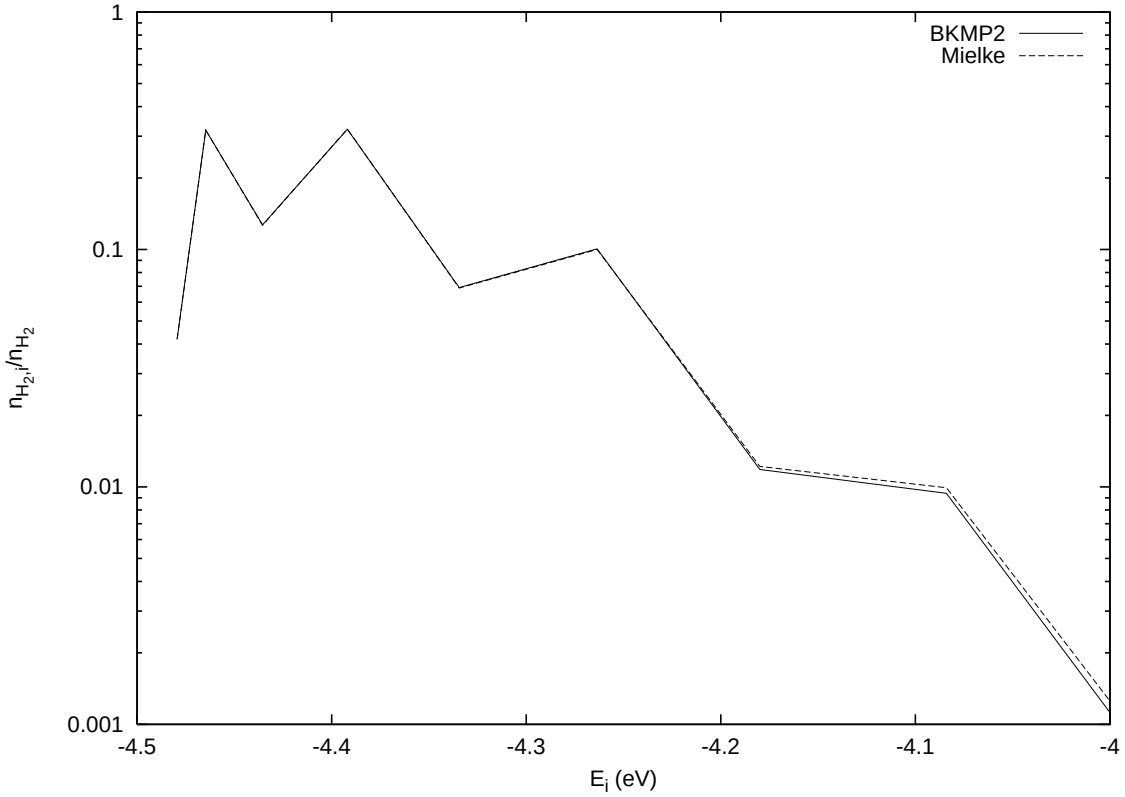

Figure 7 Level Densities $\mathrm{T} = 10000\mathrm{K}, \mathrm{n_H} = 1\mathrm{cm}^{-3}$

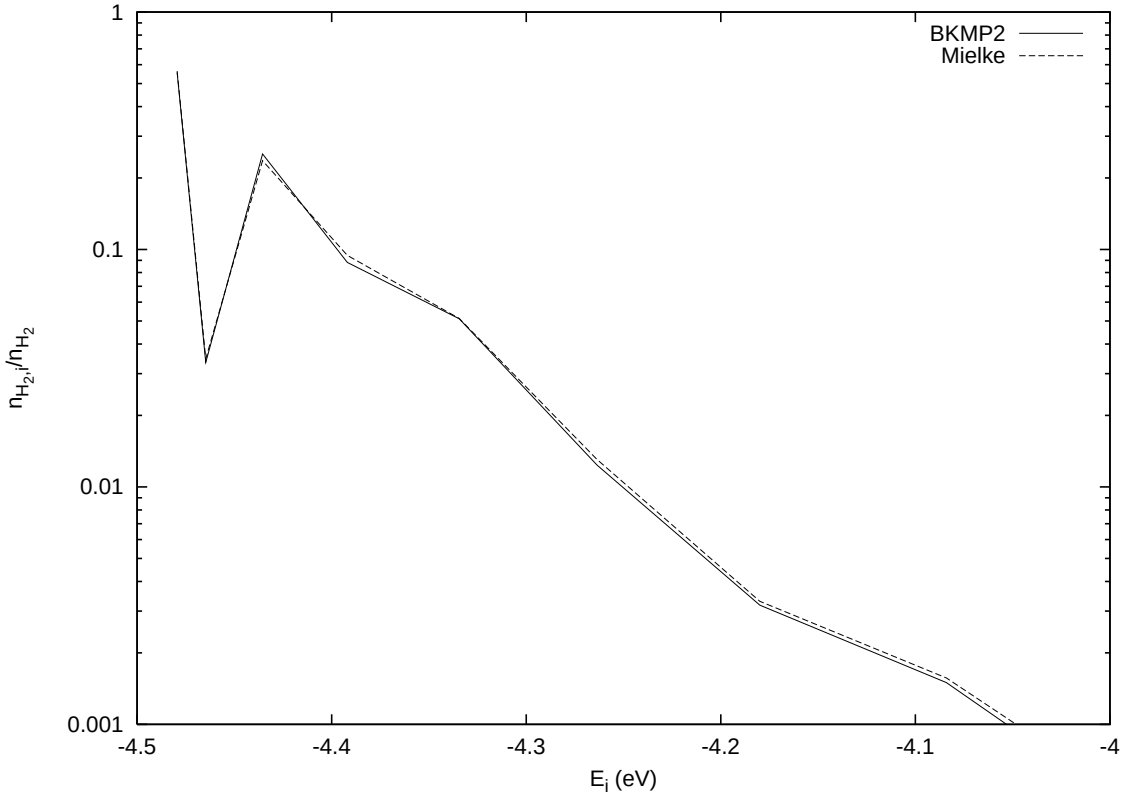

Figure 8 Level Densities $\mathrm{T} = 10000\mathrm{K}, \mathrm{n_H} = 1E4\mathrm{cm}^{-3}$

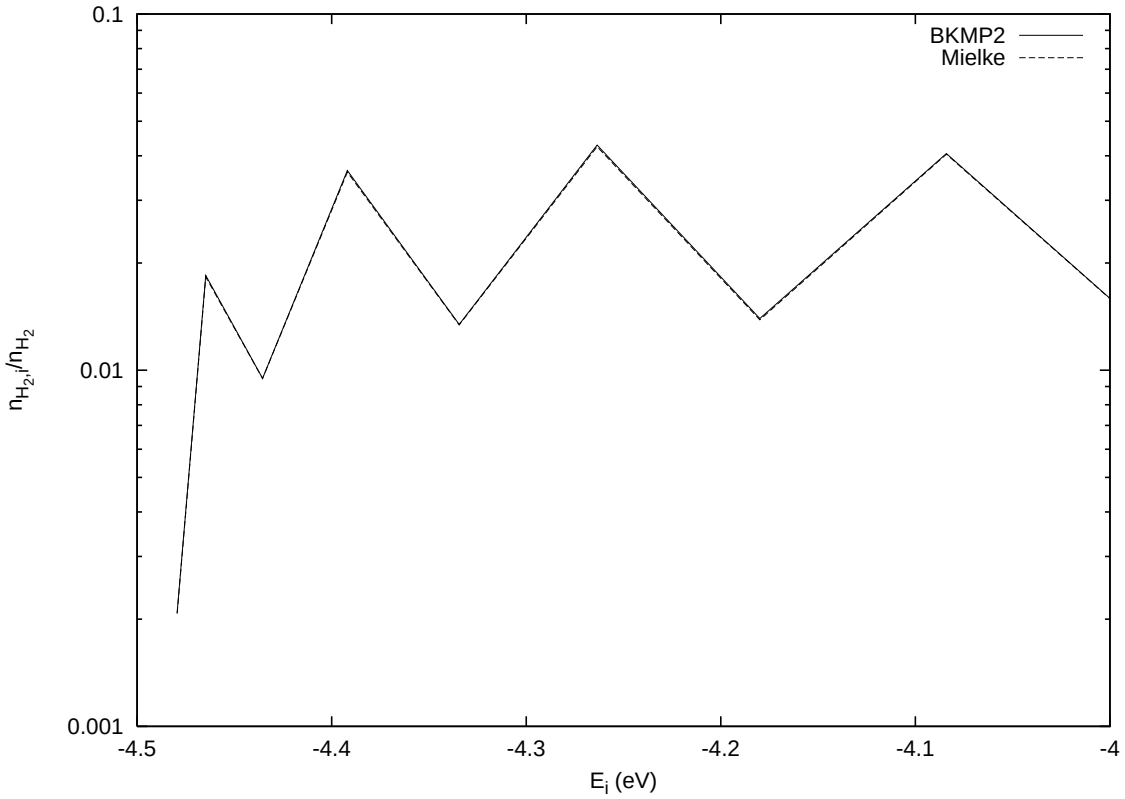

Using the energy level densities, the cooling rates can now be calculated. Note, only radiative transitions result in cooling. This is a result of the selection rules for H_2. Selection rules are calculated via equation 3.11. $\mu_{z,i\rightarrow f}$ is the dipole moment, Ψ are the state wave functions, $\widehat{\mu}$ is the transition moment operator, and τ is the coordinates. The wave function for the electronic ground states were calculated by James & Coolidge (1993). If this integral is not zero then the transition is an allowed transition (the transition moment function is symmetric). As is customary in these kinds of calculations I did not consider forbbiden transitions. The results of this integral show that only transitions for $\triangle$ J $= 0, \pm 2$. There is no limitation on vibrational transitions.

$$\mu_{z,i\rightarrow f} = \int_{-\infty}^{\infty} \Psi_i^* \widehat{\mu} \Psi_f d\tau \tag{3.11}$$

Referring back to equation 3.8, the cooling rate can now be calculated for the 301 energy levels using the calculated level populations and the Einstein coefficients. These rates are presented in tables 2 through 5. Notice that the rates converge as temperature and density increase. Temperatures less than ~ 1000K should be done using a quantum calculation.

Finally the shape of the emission spectrum can be calculated. Appendix A details how to do this using the program written for this study. This is done by normalizing the monochromatic flux, $F_{\nu_{i\rightarrow f}}$, for each radiative transition as in equation 3.12 for some constant C. Each transition is characterized by an emitted photon of energy E_{photon}. Figures 9 through 12 show the predicted spectrum of the BKMP2

Table 2 Calculated cooling rates in erg cm^{-3} s^{-1} for $n_H = 1 cm^{-3}$

Temperature (K)	Mielke	BKMP2
1000	$2.490E-25$	$2.976E-25$
1500	$1.664E-24$	$1.777E-24$
2000	$5.090E-24$	$5.126E-24$
3000	$1.968E-23$	$1.897E-23$
4000	$4.602E-23$	$4.389E-23$
5000	$8.601E-23$	$8.117E-23$
6000	$1.440E-22$	$1.330E-22$
8000	$3.403E-22$	$2.963E-22$
10000	$6.713E-22$	$5.625E-22$

Table 3 Calculated cooling rates in erg cm^{-3} s^{-1} for $n_H = 100 cm^{-3}$

Temperature (K)	Mielke	BKMP2
1000	$2.967E-23$	$3.324E-23$
1500	$1.819E-22$	$1.806E-22$
2000	$5.009E-22$	$4.862E-22$
3000	$1.812E-21$	$1.750E-21$
4000	$4.194E-21$	$4.061E-21$
5000	$7.706E-21$	$7.483E-21$
6000	$1.231E-20$	$1.199E-20$
8000	$2.445E-20$	$2.391E-20$
10000	$3.973E-20$	$3.902E-20$

Table 4 Calculated cooling rates in erg cm^{-3} s^{-1} for $n_H = 1E4 cm^{-3}$

Temperature (K)	Mielke	BKMP2
1000	$1.844E-21$	$1.869E-21$
1500	$8.960E-21$	$8.848E-21$
2000	$2.229E-20$	$2.175E-20$
3000	$6.678E-20$	$6.506E-20$
4000	$1.365E-19$	$1.338E-19$
5000	$2.344E-19$	$2.310E-19$
6000	$3.599E-19$	$3.569E-19$
8000	$6.692E-19$	$6.684E-19$
10000	$9.967E-19$	$9.984E-19$

Table 5 Calculated cooling rates in erg cm^{-3} s^{-1} for $n_H = 1E8 cm^{-3}$

Temperature (K)	Mielke	BKMP2
1000	$2.745E-21$	$2.745E-21$
1500	$1.732E-20$	$1.732E-20$
2000	$4.809E-20$	$4.809E-20$
3000	$1.524E-19$	$1.524E-19$
4000	$3.045E-19$	$3.045E-19$
5000	$4.971E-19$	$4.971E-19$
6000	$7.189E-19$	$7.189E-19$
8000	$1.183E-18$	$1.183E-18$
10000	$1.589E-18$	$1.589E-18$

Figure 9 BKMP2 predicted spectrum T $= 1000$K $n_H = 1 cm^{-3}$

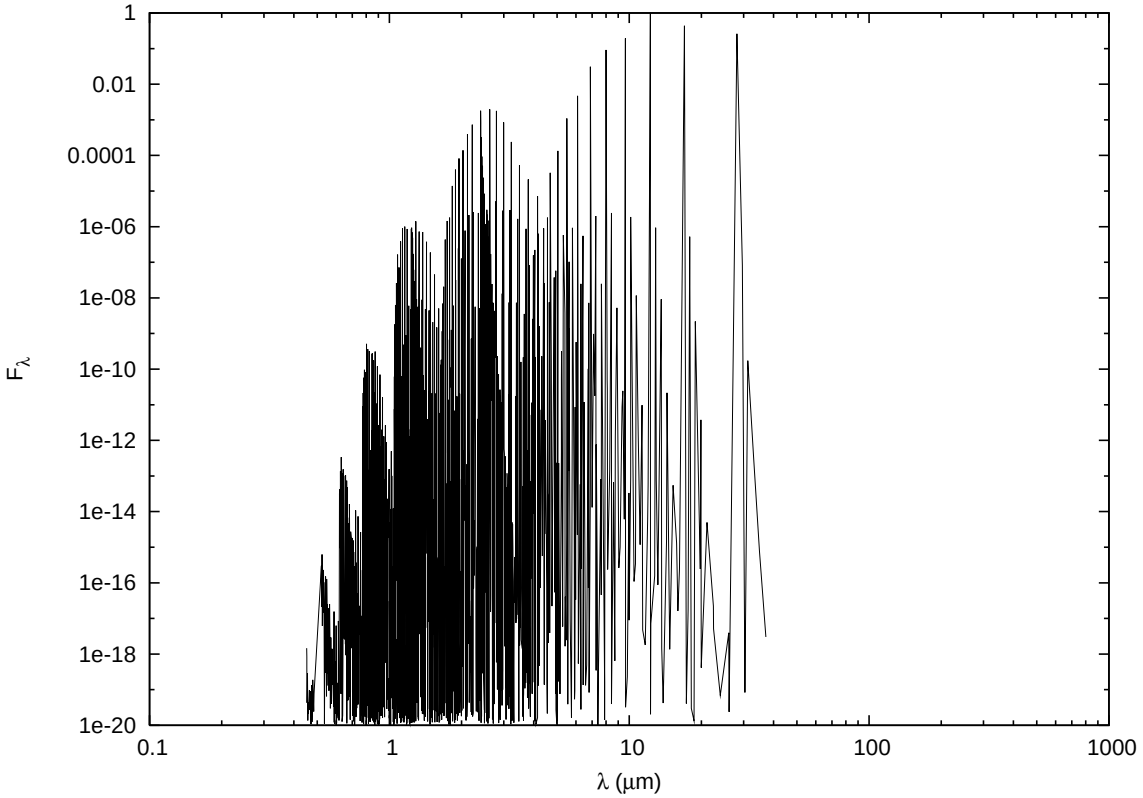

potential using this calculation.

$$\begin{aligned} F_{\nu_{i\to f}}(E_{photon}) &= CA_{i\to f}n_i \\ E_{photon} &= E_i - E_f \end{aligned} \tag{3.12}$$

The general shape of this figure can be checked by comparing it to a similar calculation performed by Shaw et al. (2005) (Shaw05). Their calculation was concerning the photo dissociation region (PDF) around a star. Figure 13 shows their results. The similarity between the calculations performed in this study compared to Shaw05 are particularly apparent when considering the 10000K spectra. In fig-

Figure 10 BKMP2 predicted spectrum T $= 1000$K $\mathrm{n_H} = 1\mathrm{E}4\mathrm{cm}^{-3}$

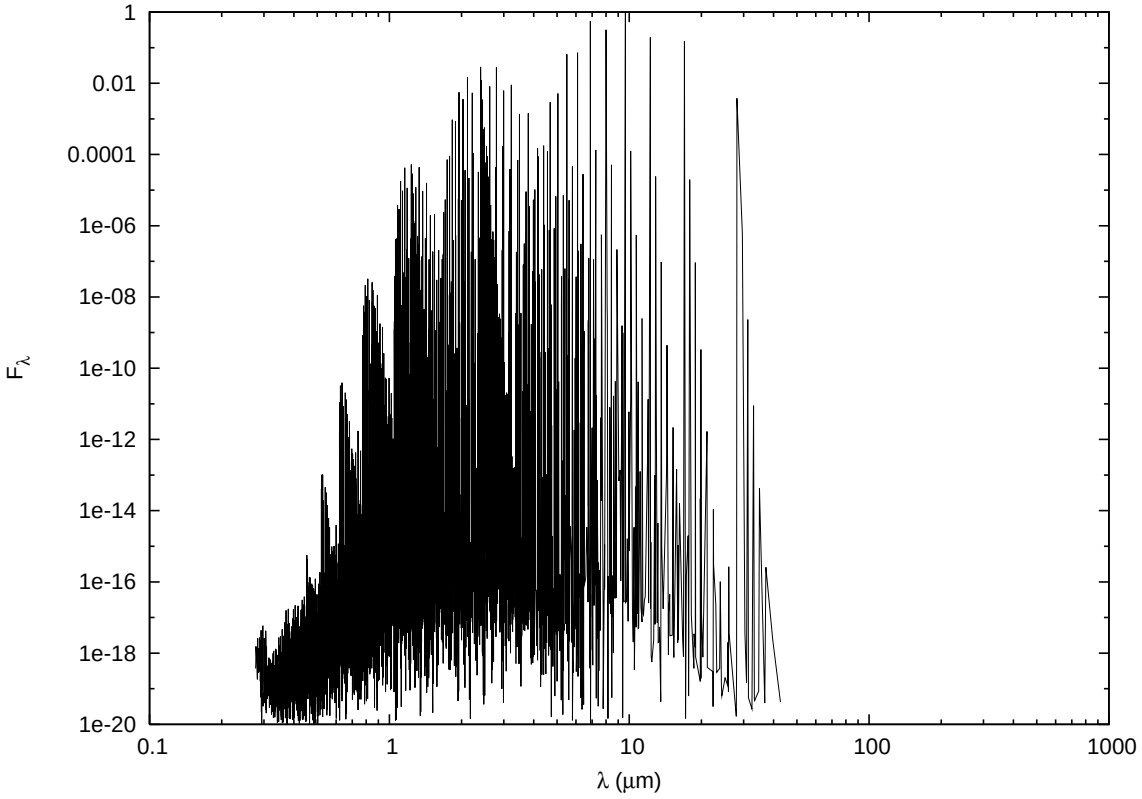

Figure 11 BKMP2 predicted spectrum T $= 10000$K $n_{\rm H} = 1$E4cm^{-3}

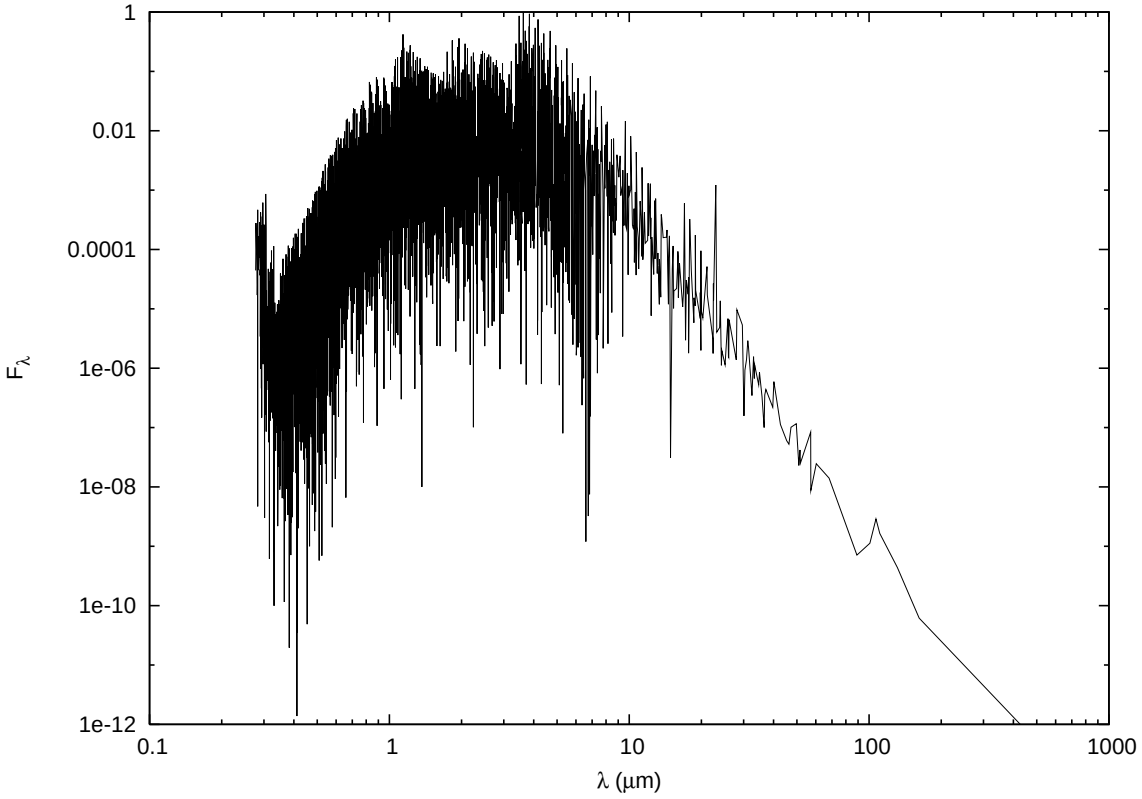

Figure 12 Mielke predicted spectrum T $= 10000$K $\mathrm{n_H} = 1\mathrm{E}4\mathrm{cm}^{-3}$

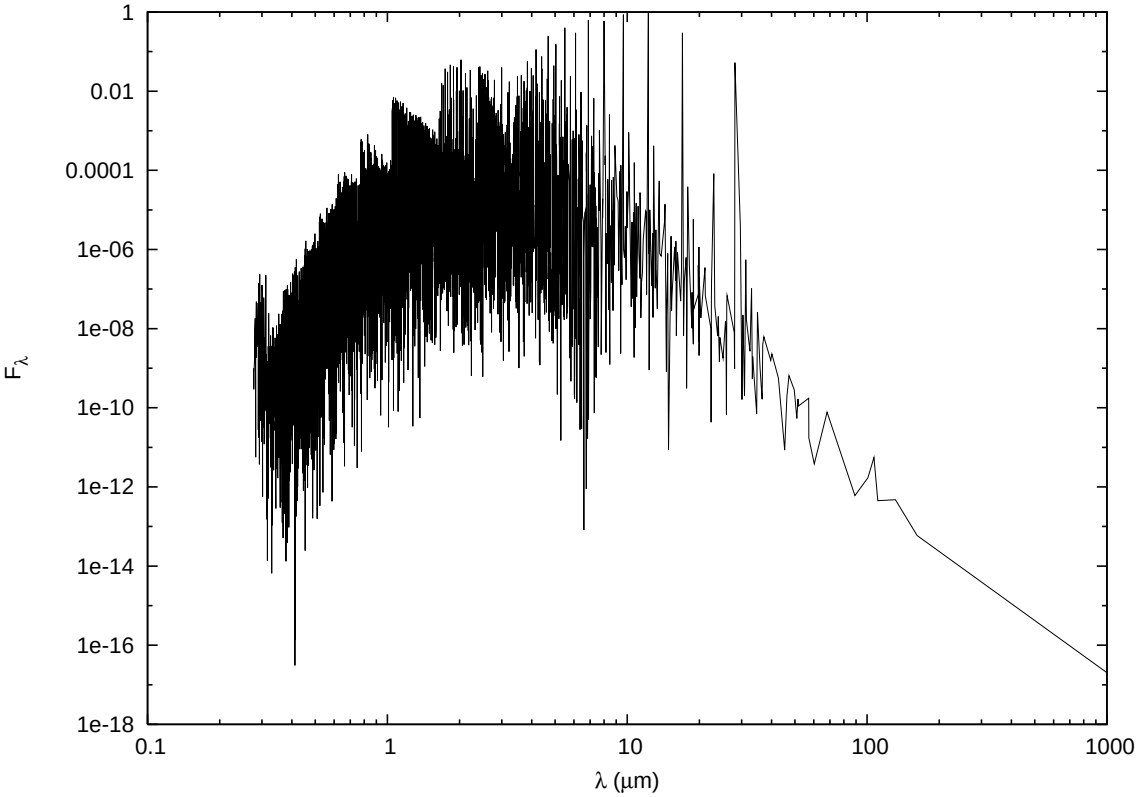

Figure 13 PDR of a Star Using CLOUDY (Shaw et al. 2005) for an ionization fraction of $.5$

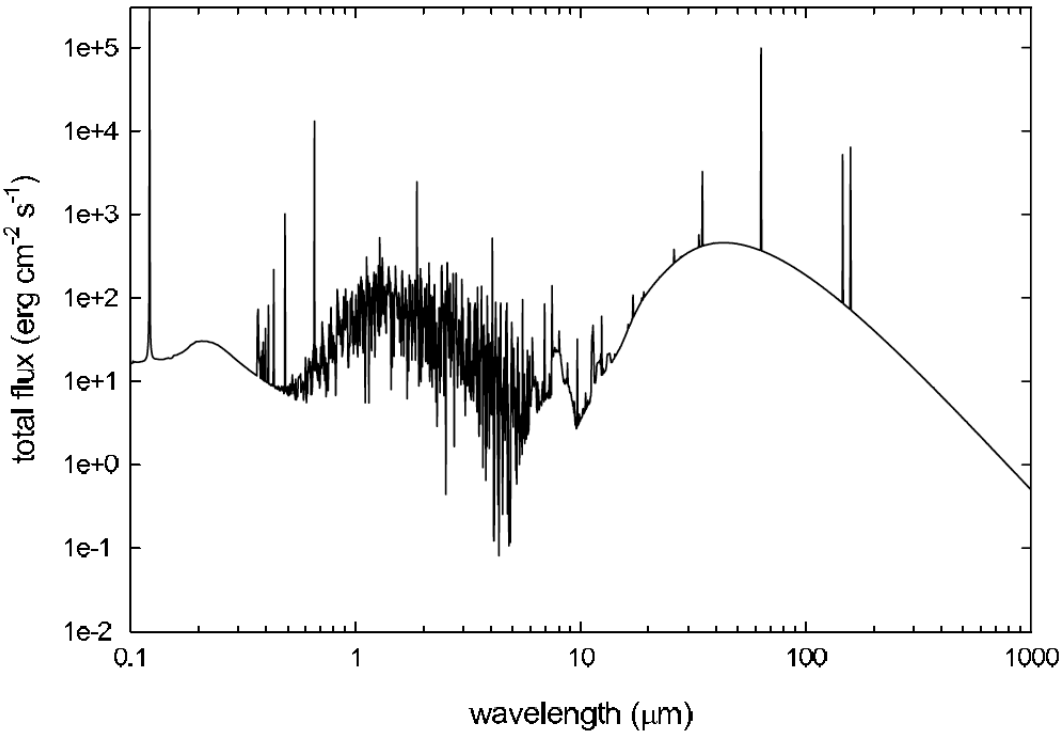

ure 13, molecular hydrogen is represented in the region of $\sim .3$ to $\sim 10\mu$m. One will also notice that the Shaw05 figure appears to have a less detailed spectrum. This is because they considered only ~ 4 percent of the ~ 12000 transitions of molecular hydrogen. They describe theirs as being a "very approximate" calculation. Finally, they used a quantum mechanical treatment performed by LeBourlot et al. (1999) and extrapolated to higher temperatures based on low temperature calculations. However, the shapes of the two calculations are similar enough to provide some confidence of this calculation as well as some perspective of how the calculation performed here can be used.

CHAPTER 4

COLLISION RATE COEFFICIENTS

The collision rate coefficients are important in calculations of gas cooling because they have a significant impact on energy level populations. Mandy & Martin (1991), Mandy & Martin (1992), Mandy & Martin (1993), and Martin & Mandy (1995) are a series of papers that lay out how to do this calculation step by step for $H + H_2$. The calculation presented in this chapter were performed following theirs. Interactions for $H + H_2$ were calculated using the quasiclassical trajectory method (QCT) (Blais & Truhlar 1976). Given a set of 31 rotational energy levels and 15 vibrational levels, this method predicts the outcome of a collision for a variety of geometries and counts the number of times a particular transition occurs. The work presented here used BKMP2 trajectories calculated by Archer (2006) and Mielke trajectories courtesy of Stephen Lepp. Using these trajectories, a series of FORTRAN programs were written to calculate the cooling rates for a variety of hydrogen densities and temperatures.

COLLISION CROSS SECTIONS

Each collision has two trajectories associated with it. The first are non-reactive collisions in which the atomic hydrogen interacts with the molecular hydrogen but no atomic exchange occurs. These trajectories are denoted $N_{i\rightarrow f,N}$. The i and f represent the initial and final energy states. Next there are collisions with an exchange reaction in which the incoming hydrogen atom changes place with one of the atoms in the molecule. These trajectories are denoted $N_{i\rightarrow f,E}$. In an exchange reaction, 3/4 of each reactive transition goes to a ortho state (odd J) and 1/4 goes to a para state (even J) as a result of nuclear spin selection rules (Oka 2004). There are

also trajectories that lead to dissociation though they are ignored when calculating level populations. The QCT code (courtesy of Stephen Lepp) will automatically assume this selection rule. Each exchange reaction then needs to be divided by 4 in order to prevent the total number of trajectories from exceeding the sample size. Equation 4.1 calculates the cross section, $\sigma_{\mathrm{i}\to\mathrm{f}}(\mathrm{T}')$ of a collision. S is the sample size and $\mathrm{b_{max}}$ is the maximum impact parameter. In this case $\mathrm{b_{max}}$ is 5a.u. for the BKMP2 potential and varied for the Mielke potential (See appendix C).

$$\sigma_{i\to f}(T') = \frac{N_{i\to f,N} + \frac{N_{i\to f}}{4}}{S}\pi b_{max}^2 \tag{4.1}$$

$$S = \sum_{i=1}^{301}\sum_{f=1}^{301}(N_{i\to f,N} + \frac{N_{i\to f}}{4} + N_{i\to dissociation}) \tag{4.2}$$

Only the de-excitation coefficients were calculated from trajectories. The excitation coefficients were calculated via detailed balance. Also, bearing in mind that the QCT uses a Monte Carlo method, the law of large numbers shows that the solution has a $\mathrm{S}^{-\frac{1}{2}}$ convergence. It stands to reason that with an increased sample size, the uncertainty should decrease.

Figures 14 through 19 are a sampling of plotted cross sections. They include, vibrational, ro0tational, and ro-vibrational transitions for both ortho and para states. As shown in the plots, both potentials show very similar behavior for each transition. Cross sections were calculated for temperatures of 500, 1000, 2000, 5000, 7000, 10000, 20000, 30000K. $\sigma_{\mathrm{i}\to\mathrm{f}}(0\mathrm{K})$ is assumed to be zero and $\sigma_{\mathrm{i}\to\mathrm{f}}(\infty)$ is assumed to be equal to the cross section at 30000K.

The cross sections were fit to a cubic spline to make them easier to work with mathematically. This was done via the form of equation 4.3. Maxima (Vodopivec & Lenarcic 2010) was used to solve for a general cubic spline for the temperature

Figure 14 An example of a vibrational transition to a para state

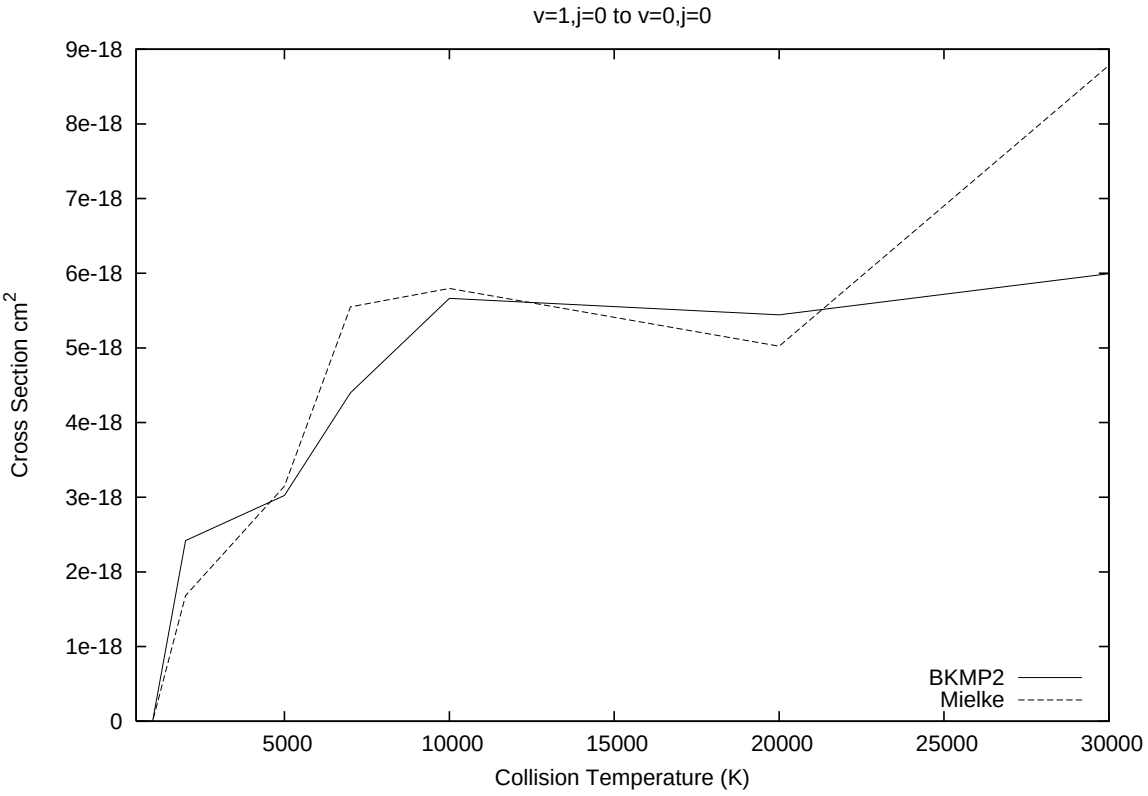

intervals used as the collision temperatures identified earlier.

$$\begin{aligned} \sigma_{i\to f,k\to k+1} &= \mathrm{a}_{k\to k+1}(T' - T'_{k\to k+1})^3 + b_{k\to k+1}(T' - T'_{k\to k+1})^2 \\ &\quad +\mathrm{c}_{k\to k+1}(T' + T'_{k\to k+1}) + d_{k\to k+1} \\ \mathrm{k} &= 1{,}9 \\ \mathrm{T}_k &= 0,\ 500,\ 1000,\ 2000,\ 5000,\ 7000,\ 10000,\ 20000,\ 30000\ \mathrm{K} \end{aligned} \tag{4.3}$$

Figure 15 An example of a vibrational transition to a ortho state

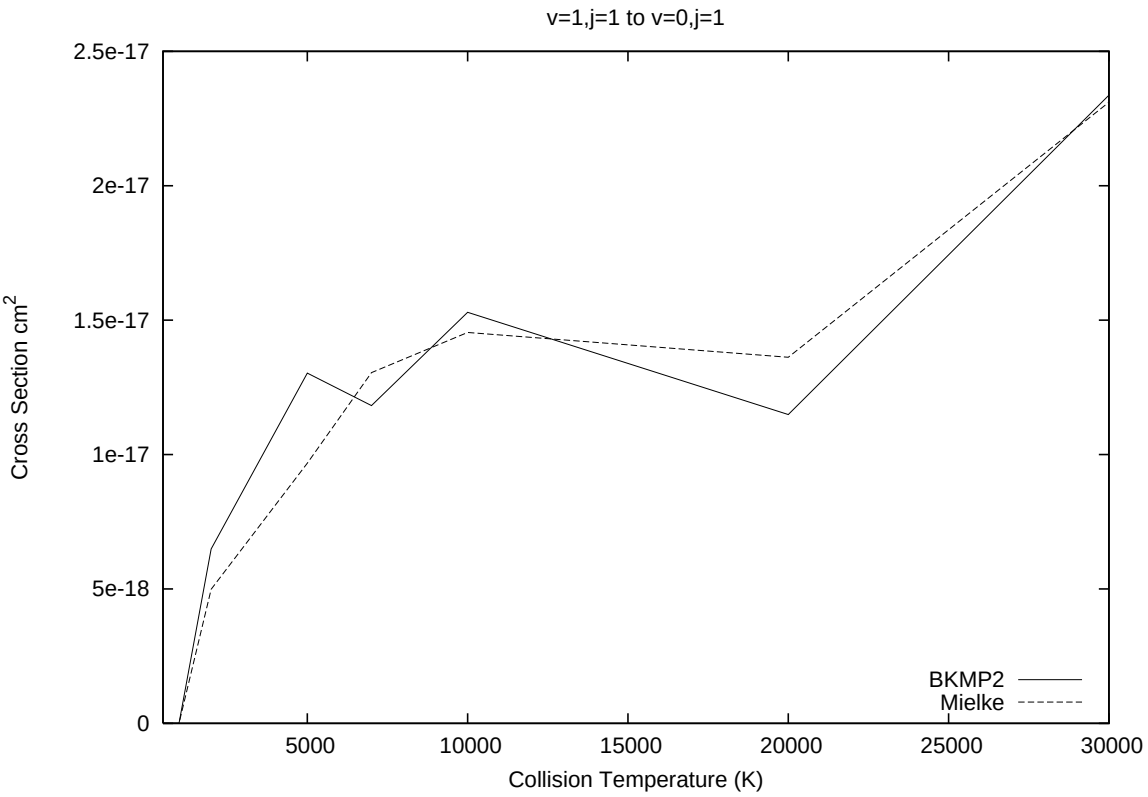

Figure 16 An example of a rotational transition to a ortho state

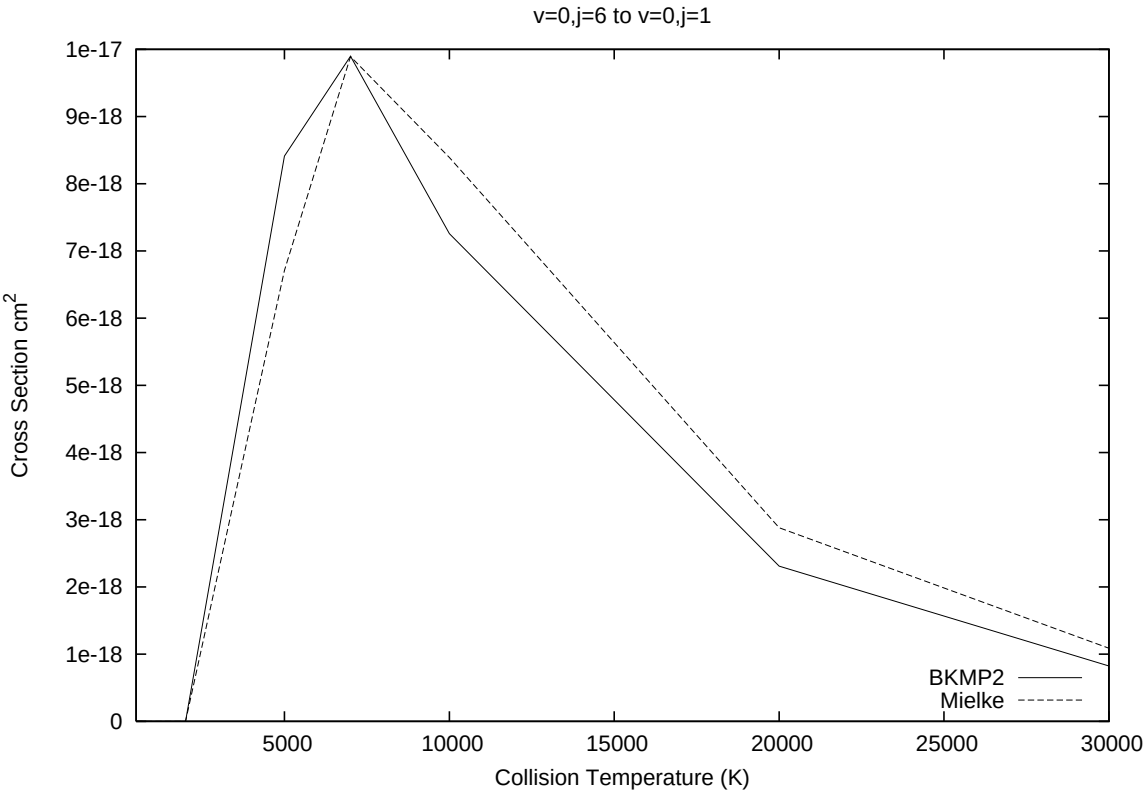

Figure 17 An example of a rotational transition to a para state

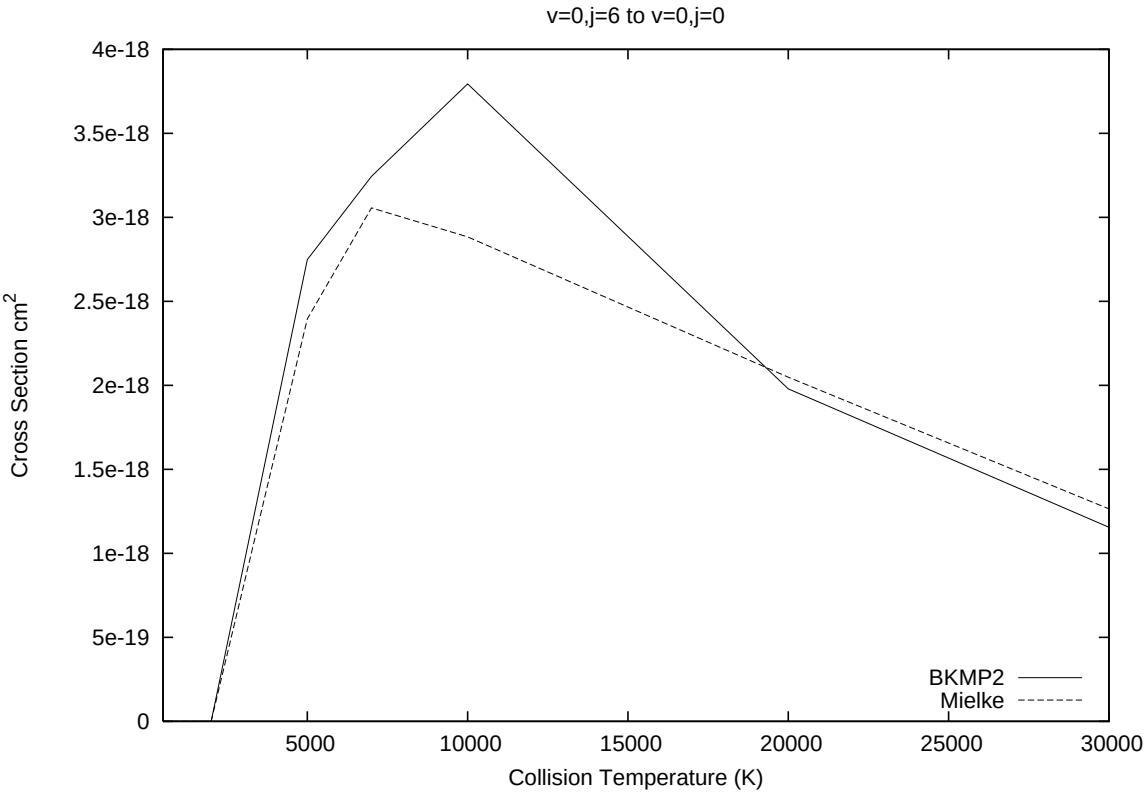

Figure 18 An example of a ro-vibrational transition to a para state

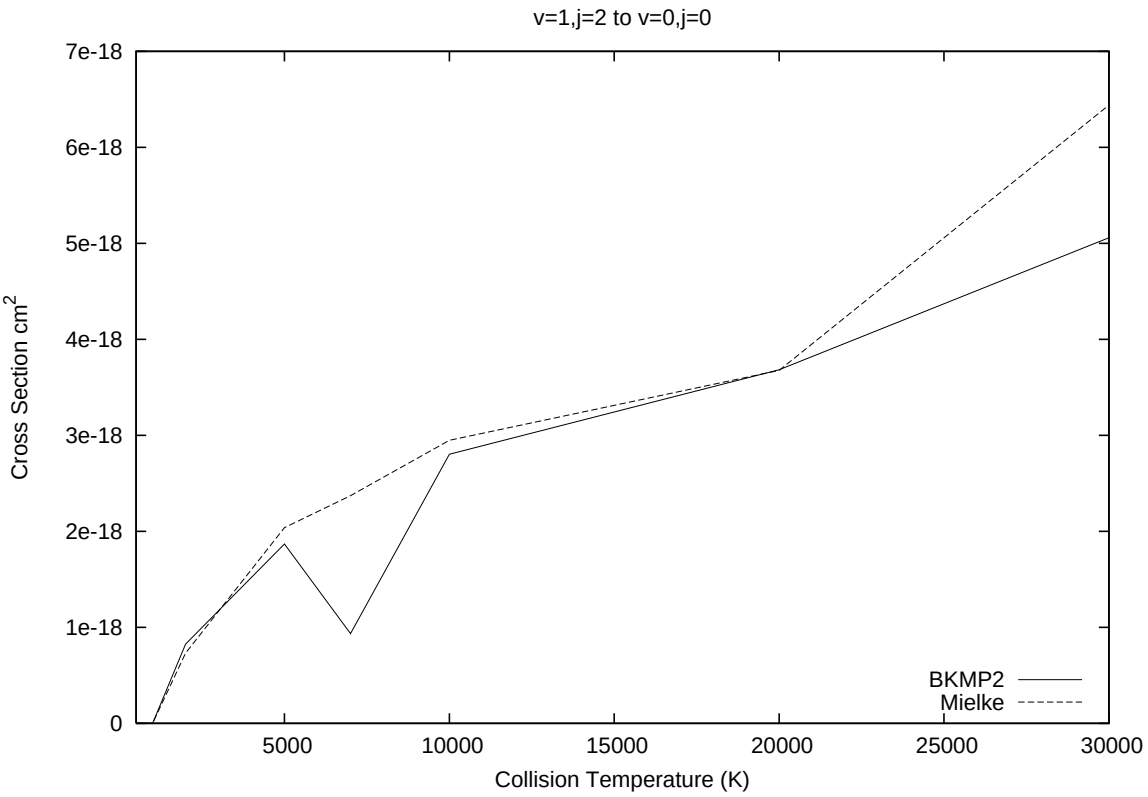

Figure 19 An example of a ro-vibrational transition to a ortho state

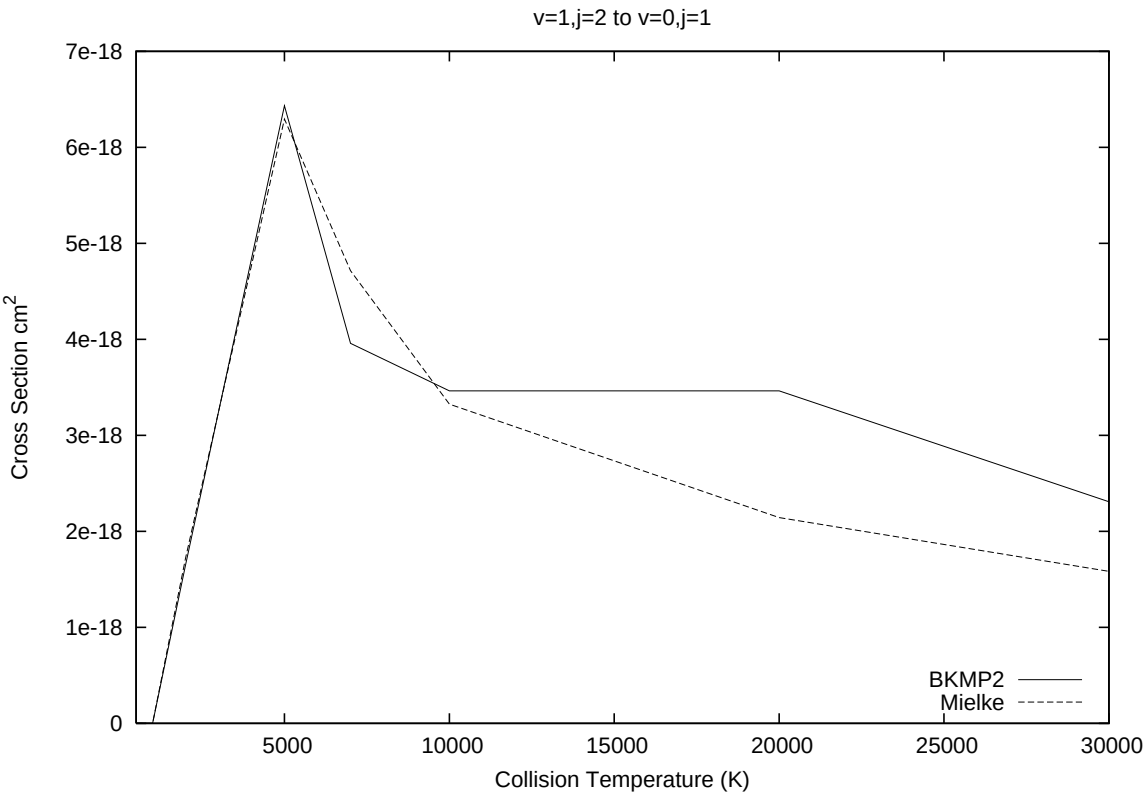

THE MAXWELL-BOLTZMANN VELOCITY DISTRIBUTION

The Boltzmann distribution, equation 4.4, gives the kinetic energy distribution of molecules in thermal equilibrium. T is the gas temperature, k is the Boltzmann factor, 8.617×10^{-5}eV/K, A is a normalization constant, and E is the kinetic energy. The Boltzmann distribution is a classical approximation of the Fermi-Dirac distribution used for spin 1/2 particles (Fermions) and the Bose-Einstein distribution used for spin 1 particles (Bosons).

$$f(E) = Ae^{-\frac{E}{kT}} \tag{4.4}$$

The Boltzmann distribution can be used to describe the number of particles within a system with a particular energy. This is given by equation 4.5. Equation 4.5 will become significant later in this section.

$$n(E) = g(E)f(E) \tag{4.5}$$

Equation 4.4 can be rewritten in terms of velocity by substituting the kinetic energy E = $\frac{1}{2}$mv^2. This gives equation 4.6.

$$f(v) = Ae^{-\frac{mv^2}{2kT}} \tag{4.6}$$

Next, the Boltzmann distribution can be normalized and solved for A as seen in equations 4.7 and 4.8 respectively.

$$\int_{-\infty}^{\infty} f(v)dv = 1 \tag{4.7}$$

$$A = (\frac{m}{2\pi kT})^{\frac{1}{2}} \tag{4.8}$$

In three dimensions this becomes equation 4.9.

$$f(v) = f(v_x, v_y, v_z) = f(v_x)f(v_y)f(v_z)F(v)dv = \int f(\overrightarrow{v})d^3(\overrightarrow{v}) \tag{4.9}$$

Since the velocity vectors are on average the same length in each direction throughout the gas, the volume of the spherical shell represented by this integeral can be written as equation 4.10. This equation represents the Maxwell velocity distribution.

$$\begin{aligned} \text{F(v)dv} &= 4\,\pi f(v)v^2dv \\ &= 4\,\pi(\tfrac{m}{2\pi kT})^{\frac{3}{2}}v^2e^{-\frac{mv^2}{2kT}}dv \end{aligned} \tag{4.10}$$

COLLISION RATE COEFFICIENTS

The mean velocity can now be described using the mean value theorem for integrals, equation 4.11.

$$< v >= \int_0^\infty F(v)vdv \tag{4.11}$$

Finally, the collision rate coefficient between two moving particles can be described based on classical mechanics as the velocity$\times$collision cross section as in equation 4.12.

$$\begin{aligned} \gamma_{i\to f} &= < \sigma_{i\to f}v > \\ &= \textstyle\int_0^\infty F(v)v\sigma_{i\to f}(v)dv \\ &= 4\,\pi(\tfrac{\mu}{2\pi kT})^{\frac{3}{2}}\textstyle\int_{-\infty}^\infty \sigma_{i\to f}(v)v^3e^{\frac{\mu v^2}{2kT}}dv \end{aligned} \tag{4.12}$$

Note that instead of mass, reduced mass is used to better represent the system of particles. Next, the substitution in equation 4.13 is made relating the velocity of

the collisions to the temperature of the collision. The result is equation 4.14 which is the equation to calculate the collision rate coefficients given a gas temperature T and collision temperature T'.

$$E = \frac{1}{2}\mu v^2 = kT' \tag{4.13}$$

$$\gamma_{i\to f} = (\frac{2}{T})^(\frac{3}{2})(\frac{k}{\pi\mu})^{\frac{1}{2}} \int_0^\infty \sigma_{i\to f}(T')e^{-\frac{T'}{T}}dT' \tag{4.14}$$

Performing this integral by hand would be too complicated tedious. So instead there are a number of numerical methods available to calculate these integrals. A Fortran program was written to calculate this integral using Simpson's 3/8th rule, equation 4.15, for the de-excitation coefficients for gas temperatures of 100, 500, 1000, 2000, 5000, 7000, 10000, 15000, 20000, 25000, 30000, and 40000 K.

$$\begin{aligned} \mathrm{h} &= \tfrac{b-a}{3n} \\ \int_a^b f(x)dx &\approx \tfrac{3h}{8}\textstyle\sum_{k=1}^{n}[f(x_{3k-2}) + 3f(x_{3k-2}) + 3f(x_{3k-1} + f(x_{3k})] \end{aligned} \tag{4.15}$$

Referring back to equation 4.5, the populations for two energy levels can be written as equation 4.16.

$$\frac{n_f}{n_i} = \frac{g_f e^{-\frac{E_f}{kT}}}{g_i e^{\frac{-E_i}{kT}}} = \frac{g_f}{g_i}e^{-\frac{(E_f - E_i)}{kT}} \tag{4.16}$$

As stated in the previous chapter, when the system is in steady state, the excitation transitions must equal the de-excitation transitions. This can be written in

the form of equation 4.17.

$$n_i n_H \gamma_{i\to f} = n_f(n_H \gamma_{f\to i} + A_{f\to i}) \tag{4.17}$$

By detailed balance, equation 4.17 can be rewritten as equation 4.18.

$$\frac{n_f}{n_i} = \frac{\gamma_{i\to f}}{\gamma_{f\to i}} \tag{4.18}$$

So now the excitation coefficients can be calculated as equation 4.19.

$$\frac{\gamma_{i\to f}}{\gamma_{f\to i}} = \frac{g_f}{g_i} e^{-\frac{(E_f - E_i)}{kT}} \tag{4.19}$$

FITTING THE RATE COEFFICIENTS

Next, the rate coefficients were fit to equation 4 from Martin & Mandy (1995), equation 4.20 in this discussion, to the parameters a, b, c, and d. This was done using the general least squares fitting algorithm from section 15.4.1 from Press et al. (2007). This section describes this algorithm and how it was used.

$$\begin{aligned} \log_{10}\gamma(t) &= \text{a+bz+cz}^2 - d(\tfrac{1}{t} - 1) \\ \text{t} &= \text{T/4500 K} \\ \text{z} &= \log_{10} t \end{aligned} \tag{4.20}$$

This algorithm works by finding the solution that minimizes χ^2 (equation 4.21) for equation 4.20 written as a system of 12 equations for the temperatures $\text{T}_\text{i} =$

$100 \rightarrow 40000$K identified earlier.

$$\begin{aligned} \chi^2 &= \textstyle\sum_{i=1}^{12}[log_{10}\gamma(t_i) - (a + bz + cz^2 - d(\frac{1}{t} - 1)]^2 \\ &= \textstyle\sum_{i=1}^{12}[y_i - \sum_{k=1}^{4} a_k X_k(t_i)]^2 \\ \mathrm{y}_i &= \log_{10}\gamma(t_i) \\ \mathrm{a}_k &= \text{a, b, c, and d respectively} \\ X_k(t_i) &= 1, \mathrm{z}_i, z_i^2, \text{ and } \tfrac{1}{t_i} - 1 \text{ respectively} \end{aligned} \tag{4.21}$$

Following the algorithm as in Press et al. (2007), three matrices $\mathbf{b} = \mathrm{b_i}$, a vector of 12 elements, $\mathbf{A} = \mathrm{A_{ij}}$, a 12×4 matrix of the values of $\mathrm{X_k(t_i)}$, and **a**, a 4 element vector with unknown values of $\mathbf{a} = \mathrm{a_k}$ were identified. The goal is to solve for the vector **a**. Taking the derivative of equation 4.21 and setting it equal to zero gives equation 4.22.

$$\begin{aligned} 0 &= \textstyle\sum_{i=1}^{12}[y_i - \sum_{j=0}^{4} a_j X_j(t_i)]X_k(t_i) \\ \mathrm{k} &= 1{,}4 \end{aligned} \tag{4.22}$$

Equation 4.22 is then solved for $\mathrm{a_j}$ giving the values of the coefficients of the fit. This is done as represented by equations 4.23.

$$\begin{aligned} \alpha &= A^T \cdot \mathbf{A} \\ \beta &= A^T \cdot \mathbf{b} \\ \alpha \cdot \mathbf{a} &= \beta \\ \mathbf{a} &= \alpha^{-1} \cdot \beta \end{aligned} \tag{4.23}$$

This procedure was done using a program I wrote in Fortran. Figures 20 through 24 show some examples of fits to the collision rate coefficients using equation 4.20.

When considering the error bars it is clear that the fit is sufficient even for the largest RMS error (table 2) for a calculation with a large value range. Martin and Mandy (1995) report this fit to be sufficient to 5 percent of the calculated data points. All the significant transitions (low initial energy) are well behaved and well fit. Any difficulty in fitting is a result of the fact that these cross sections can behave very erratically due to few trajectories. They also have many different behaviors at various temperatures. However, equation 4.20 works very well for most of the cross sections. A new trajectory calculation with a larger sample may produce better results. Of course a new function may also be required for more precision.

COMPARISON WITH OTHER CALCULATIONS

The coefficient fits can now be compared with previous work. The rate coefficients presented in Martin & Mandy (1995) are available at Martin (1996). The calculations presented here match within an order of magnitude of the Martin & Mandy (1995) calculations. These plots include the calculations for the Mielke potential with $b_{max} = 5$a.u. and for a varying maximum impact parameter. Varying the impact parameter appears to have minimal significance. At the most extreme the varying impact parameter is still within 10 percent of the constant impact parameter (eg. table 7 for the 0,4 to 0,2 transition) . In each instance this difference is less than 10 percent. However, for the cooling calculation the varying impact parameter for the Mielke potential was used. For the BKMP2 potential the impact parameter was fixed at 5a.u. Figures 25 through 33 compare the Martin & Mandy (1995) BKMP coefficients to the coefficients calculated here.

Figure 20 v=0,j=4 to v=0,j=2

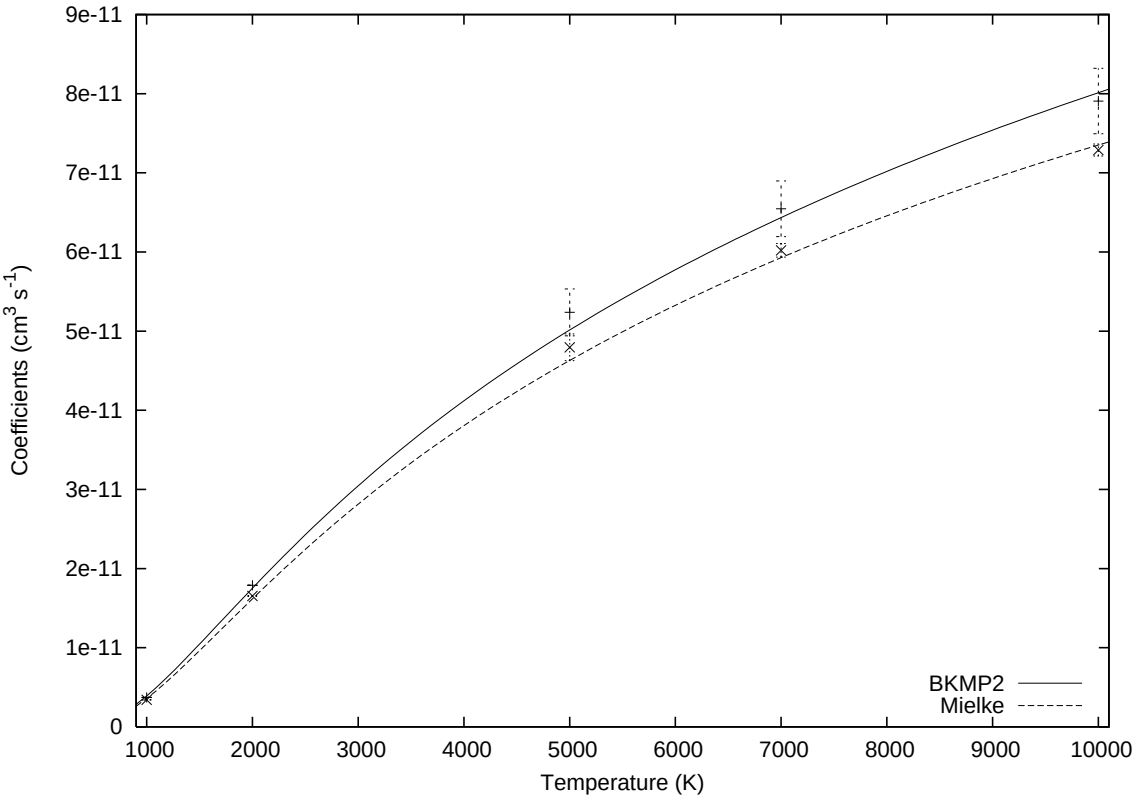

Figure 21 v=0,j=6 to v=0,j=2

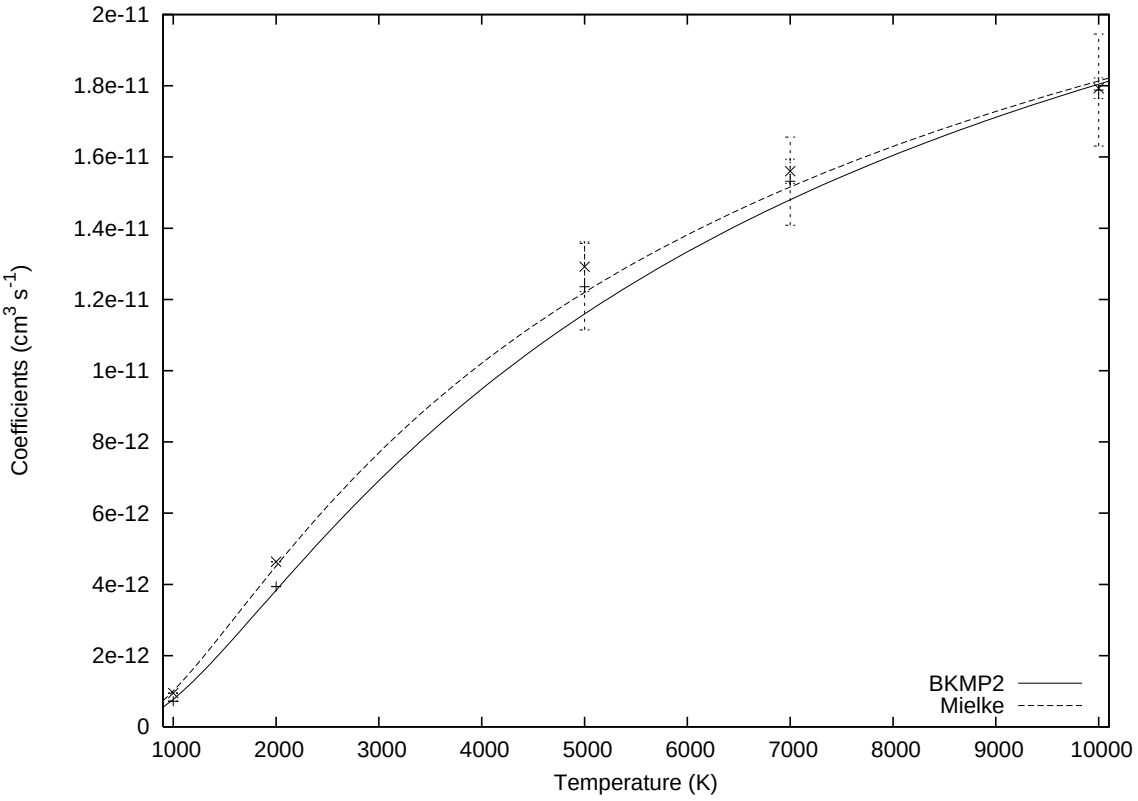

Figure 22 v=1,j=0 to v=0,j=0

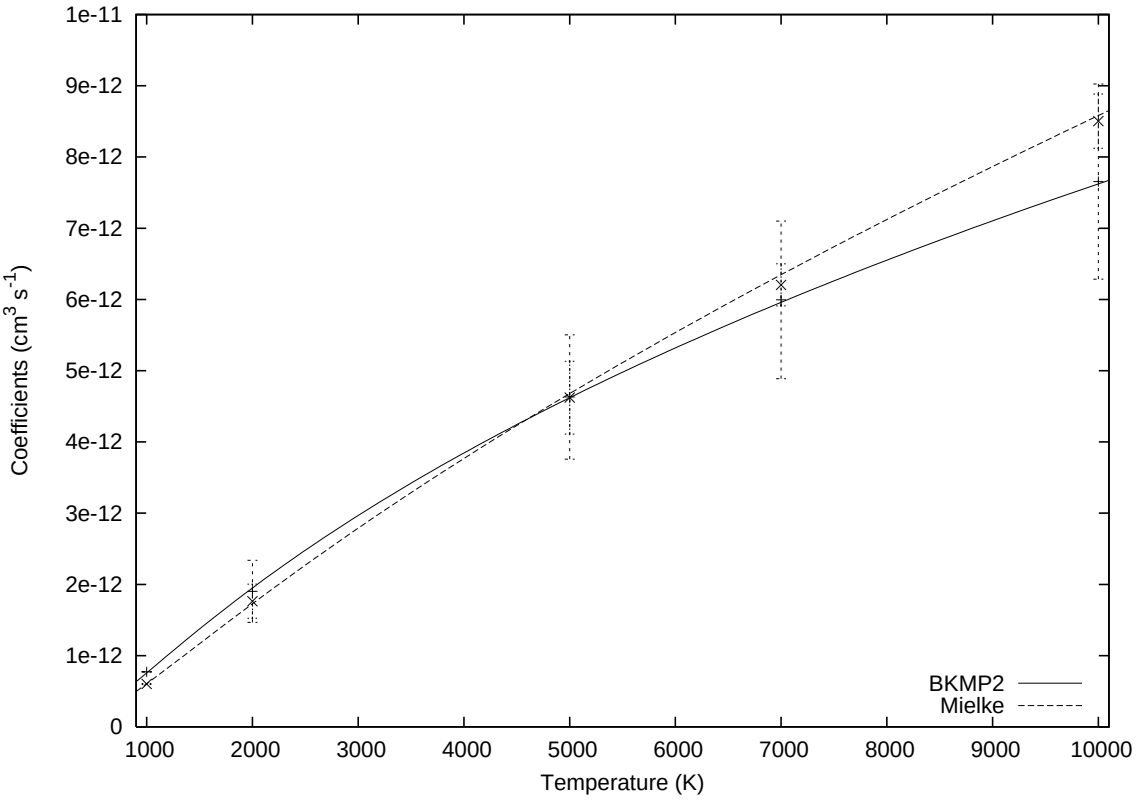

Figure 23 v=1,j=5 to v=0,j=5

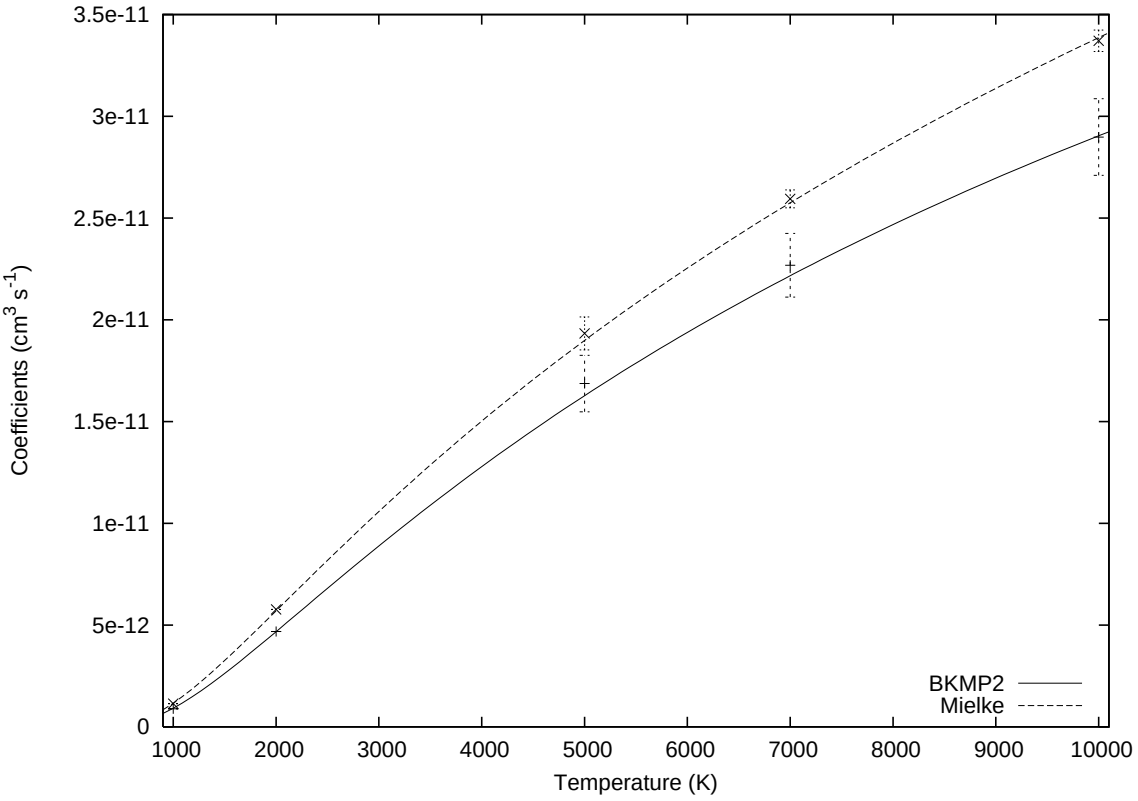

Figure 24 v=0,j=1 to v=0,j=0

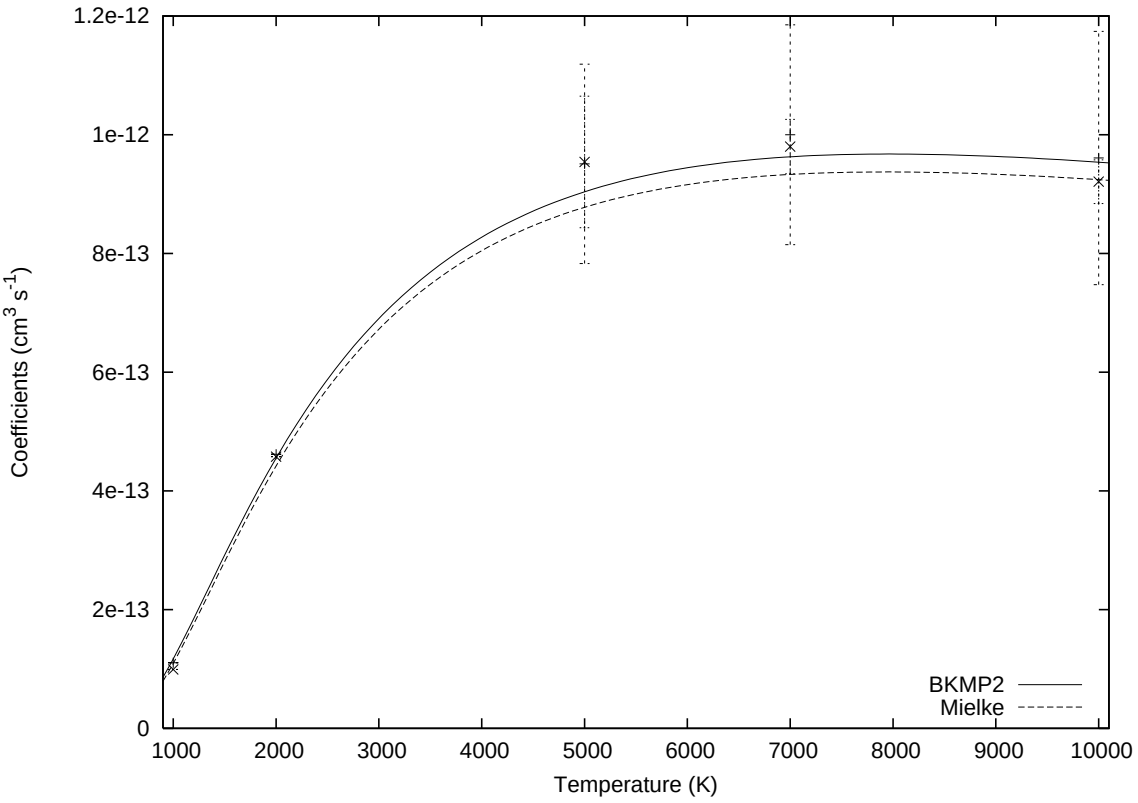

Table 6 RMS error of the randomly selected fits presented in figures 20 through 24 as a percentage

Transition	BKMP2	Mielke
$\mathrm{v} = 0, \mathrm{j} = 1$ to $\mathrm{v} = 0, \mathrm{j} = 0$	2.767	3.978
$\mathrm{v} = 0, \mathrm{j} = 4$ to $\mathrm{v} = 0, \mathrm{j} = 2$	2.325	1.358
$\mathrm{v} = 0, \mathrm{j} = 6$ to $\mathrm{v} = 0, \mathrm{j} = 2$	276.4	234.4
$\mathrm{v} = 1, \mathrm{j} = 0$ to $\mathrm{v} = 0, \mathrm{j} = 0$	0.138	1.219
$\mathrm{v} = 1, \mathrm{j} = 5$ to $\mathrm{v} = 0, \mathrm{j} = 5$	1.395	0.958

Table 7 Discrepency between coefficients calculated using $b_{max} = 5$a.u. and a varying maximum impact parameter for the 0,4 to 0,2 transition (cm^3s^{-1})

T(K)	$b_{max} = 5$ a.u.	$b_{max} = varying$	percent difference
1000	$3.589E-12$	$3.265E-12$	9.030
2000	$1.618E-11$	$1.512E-11$	6.588
3000	$2.815E-11$	$2.673E-11$	5.051
4000	$3.807E-11$	$3.654E-11$	4.016
5000	$4.629E-11$	$4.477E-11$	3.273
6000	$5.325E-11$	$5.180E-11$	2.716
7000	$5.926E-11$	$5.790E-11$	2.285
8000	$6.453E-11$	$6.328E-11$	1.945
9000	$6.923E-11$	$6.807E-11$	1.671
10000	$7.347E-11$	$7.240E-11$	1.448

Figure 25 BKMP2 and Mielke coefficients for v=3,j=8 to v=2,j=10

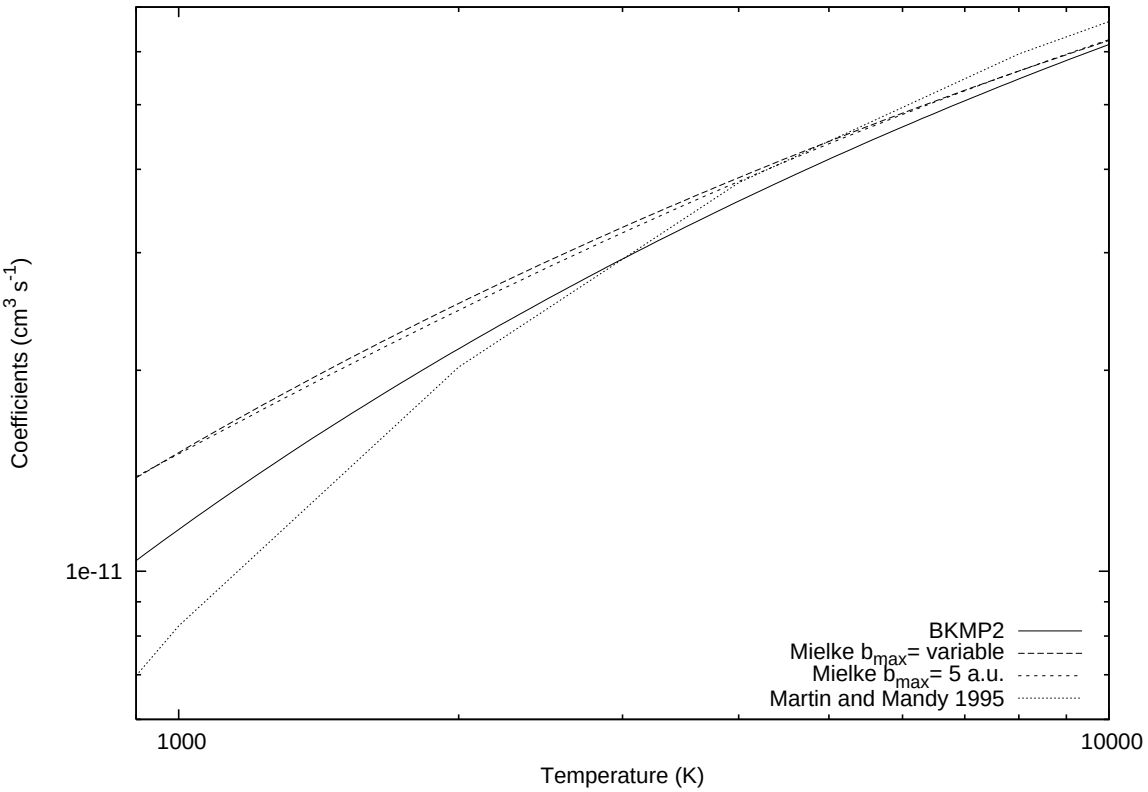

Figure 26 BKMP2 and Mielke coefficients for v=0,j=4 to v=0,j=2

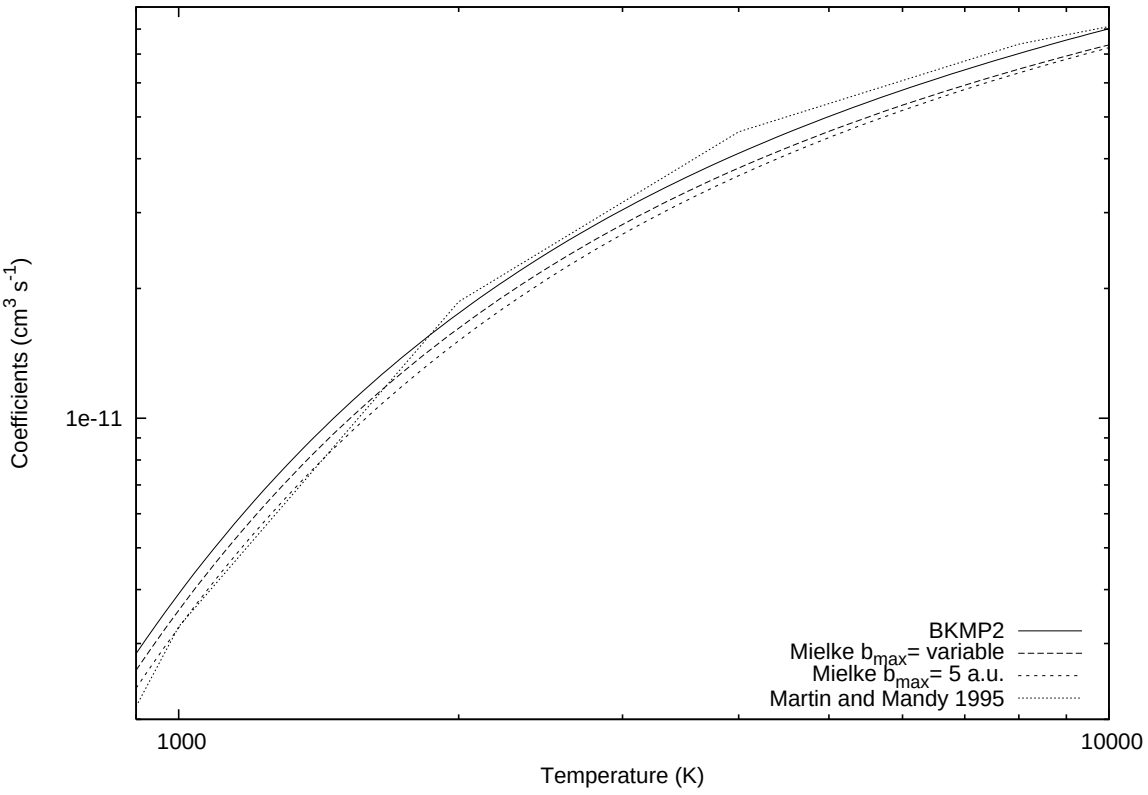

Figure 27 BKMP2 and Mielke coefficients for v=0,j=6 to v=0,j=0

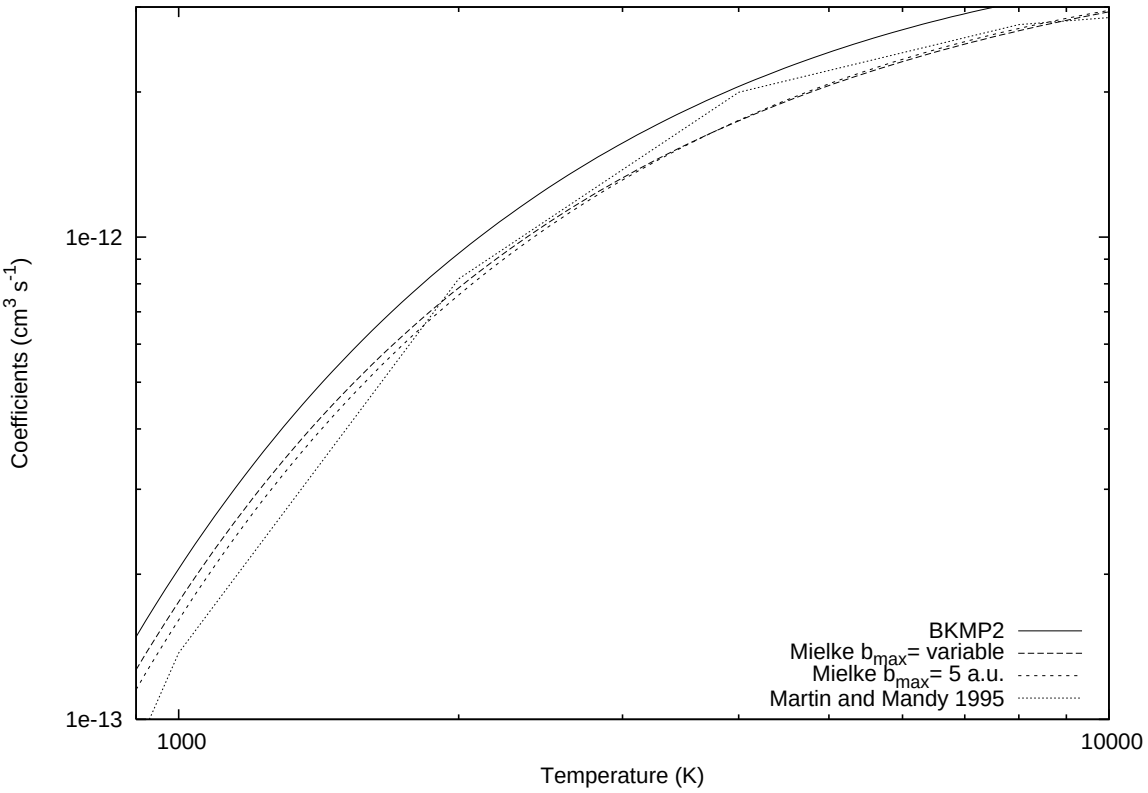

Figure 28 BKMP2 and Mielke coefficients for v=0,j=6 to v=0,j=2

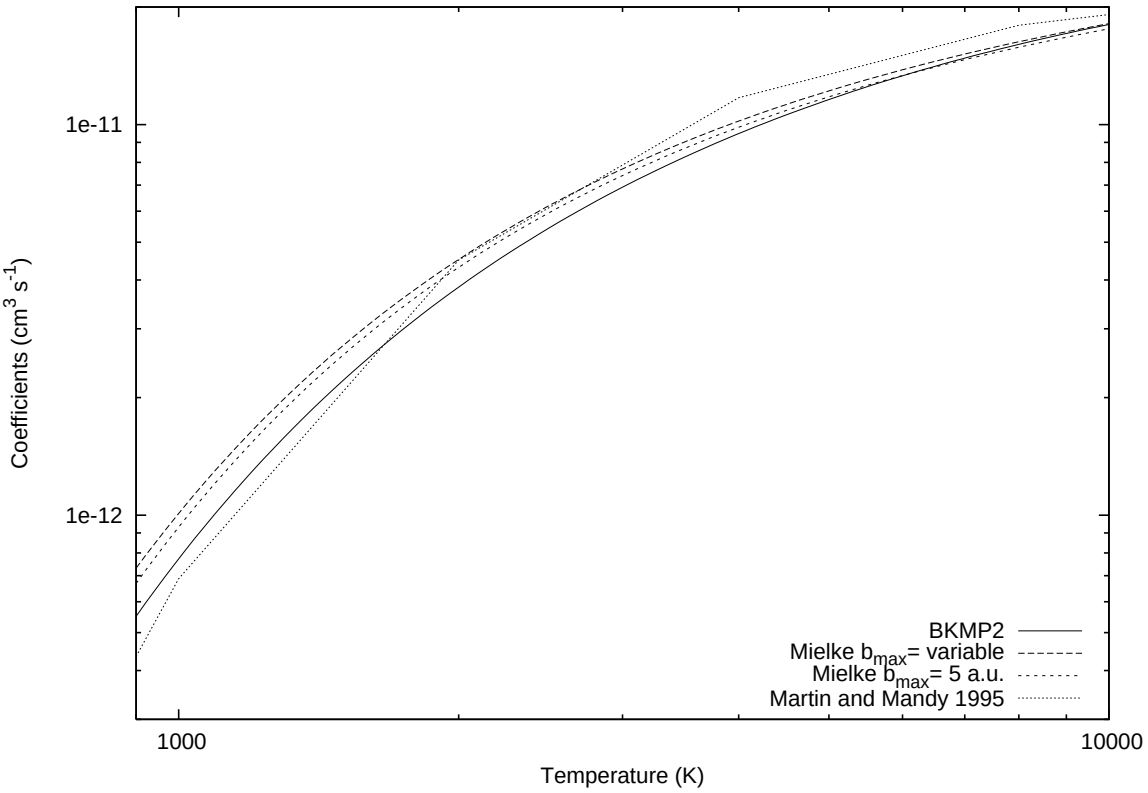

Figure 29 BKMP2 and Mielke coefficients for v=0,j=8 to v=0,j=6

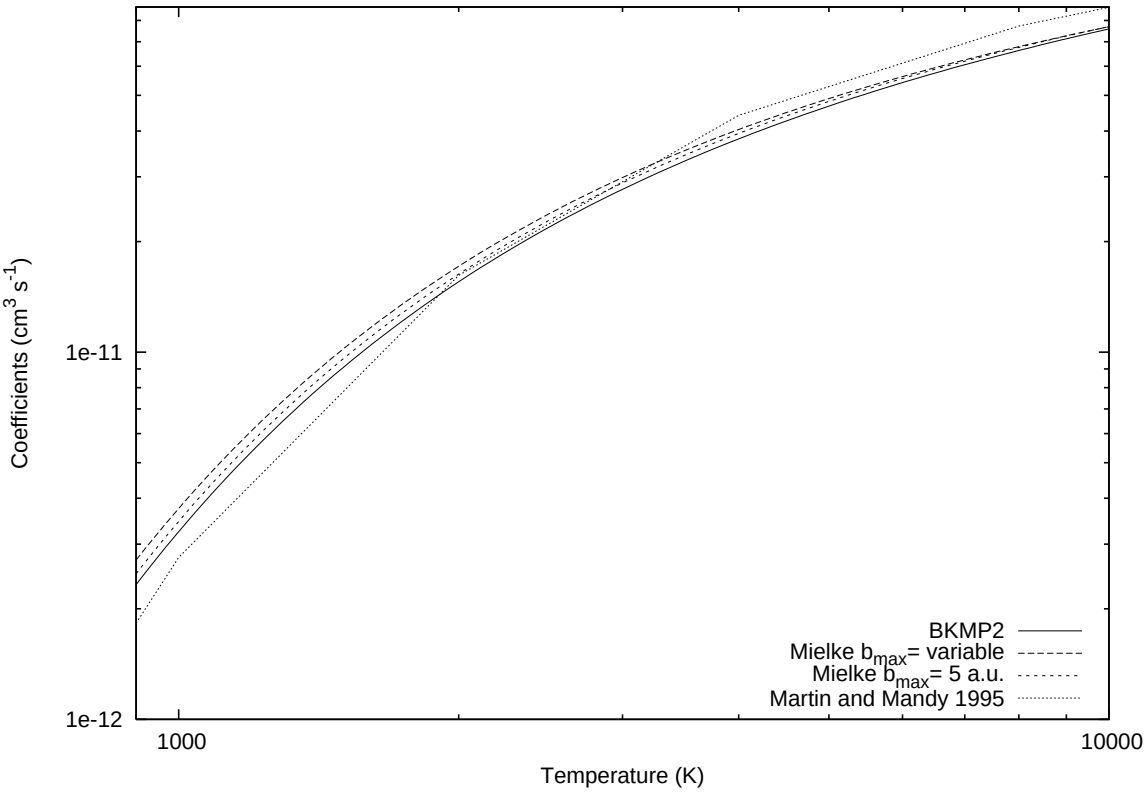

Figure 30 BKMP2 and Mielke coefficients for v=1,j=2 to v=1,j=0

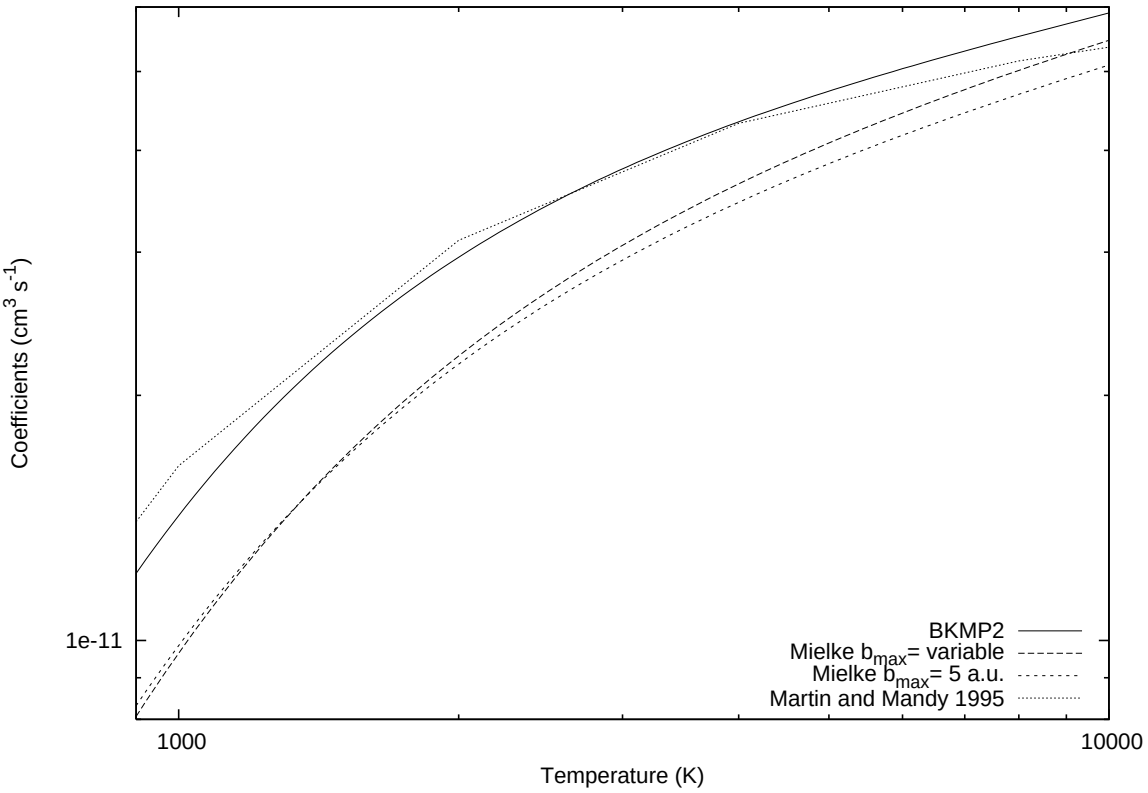

Figure 31 BKMP2 and Mielke coefficients for v=1,j=5 to v=0,j=5

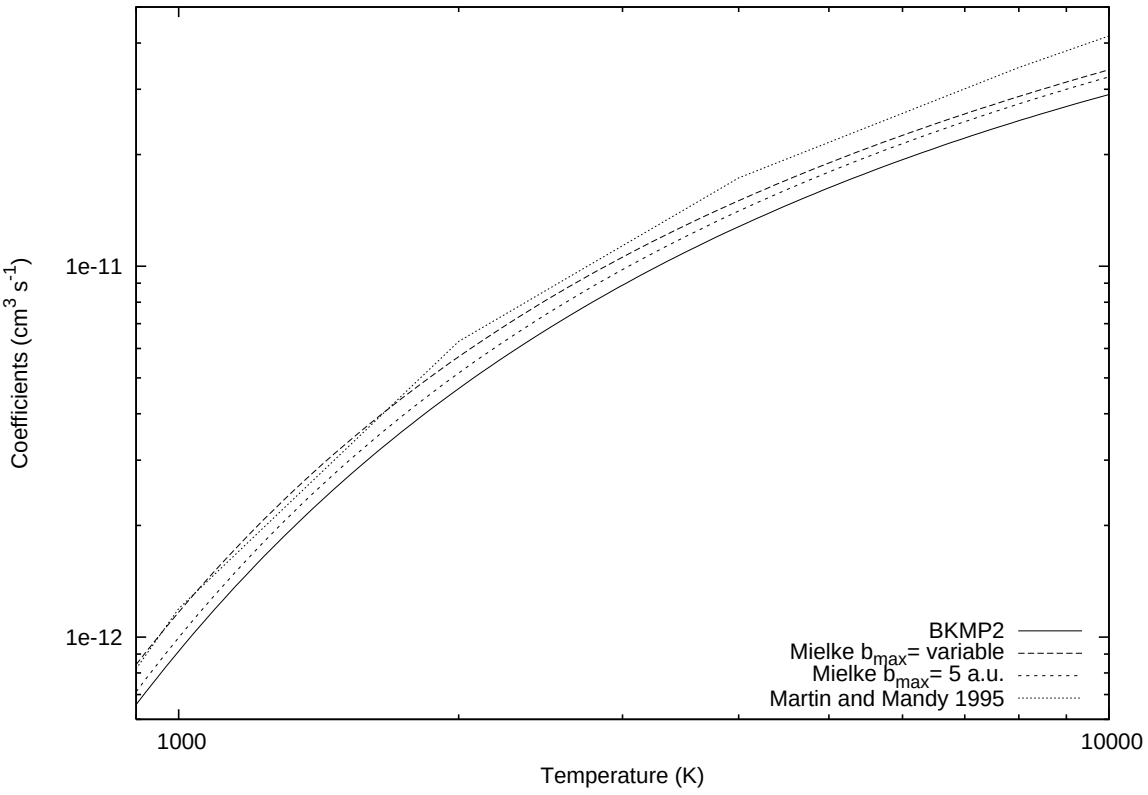

Figure 32 BKMP2 and Mielke coefficients for v=1,j=7 to v=1,j=1

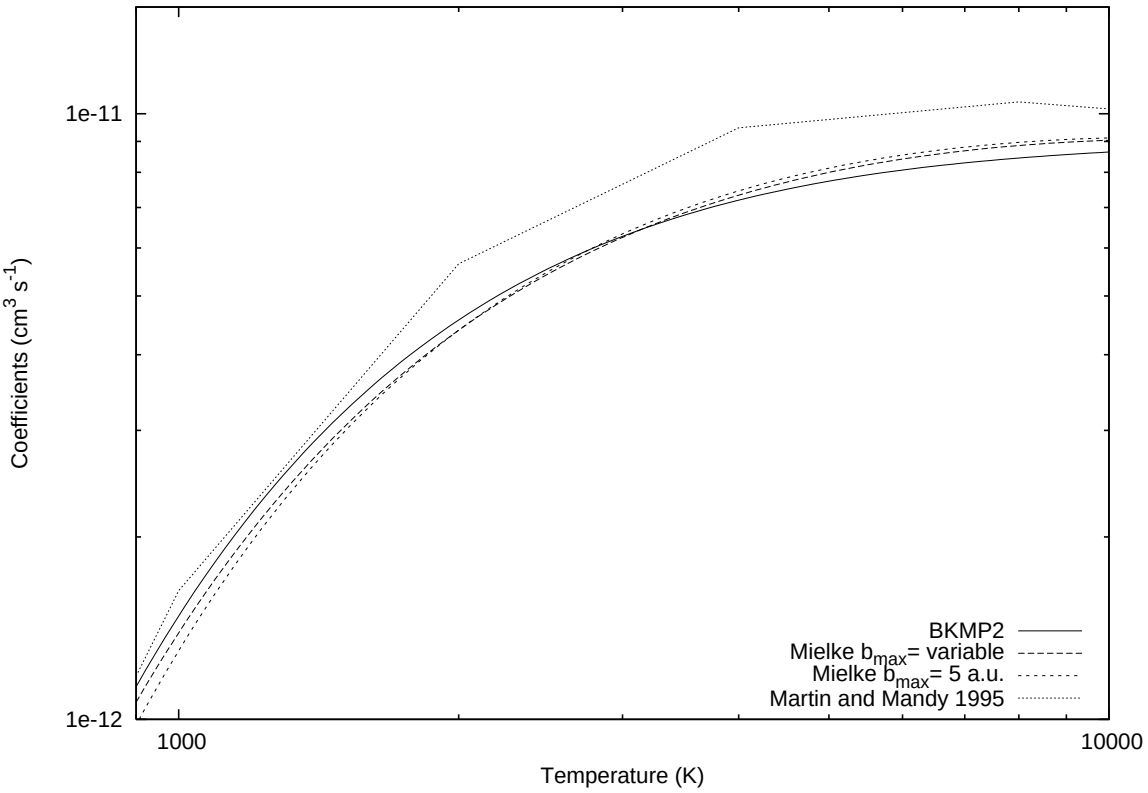

Figure 33 BKMP2 and Mielke coefficients for v=2,j=1 to v=0,j=1

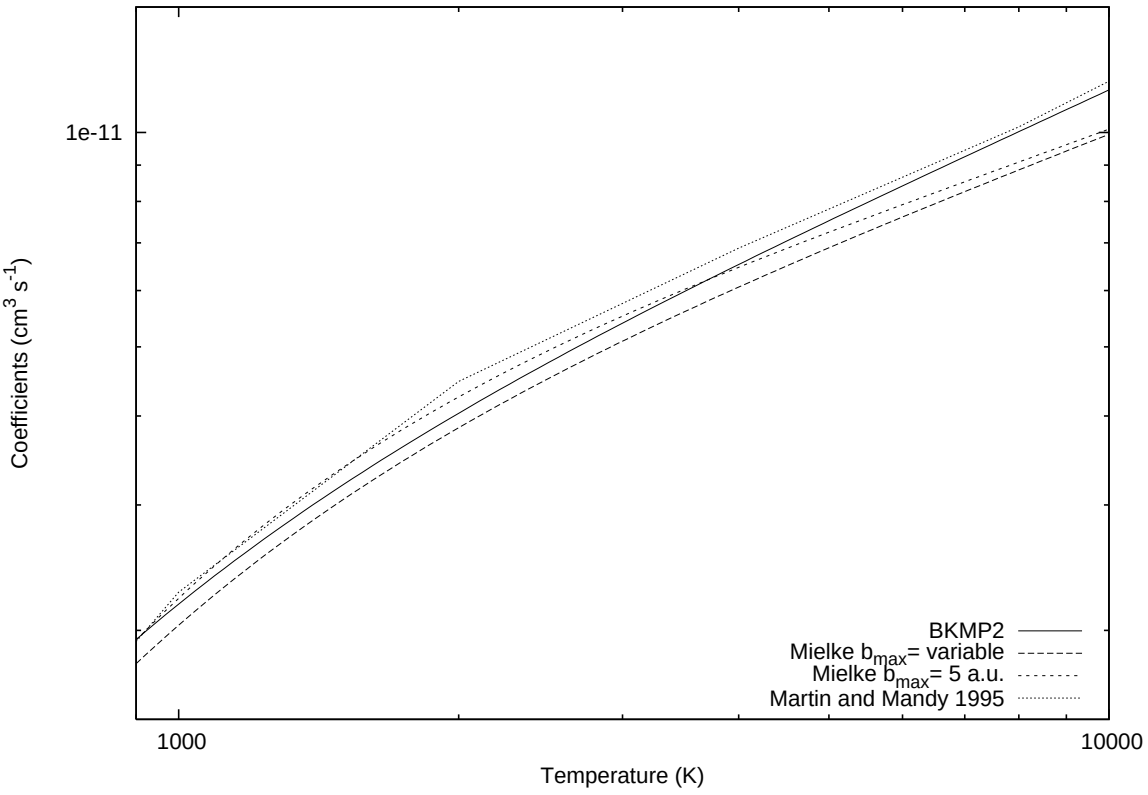

CHAPTER 5

EINSTEIN COEFFICIENTS

In this calculation, the Einstein coefficients for spontaneous emission used are the ones calculated by Turner et al. (1977). There are 3 coefficients to consider in this case; $A_{i,f}(i > f)$ is the spontaneous emission coefficient, $B_{i,f}(i > f)$ is the stimulated emission coefficient, and $B_{fi}(f < i)$ is the absorption coefficient. Again, this calculation considers only spontaneous emission because it assumes a low H_2 density, as well as a low photon flux, however, this discussion is necessary to understand detailed balance in the previous chapter and because the code used in this calculation has the stimulated emission and absorption capabilities already written into it if one wishes to redo the calculation to include these values. It is standard to only consider spontaneous emission in these types of calculations making the low density assumption necessary when comparing a calculation to previous results. The absorption and stimulated emission coefficients would become significant in systems such as a maser where the gas is subjected to a very intense photon field.

EINSTEIN COEFFICIENTS DERIVATION

The following discussion summarizes the calculation presented by Turner et al. (1977). Where it doesn't conflict with what was used so far in this document, their notation is preserved. The spontaneous emission coefficients from state i to f is simply the probablility of a spontaneous emission to occur. It is given by equation 5.1. J is the rotational quantum number, Ψ_i is the nuclear rotation-vibration wave function, Q(R) is the quadrupole moment, R is the distance between nuclei, f(JJ')is

the branching ratio, and $E_{i,f}$ are the energies of states i and f.

$$A_{i\to f} \propto (E_i - E_f)^5 | < \Psi_i | Q(R) | \Psi_f > |^2 f(JJ') \tag{5.1}$$

The branching ratio is the ratio of the number of transitions from i $\rightarrow$ f to the sum of the number of transitions from i $\rightarrow$ f$'$ and i $\rightarrow$ f$''$. In the case of H_2 the selection rules state that only three transitions can occur; J $\rightarrow$ J + 2, J $\rightarrow$ J $-$ 2, and J $\rightarrow$ J. The ratios are presented in equation 5.2 as presented in Turner et al. (1977).

$$\begin{aligned} f(JJ') &= \tfrac{3(J+1)(J+2)}{2(2J+1)(2J+3)} \quad J' = J+2 \\ &= \tfrac{J(J+1)}{(2J-1)(2J+3)} \quad J' = J \\ &= \tfrac{3J(J-1)}{2(2J-1)(2J+1)} \quad J' = J-2 \end{aligned} \tag{5.2}$$

They solved for the wave functions by solving the radial Schrodinger equation (equation 5.3). μ is the reduced mass, V(R) is the potential calculated by Kolos & Wolniewicz (1965, 1968). Q(R) is calculated by Kolos & Wolniewicz (1965) and Dalgarno et al. (1969).

$$\frac{d^2}{dR^2}\Psi_i(R) + 2\mu[E_i - V(R) - \frac{J(J+1)}{2\mu R^2}]\Psi_i(R) = 0 \tag{5.3}$$

ABSORPTION AND STIMULATED EMISSION

The coefficients for spontaneous emission, absorption, and stimulated emission must balance each other in thermal equilibrium. That is, for every molecular transition into an energy level there must be a transition out of the energy level so that the population of each energy level remains the same. This is represented by equa-

tion 5.4. $u_{E_i \to E_f}$ is the energy density for photons of energy $E_i - E_f$. Note that the energy density would be the place to include the contribution from CMB photons. This can be done by modifying the code in the appendix CD. For the purposes of the calculation presented in this paper, the CMB is coupled to the gas temperature particularly at high redshifts but must be included separately at lower redshifts.

$$n_i(A_{i\to f} + B_{i\to f} u_{E_i \to E_f}) = n_f B_{f\to i} u_{E_i \to E_f} \tag{5.4}$$

The derivation of the B coefficients can be found in any undergraduate modern physics textbook so it won't be described here. However, the end result is that they are related to the A coefficients by equation 5.5. These can easily be included in the calculation presented here by uncommenting the subroutine Bvalues in the program cooling_curve_BDF.f95 (Appendix A demonstrates how to do this).

$$\begin{aligned} B_{f\to i} &= \frac{g_i}{g_f} \frac{c^2}{2h\nu^3} A_{i\to f} \\ B_{i\to f} &= \frac{c^2}{2h\nu^3} A_{i\to f} \end{aligned} \tag{5.5}$$

CHAPTER 6

COOLING FITS

The final step was to fit the cooling rates to a function of temperature and n_H. This was done by first fitting the low and high density limits then determining a cooling function using those limits to fit the intermediate densities. Finally, errors were calculated for the fits and compared to previous work. Fits in previous work have been known to be very complicated. For example, Martin et al. (1996) used a fit that was a function of 21 parameters. Tiné et al. (1998) used 3 low density limit and 3 high density limit equations each representing a temperature range as well as 2 temperature dependent parameters to fit their curves.

LOW AND HIGH DENSITY LIMITS

In order to fit the low and high density limits a very generalized equation was selected. 2 functions L and H were defined which have the forms of equations 6.1. Here the high density limit is defined as $n_H = 1E8 cm^{-3}$ which is consistent with Martin et al. (1996). The high density limit is defined as a value that the cooling approaches where increasing the hydrogen density doesn't lead to an increase in cooling. The low density limit was found by plotting the cooling for a range of densities and determining the limit. The low density limit is acheived when $\triangle\Lambda/N_{H_2} \propto \triangle N_H$. In this calculation the low density limit is $n_H = .01 cm^{-3}$ but realistically could be set as high as $10 cm^{-3}$. Figure 34 demonstrates this. Notice that at low densities the cooling changes proportionally to hydrogen density and at high density the curve flattens out. Also defined were two intermediate limits at $n_H = 1E4 cm^{-3}$, an intermediate high density limit H_1, and $n_H = 1E5 cm^{-3}$, an intermediate low density limit L_2. The purpose for these limits will become clear

Figure 34 Cooling vs. Density for the Mielke Potential T $= 3000$K

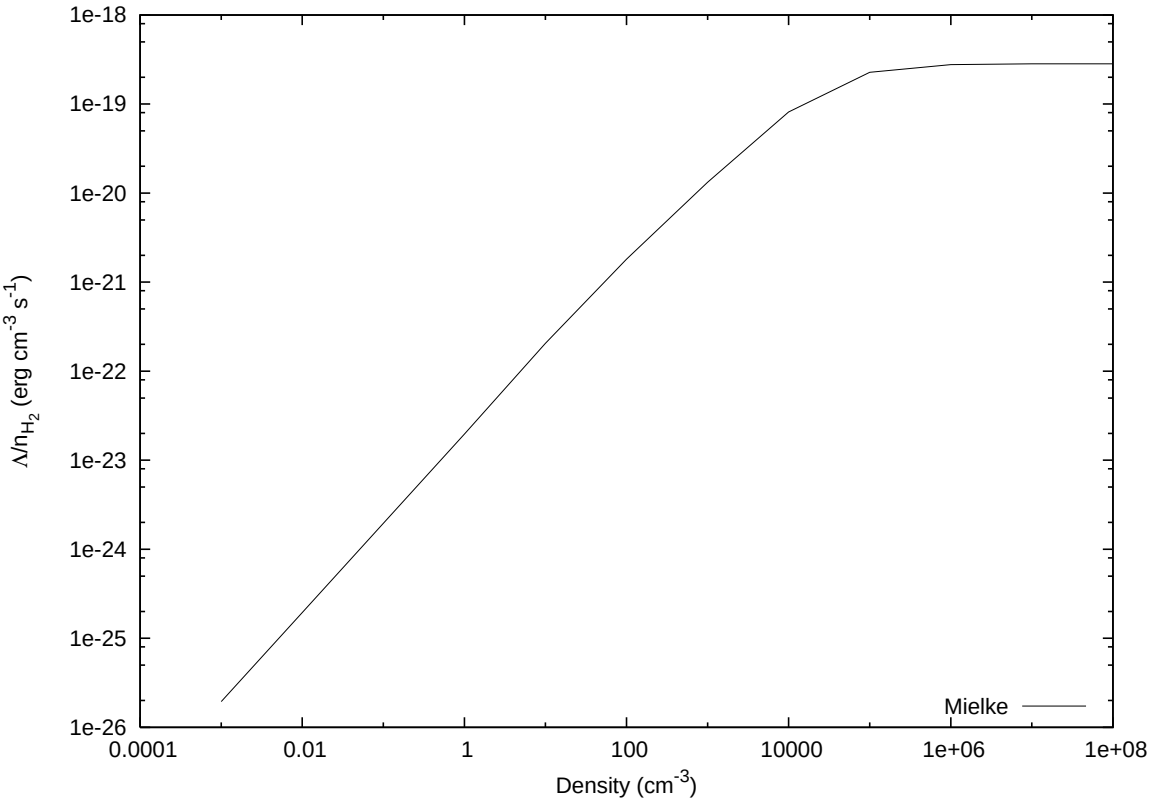

later.

$$\begin{aligned}
\frac{\Lambda_{n_H=.01cm^{-3}}}{n_{H_2}} &= (.01\text{cm}^{-3})\text{L} \\
\frac{\Lambda_{n_H=1E4cm^{-3}}}{n_{H_2}} &= \text{H}_1 \\
\frac{\Lambda_{n_H=1E5cm^{-3}}}{n_{H_2}} &= (1\text{E5cm}^{-3})\text{L}_2 \\
\frac{\Lambda_{n_H=1E8cm^{-3}}}{n_{H_2}} &= \text{H}
\end{aligned} \tag{6.1}$$

Next a functional form to fit the limits was selected based on their logarithmic behavior. This was done, after considerable trial and error, using equation 6.2 for the 24 parameters $\text{a}_i, \text{b}_i, \text{c}_i, \text{d}_i, \text{e}_i, \text{f}_i$ where i $= 1$ to 4 . The fitting was done using GNUPLOT (Williams & Kelley 2004) which uses the Levenberg-Marquardt method for non linear least squares fitting. The calculated parameters are presented in table 9. Figure 35 is a plot of equation 6.2. The plots show that the low and high density limits of each potential are almost identical. Table 10 shows the normalized RMS error of the fits. From this table it is clear that the fitting equations are very good approximation of the calculated low and high density limit data values.

$$\begin{aligned}
log_{10}H &= \text{a}_1 log_{10}T + b_1(log_{10}T)^{c_1} + d_1(log_{10}T)^{e_1} + T/f_1 \\
log_{10}[(.01cm^{-3})L] &= \text{a}_2 log_{10}T + b_2(log_{10}T)^{c_2} + d_2(log_{10}T)^{e_2} + T/f_2 + log_{10}.01 \\
log_{10}H_1 &= \text{a}_3 log_{10}T + b_3(log_{10}T)^{c_3} + d_3(log_{10}T)^{e_3} + T/f_3 \\
log_{10}[(1E5cm^{-3})L_2] &= \text{a}_4 log_{10}T + b_4(log_{10}T)^{c_4} + d_4(log_{10}T)^{e_4} + T/f_4 + log_{10}\text{1E5}
\end{aligned} \tag{6.2}$$

Table 8 Parameters for the high and low density limits for the BKMP2 potential

Parameter	1	2	3	4
a	-1.964	-0.087	-0.964	-2.414
b	-42.364	-21.979	-30.251	-32.382
c	-1.137	-0.523	-0.608	-1.110
d	-43.255	-21.979	-31.665	-32.382
e	-2.593	-0.556	-2.376	-1.190
f	-1.073	0.472	-0.364	0.439

Table 9 Parameters for the high and low density limits for the Mielke potential

Parameter	1	2	3	4
a	-2.248	-0.0822	-1.697	-3.008
b	-38.483	-21.978	-34.678	-58.027
c	-1.580	-0.528	-1.314	-1.359
d	-38.483	-21.978	-34.678	-58.441
e	-1.585	-0.551	-1.347	-2.529
f	0.0778	0.472	0.432	-1.627

Figure 35 Low and High Density fits

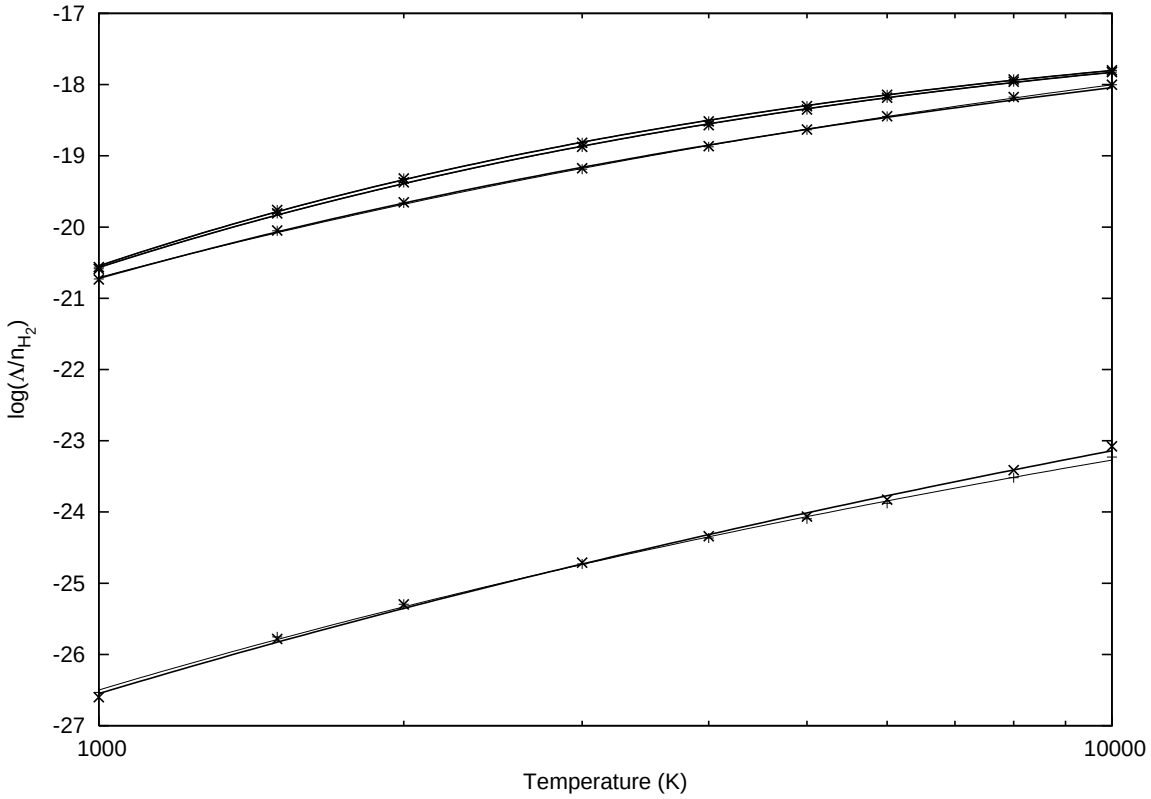

Table 10 Normalized RMS Error of the Limit Fits T ≥ 800K Expressed as a percentage

potential	L	H	L_2	H_1
Mielke	4.38	.859	.0438	3.29
BKMP2	3.03	.769	.0697	2.377

FITTING FUNCTION

The final step was to select a function that would accurately predict the cooling curve between the limits while at the same time approaching the limits at their respective densities. Equation 6.3 was an inital attempt. It accurately predicted the limits however it failed to predict the intermediate ranges particularly at $n_H = 1E4 cm^{-3}$ as seen in figure 36 for the BKMP2 and Mielke potentials. Table 11 shows the error using this fit at $n_H = 1E4 cm^{-3}$.

$$\frac{\Lambda}{n_{H_2}} = \frac{n_H L}{1 + \frac{n_H L}{H}} \tag{6.3}$$

After plotting the cooling rates for densities of $.001 cm^{-3}$ to $1E8 cm^{-3}$ it became clear that the function needed to be fit to density. This can be done using the intermediate limits to define two separate critical densities, equation 6.4.

$$n_{cr,i} = \frac{H_i}{L_i} \tag{6.4}$$

This has the effect of separating the cooling curve into two separate components such that $H = H_1 + H_2$ and $L = L_1 + L_2$. H_1 is defined as the cooling at $n_H = 10^4 cm^{-3}$ and $L_2 10^5$ is the cooling at $n_H = 10^5 cm^{-3}$. L_1 and H_2 can then be calculated using equation 6.5.

$$\begin{aligned} H_2 &= H - H_1 \\ L_1 &= L - L_2 \end{aligned} \tag{6.5}$$

Figure 36 Fit from equation 6.3 for $n_H = 1E4$ cm^{-3}

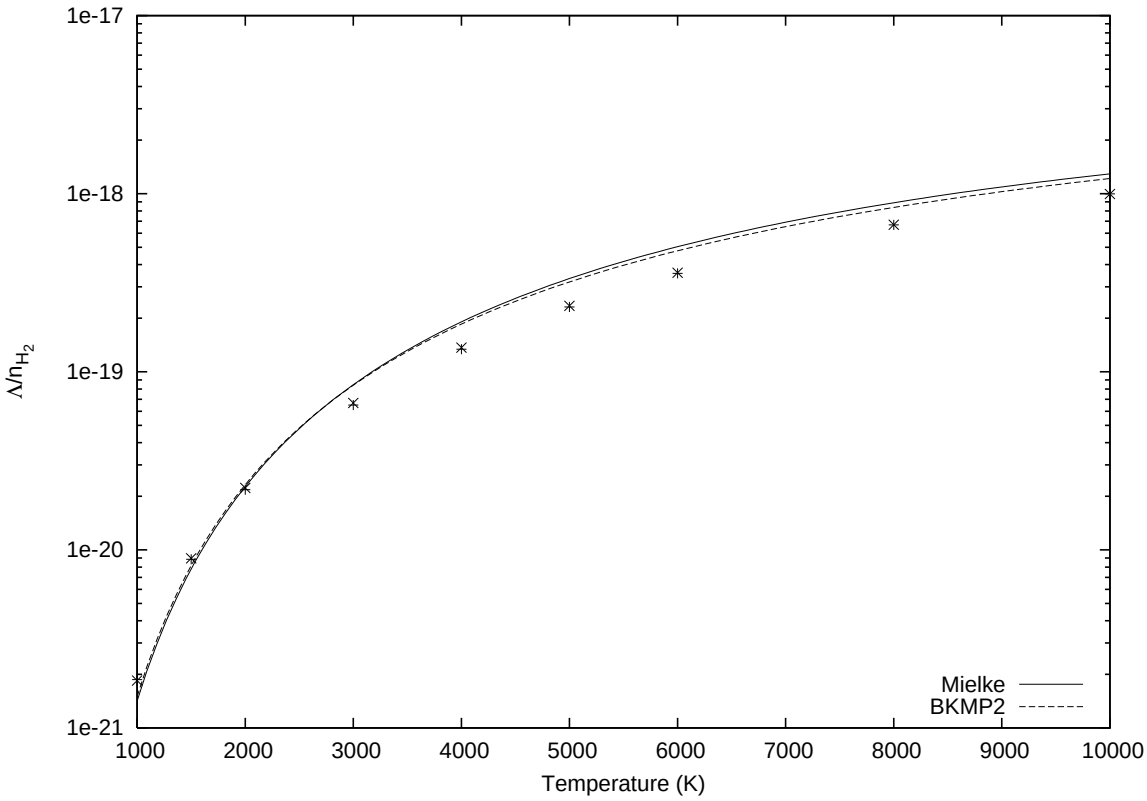

Table 11 Relative error of the fit from equation 6.3 for the BKMP2 potential at $n_H = 1E4 cm^{-3}$

T(K)	Data value (ergs^{-1}cm^{-3})	Fit Value (ergs^{-1}cm^{-3})	Relative Error as a percentage
1000	$6.680E-22$	$1.981E-21$	196.473
1500	$4.489E-21$	$1.070E-20$	138.469
2000	$1.652E-20$	$3.067E-20$	85.691
3000	$7.971E-20$	$1.135E-19$	42.440
4000	$2.013E-19$	$2.557E-19$	26.983
5000	$3.774E-19$	$4.492E-19$	19.038
6000	$5.974E-19$	$6.817E-19$	14.109
8000	$1.104E-18$	$1.215E-18$	10.054
10000	$1.591E-18$	$1.775E-18$	11.555

The two individual cooling curves can now be summed to get the total cooling as in equation 6.6. Figures 37 and 38 show the fit when applied to the data. Tables 12 and 13 show the relative errors for a range of temperatures for densities $n_H = 1E4$ and $1E8 cm^{-3}$. The high rms error for the mid densities come from the high temperatures ($T7000K$) where the calculation should be taken with caution. At these high temperatures dissociation would be important making this fit less reliable anyway. The conclusions section offers a possible fix to this.

$$\frac{\Lambda}{n_{H_2}} = \frac{L_1 n_H}{1 + \frac{L_1 n_H}{H_1}} + \frac{L_2 n_H}{1 + \frac{L_2 n_H}{H_2}} \tag{6.6}$$

RESULTS

The resulting cooling curves are plotted in figures 39 through 42 for various densities. Also plotted are the results of Hollenbach & Mckee (1979), Lepp & Shull (1983), and Martin et al. (1996).

COSMIC COOLING CURVE

Referring back to the application of this calculation to the early universe, it is possible to calculate the cooling rate as a function of redshift. Since most of the baryons in the early universe were atomic hydrogen, one can assume that the number density of hydrogen in the early universe is equal to .9 times the baryonic density. The baryonic number density as a function of redshift can be estimated using Friedmann's equations. The result is equation 6.8 where $n_{\gamma,CMB}$ is the baryon to photon density (equation 6.7), n_B is the baryon density, ρ_c is the critical density,

Figure 37 BKMP2 and Mielke cooling $n_H = 1E4 cm^{-3}$

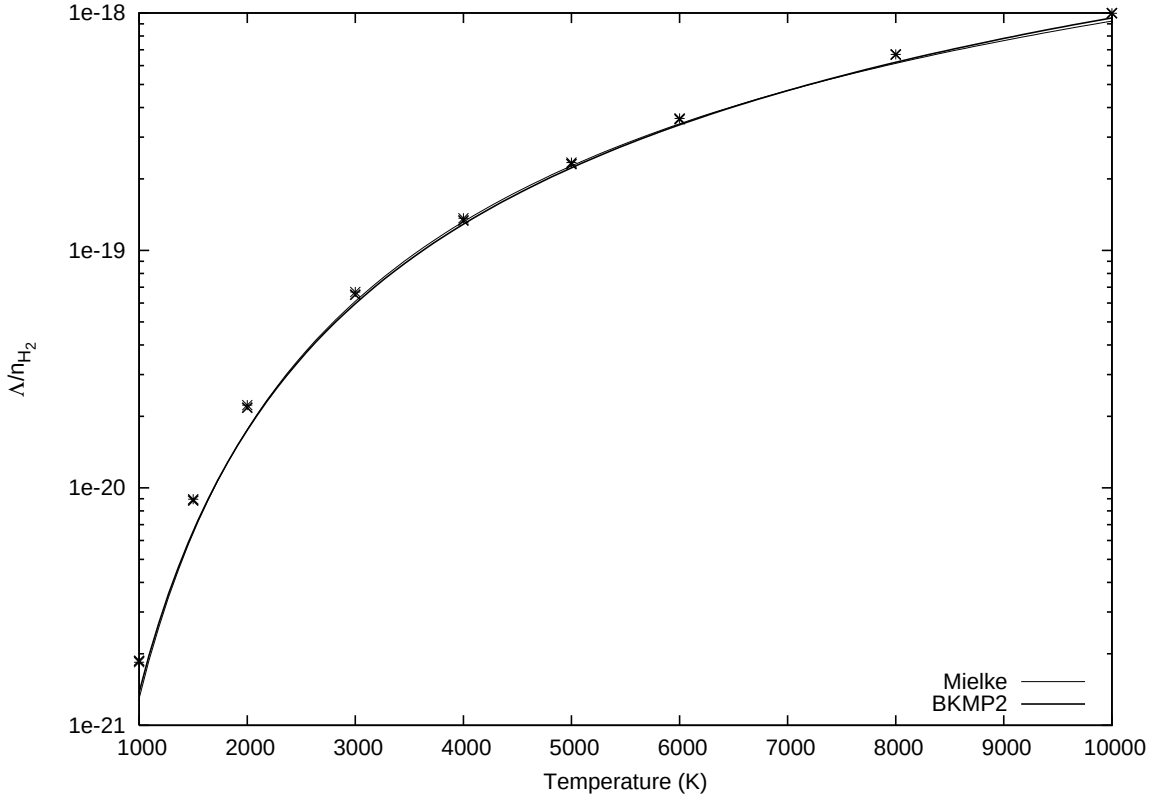

and m_p is the mass of a proton. Also present are the gravitational constant, G = 6.7×10^{-8} erg cm g^{-2}, the Hubble constant, $H_0 = 69.7$ km s^{-1} Mpc^{-1}, and w = $-.94$. H_0 and w were calculated by Suyu et al. (2010).

$$n_{\gamma,CMB} \sim \frac{aT^4}{2.8kT} \tag{6.7}$$

$$n_B(z) \approx \frac{n_{\gamma,CMB}\rho_c}{m_p} = \frac{n_{\gamma,CMB}3H^2}{m_p 8\pi G} = \frac{3n_{\gamma,CMB}}{8\pi m_p G}[H_0(1+z)^{3(1+w)/2}]^2 \tag{6.8}$$

The temperature of matter in the universe can be set to approximately the radiation temperature until z~ 100 when Compton heating from the CMB can no longer

Figure 38 BKMP2 and Mielke cooling $n_H = 1E8 cm^{-3}$

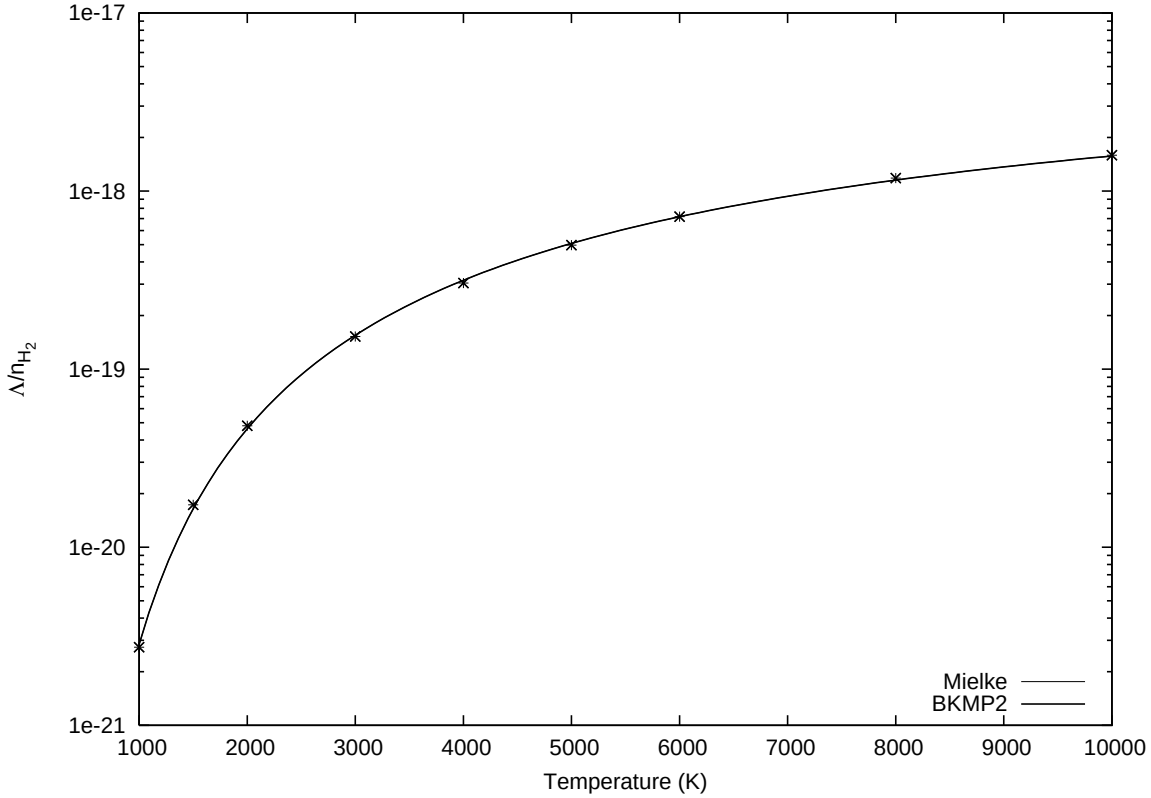

overcome the adiabatic cooling of the universe due to large heating timescale. However, for calculations requiring more precision, adiabatic cooling of baryons should be considered around $z \sim 500$. Here, however, since the matter temperature is set to the radiation temperature, it goes as $T \propto (1 + z)$. Figure 43 shows the behavior of the cooling over redshift with the assumption that the matter temperature is coupled to the CMB via compton heating. Studies have been conducted since Gamow (1949) to determine the matter temperature in terms of the radiation temperature more precisely for applications to lower redshifts. A difinitive determination of the matter temperature evolution of the early universe will be vital for an accurate cosmological cooling calculation.

Table 12 Relative error of the fit from equation 6.6 for the BKMP2 and Mielke potentials at $n_H = 1E4 cm^{-3}$

T(K)	Mielke	BKMP2
1000	5.325	4.956
1500	12.848	17.574
2000	1.658	6.146
3000	10.059	7.722
4000	13.393	12.996
5000	14.086	15.331
6000	13.554	16.196
8000	9.034	14.077
10000	.0241	7.423

Table 13 Relative error of the fit from equation 6.6 for the BKMP2 and Mielke potentials at $n_H = 1E8 cm^{-3}$

T(K)	Mielke	BKMP2
1000	2.335	2.525
1500	5.205	5.419
2000	1.234	1.466
3000	4.585	4.563
4000	3.387	3.505
5000	0.454	0.273
6000	3.278	3.098
8000	2.902	2.885
10000	2.557	2.286

Table 14 RMS of the fit from equation 6.6 for the BKMP2 and Mielke potentials

$log_{10}(n_H \text{ cm}^{-3})$	Mielke	BKMP2
-3	4.424	3.127
-2	4.358	3.117
0	4.007	1.814
1	23.878	7.922
2	28.106	12.464
3	20.171	9.159
4	2.982	4.757
5	4.790	5.042
6	1.629	1.578
7	1.335	1.264
8	1.320	1.248
9	1.318	1.245

Figure 39 BKMP2 and Mielke with previous calculations $n_H = 1 cm^{-3}$

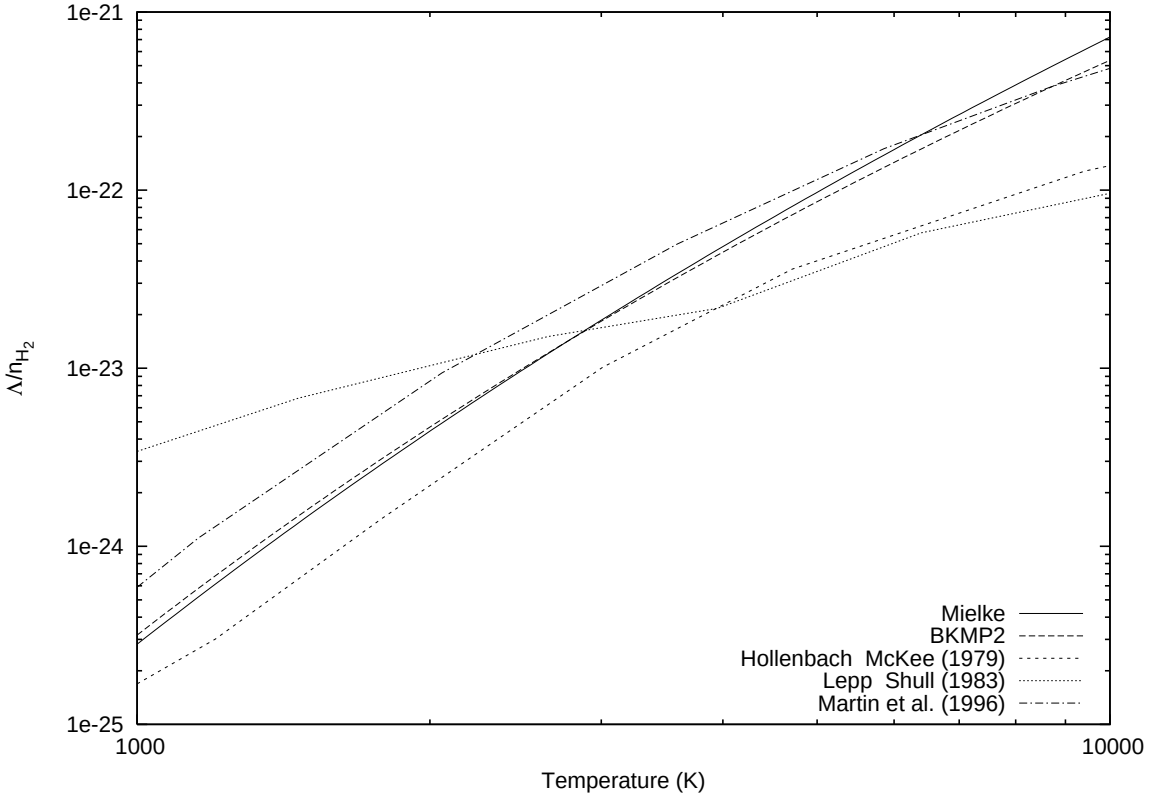

Figure 40 BKMP2 and Mielke with previous calculations $n_H = 100 cm^{-3}$

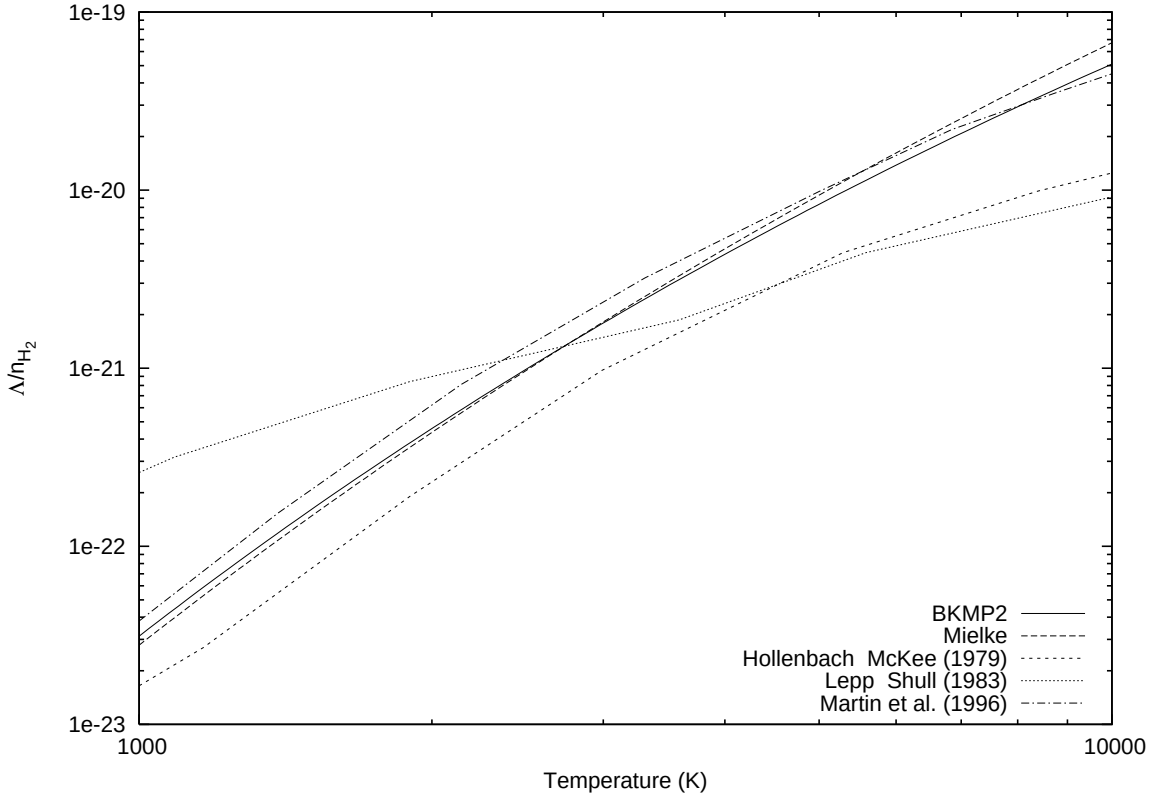

Figure 41 BKMP2 and Mielke with previous calculations $n_H = 1E4 cm^{-3}$

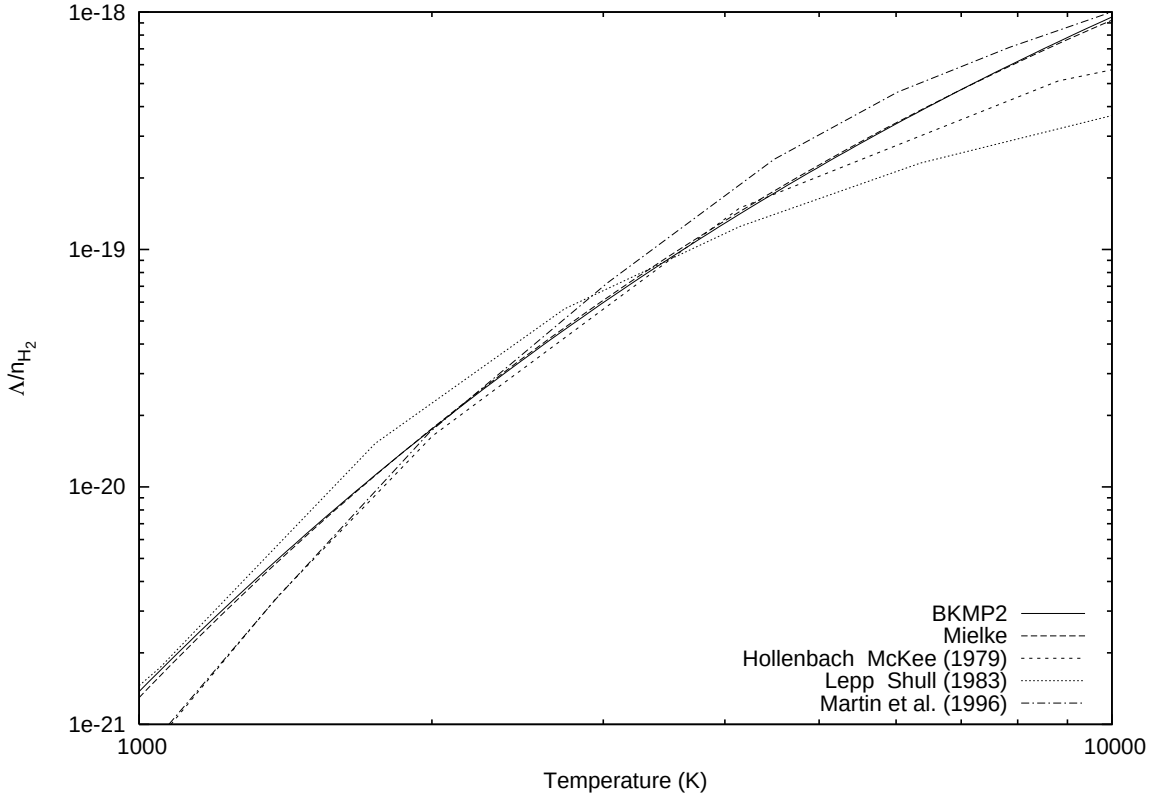

Figure 42 BKMP2 and Mielke with previous calculations $n_H = 1E8 cm^{-3}$

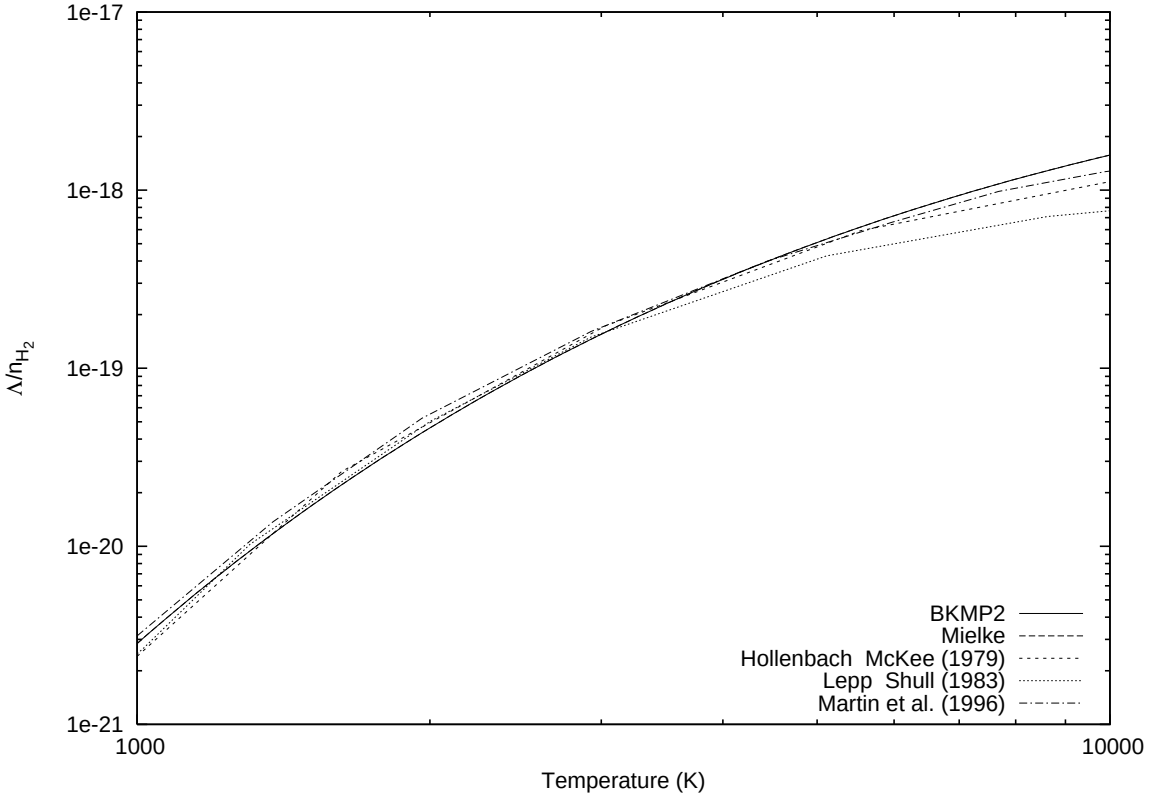

Figure 43 Evolution of the BKMP2 and Mielke potentials over cosmic timescale

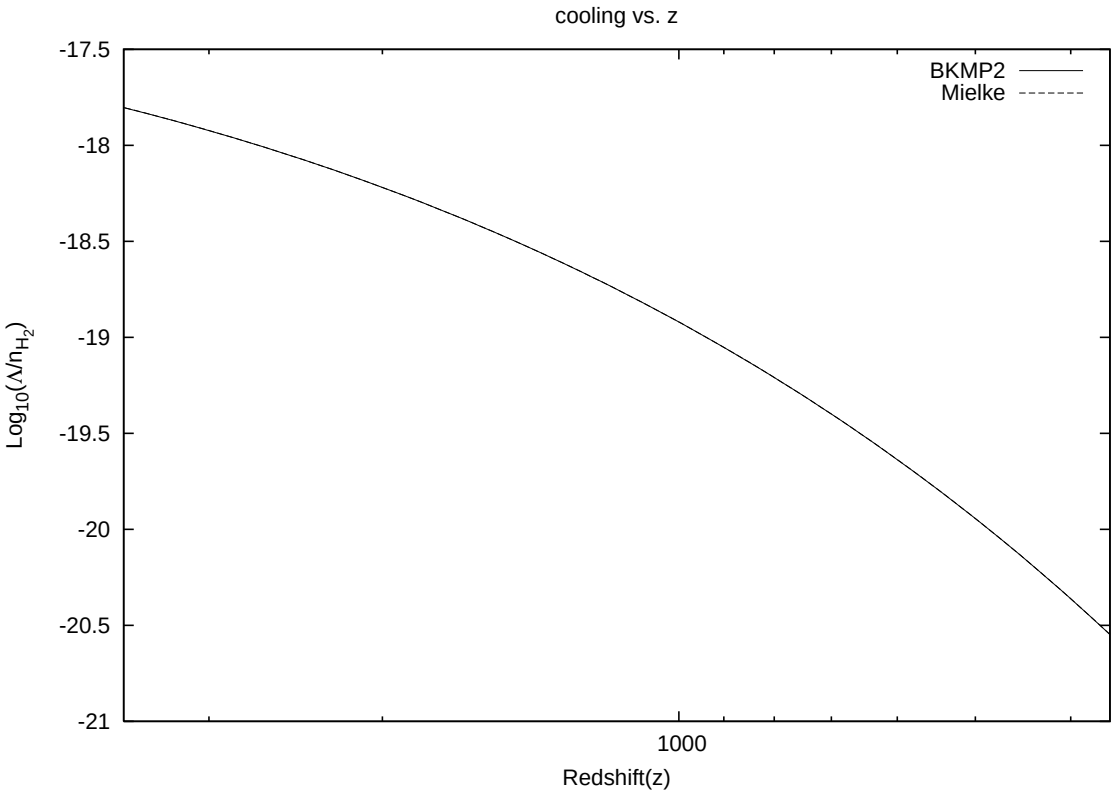

CHAPTER 7

CONCLUSIONS

Overall, the calculations presented here are consistent with previous calculations particularly at intermediate temperatures and higher densities. At lower temperatures ($T \leq 500$K) the calculation needs to include a quantum mechanical method as the quasi-classical method is no longer sufficient. The discrepency of the cooling curves calculated here with respect to the calculations by Hollenbach & Mckee (1979) and Lepp & Shull (1983) could possibly be explained by the use of different potential energy surfaces and improved computational methods and capabilities. Also it should be noted that H_2 dissociation (Appendix B) was not considered in this calculation. However, for example, in the case of the BKMP potential, Martin et al. (1996) did include dissociation.

Also, one will notice that most of the plots presented in this document were confined to the 1000 to 10000K range. This was done because the collision cross sections were only calculated for temperatures up to 30000K. So, in order to avoid contributions from temperatures greater than 30000K, the maxwellian velocity distribution was only integrated up to 10000K. All the fits were performed for temperatures in the range of 1000 to 10000K. Also, since this is a quasi-classical trajectory calculation that does not include unbound energy levels or dissociation, the range of 1000 to 10000K is the applicable range for this calculation.

Another option for improving the fit is to perform the fit in stages. Planned improvements to this fit will involve fitting some of the major transitions individually. For example, cooling from transitions to the $0,0$ energy level can be picked out from the total cooling, fit by itself, and added to the cooling from the rest of the transitions. Since $0,0$ will have a significant number of transitions, fitting this

energy level alone should significantly improve the fit. The results of this fitting technique will be the subject of a future publication (Kelley & Lepp 2012).

As far as application to the early universe is concerned, this calculation is a good step. However, a more complete study would include helium, deuterium, and lithium. Also it would include all the molecules they form with each other and their ions, and the collisions between them.

Luckily the universe has provided almost unlimited astrophysical environments to use as laboratories in the form of nebulae. However, no nebula is pure; so again, H_2 collisions with other elements and molecules need to be understood better as well. Also, with improved instrumentation, our ability to probe these processes in the early universe will also improve. For example, missions such as WMAP and follow up missions will provide information about the last scattering surface. Someday perhaps neutrino detectors will achieve the sensitivity to peer past the last scattering surface. Unfortunately modern neutrino detectors have only enough sensitivity to observe the milkyway and the very local universe. Any number of instruments are possible to study the universe at this early, and crucial, time in our universe's evolution.

APPENDIX A

CODE DOCUMENTATION

This section outlines the Fortran 95 code used to do the calculations presented in this document. This code was designed by the author specifically for this calculation and is not recomended for use other than $H + H_2$ cooling. It comes with no guarantees or warranty. It consists of 16 files (some of which are optional) which must be executed and/or modified only as described in this appendix. As an additional warning, these programs are by no means elegant but they are functional. There are certainly more efficient means to conduct these calculations but the code presented here was the quickest and most intuitive to the author to write. These programs assume access to the open source programs Maxima and Octave. All of these programs are available on the appendix CD. The calculations were done using gcc fortran on a Fedora 10 laptop. gfortran on Mac OSX 10.6.8 gave erroneous results or at times failed to compile all together. The reason for this is unclear. An Ubuntu computer using f95 was also used successfully for the cooling calculation, but failed when used for the spectrum predictions. Other compilers have not been tested. Units used in these programs are cm, s, eV, K, and eV/c^2 for mass.

RATE COEFFICIENTS

mcr2c.f95 (Molecular Collision Rate Coefficient Calculator) takes trajectories provided by Dr. Stephen Lepp, calculates the cross sections, fits them to a cubic spline and then integrates using Simpson's rule as described in chapter 4. It is composed of two subroutines; "cross_sections" and "fitting." It does not work with other data files. The original trajectory data files were in 31 smaller files for initial rotational states 0 to 31, which were compressed to 1 large file named

"cross_section.dat" to add more autonomy to this program. A cross_section.dat file must be placed in the main directory. The first part of the code is fairly straight forward. It calculates collision cross sections for temperatures T $= 500, 1000, 2000,$ $5000, 7000, 10000, 20000,$ and 30000K and passes them to the subroutine "fitting."

The subroutine fitting fits the coefficients to a cubic spline and integrates them. To get an expression for the cubic spline Maxima was used. The cubic spline can be calculated by running the script "spline.wxm" under Maxima. Maxima then produces an 8 term equation that calulates the cross sections for the ranges $0 \rightarrow 500$, $500 \rightarrow 1000$, $1000 \rightarrow 2000$, $2000 \rightarrow 5000$, $5000 \rightarrow 7000$, $7000 \rightarrow 10000$, $10000 \rightarrow 20000$, and $20000 \rightarrow 30000$K. Cross sections are then calculated for every 10K for temperatures $1 \rightarrow 30000$K. These are then integrated using Simpson's rule as explained in chapter 4. It produces rate coefficients for temperatures listed in the file "templist."

Now the rate coefficients can be fit to the functional form of Martin & Mandy (1995) discussed in chapter 4. This is done through the linear regression algorithm also discussed in chapter 4 using the program fitting.f95. This program reads in the file coefficients from clean.f95 and produces a file called "fit_parameters." As its name indicates it is simply a list of the individual fit parameters (a,b,c, and d) of all the rate coefficients. Also this program weeds out any coefficients of zero. The file templist is also required for this program with the exact same temperatures used in mcr2c.f95. An executable called cooling.sh allows one to automatically execute all these codes.

COOLING RATES

The program used to actually calculate the cooling rates is cooling_curve.f95. It comes with a number of options that were used to study different master equa-

tions. It starts by asking the user to enter a density in cm^{-3}. The program begins by reading in the Einstein coefficients for spontaneous emission from the files A_values.dat and A_values2.dat which it then uses to calculate the absorption and stimulated emission coefficients. Next it collects the collision rate coefficient fit parameters and determines the total number of state transitions. Next it calls up the subroutine curves. Line 33 names the output file that should be changed for each density. In the case presented in the appendix CD, the output file will be named b.E8.txt. The code then calls up "templist2.txt" which contains a list of user specified gas temperatures to calculate cooling rates for. This list has the same format as "templist" and can contain as many temperatures as the user desires. Since this is a quasi-classical calculation, temperatures below ~ 500K should be avoided. Next the radiation density is calculated based on the temperatures in templist2. Then the level densities are calculated using the subroutine "density."

At this point the user has two options. 1) A backward differentiation (BDF) can be used or 2) a singular value decomposition (SVD). This can be done by uncommenting the desired method on lines 368 and 369. The BDF has the advantage that it produces less residual error, however it takes as much as a day to do a single density (the higher the density the longer it takes). While the SVD is fast, it seems to produce a significant amount of error. Both methods are valid and in fact produce very similar results. The calculations presented in this discussion were done using the BDF method.

BDF

The only thing the BDF requires is for the user to decide if they would like to include dissociative tunneling, absorption, and stimulated emission. Dissociatve tunneling requires the data file "dissociative_tunneling.dat." This contains some

of the dissociative tunneling coefficients used by Martin et al. (1996) which can be easily modified for different coefficients. Dissociative tunneling can be included by uncommenting the variable "dis" on line 420. Stimulated absorption and emission can be included by uncommenting the u and B1 variables on lines 405, 417, and 425. The program will then calculate the level populations using Octave, and pass them on to calculate the cooling rates. The level populations are printed out in the file on line 477 which is "bT=1000" in this case. Lines 480-483 must also be uncommented to print energy level densities. Line 477 must be commented out if the user wants to calculate cooling for multiple temperatures. There is an optional stop command on line 485 if the user is only interested in the level populations. This can be commented on or off depending on the user's desire.

SVD

As in the BDF, the SVD has the option of adding dissociative tunneling, absorption, and stimulated emission. These can be added via lines 523, 535, 557, and 543. Next the program calls Octave to perform the SVD. This requires the file "equations" to tell Octave to just print out the level densities. This is done as file "x.dat."

Next the user must decide what their error tolerance is. From trial and error a good number to uses is 1E-5. Also its a good idea to have the program eliminate any values less than .1 percent of the maximum population density. This can be done by editing lines 592, 595, 597, and 599. The SVD has a tendancy to multiply the densities by -1 to give an all negative density matrix. The program will automatically fix this. Again, there is an optional stop on line 617 if the user is only interested in the density matrix. This stop must be used if spectrum.f95 is going to be run. Line 607 allows the user to again specify an output file. It, along with lines 610 through 613 must be commented out if the user wants to calculate cooling for

multiple temperatures. As can be seen, the densities or the cooling curve can be calculated but not both at the same time.

ADDITIONAL CODE OPTIONS

levels.f95

An optional program "levels.f95" can also be used. It's purpose is to calculate and print out all the harmonic energy levels with their associated vibrational and rotational quantum numbers in a file called energy_levels.txt. Also, it displays the index number each energy level is assigned which is used throughout this code. This program needs to be run in order to use spectrum.f95. E.dat contains the non-harmonic energy levels.

spectrum.f95

This is another useful program that is used for plotting the predicted emission spectrum of the molecule with one of the potentials. This program works by reading in the density matrix from cooling_curve.f95 and using the Einstein coefficients as well as the output from levels.f95, and producing a normalized emission file. The only manipulation needed for this program is to define the name of the density file on line 20 and the name of the output file on line 86. It should be noted that this program suffers significantly from rounding errors however does provide a good general estimate of the emission shape.

sorttool.f95

This tool allows one to organize and pick out desired data. Simply start the program and decide which states you are interested in and all the data for that

transition is printed out in 3 files, data, errorbars, and parameters.The file data contains the calculated rate coefficients at a given temperature. The file errorbars prints out the coefficients from the Martin & Mandy (1995) fits, the errorbars, and the collision cross sections. The file parameters contains the 4 fit parameters for the Martin & Mandy (1995) fits.

APPENDIX B

QUASI-BOUND STATES

The calcuations presented in this document included only the 301 bound states. However, Martin et al. (1996) included 47 quasi bound states (302 through 348) table 15. A quasi-bound state is a state with energy higher than the dissociation energy. These states are short lived states that become important at high temperature and high hydrogen density held together by the rotational barrier which must be breached by either quantum tunneling, or the introduction of additional energy through collisions. Due to the low density, intermediate temperature considerations of this document, these quasi-bound states were intentionally ignored. Including these states would require a new master equation which would include 2 additional coefficients, the collisional dissociation and dissociative tunneling coefficients.

The dissociation coefficients result in the destruction of the H_2 molecule. Being a second order reaction, the collisional dissociation coefficients from some state i to dissociation ($\gamma_{i\rightarrow 349}$) would have units identical to the collisional rate coefficients, except they would lead to and unbound energy state (i $= 349$) thus lowering the total H_2 level populations and would not be subject to detailed balance for a reverse transition. The dissociative tunneling coefficients from some state i to dissociation ($k_{i\rightarrow 349}$) are a first order reaction with units s^{-1}. These would result in a new master equation with the form of equation B.1.

$$\frac{dn_i}{dt} = n_H(\sum_{f=1;f\neq i}^{348} n_f\gamma_{f\rightarrow i} - n_i \sum_{f=1;f\neq i}^{349} \gamma_{i\rightarrow f}) + \sum_{f=i+1}^{348} n_f A_{f\rightarrow i} - n_i(\sum_{f=1}^{i-1} A_{i\rightarrow f} + k_{i\rightarrow 349}) \quad \text{(B.1)}$$

Table 15 Bound and Unbound H_2 energy levels. i is the energy level index number (eg. level v $= 0$, j $= 0$ has an index number of i=1) and energy level with respect to dissociation (E $= 0$ eV)

i	v,j	E(eV)	i	v,j	E(eV)	i	v,j	E(eV)
1	0, 0	−4.479	117	4, 14	−1.522	233	6, 19	−0.329
2	0, 1	−4.465	118	2, 19	−1.510	234	9, 12	−0.328
3	0, 2	−4.435	119	7, 0	−1.466	235	14, 19	−0.327
4	0, 3	−4.392	120	3, 17	−1.462	236	10, 9	−0.322
5	0, 4	−4.334	121	6, 8	−1.458	237	7, 17	−0.318
6	0, 5	−4.264	122	7, 1	−1.456	238	3, 21	−0.311
7	0, 6	−4.180	123	7, 2	−1.437	239	11, 5	−0.309
8	0, 7	−4.084	124	5, 12	−1.416	240	8, 15	−0.293
9	0, 8	−3.977	125	7, 3	−1.408	241	0, 30	−0.283
10	1, 0	−3.963	126	4, 15	−1.394	242	1, 23	−0.281
11	1, 1	−3.949	127	6, 9	−1.376	243	11, 6	−0.275
12	1, 2	−3.921	128	7, 4	−1.371	244	10, 10	−0.266
13	1, 3	−3.880	129	1, 22	−1.364	245	9, 13	−0.256
14	0, 9	−3.859	130	0, 24	−1.361	246	7, 23	−0.238
15	1, 4	−3.825	131	2, 20	−1.350	247	11, 7	−0.237
16	1, 5	−3.758	132	7, 5	−1.324	248	12, 0	−0.224
17	0, 10	−3.731	133	3, 18	−1.316	249	12, 1	−0.219
18	1, 6	−3.679	134	5, 13	−1.305	250	7, 18	−0.218
19	0, 11	−3.595	135	6, 10	−1.288	251	6, 20	−2.218
20	1, 7	−3.588	136	7, 6	−1.270	252	12, 2	−0.209
21	1, 8	−3.486	137	4, 16	−1.263	253	10, 11	−0.208
22	2, 0	−3.476	138	7, 7	−1.208	254	8, 16	−0.206
23	2, 1	−3.463	139	6, 11	−1.194	255	5, 22	−0.205
24	0, 12	−3.450	140	0, 21	−1.191	256	11, 8	−0.196
25	2, 2	−3.436	141	5, 14	−1.189	257	12, 3	−0.194
26	2, 3	−3.397	142	11, 19	−1.189	258	9, 14	−0.182
27	1, 9	−3.374	143	7, 21	−1.177	259	4, 25	−0.182
28	2, 4	−3.345	144	3, 19	−1.168	260	4, 24	−0.179
29	0, 13	−3.298	145	8, 0	−1.151	261	12, 4	−0.174
30	2, 5	−3.282	146	8, 1	−1.142	262	11, 9	−0.153
31	1, 10	−3.253	147	7, 8	−1.139	263	12, 5	−0.151
32	2, 6	−3.206	148	4, 17	−1.129	264	10, 12	−0.148
33	0, 14	−3.140	149	8, 2	−1.124	265	3, 26	−0.139
34	1, 11	−3.124	150	8, 3	−1.098	266	12, 6	−0.124

i	v,j	E(eV)	i	v,j	E(eV)	i	v,j	E(eV)
35	2, 7	−3.120	151	6, 12	−1.095	267	7, 19	−0.121
36	2, 8	−3.024	152	5, 15	−1.070	268	8, 17	−0.121
37	3, 0	−3.018	153	7, 9	−1.063	269	1, 27	−0.112
38	3, 1	−3.005	154	8, 4	−1.063	270	9, 15	−0.109
39	1, 12	−2.987	155	2, 22	−1.028	271	15, 19	−0.109
40	3, 2	−2.980	156	8, 5	−1.020	272	11, 10	−0.107
41	0, 15	−2.976	157	3, 20	−1.019	273	12, 7	−9.456E − 2
42	3, 3	−2.943	158	1, 24	−1.019	274	13, 0	−9.405E − 2
43	2, 9	−2.918	159	0, 26	−0.994	275	13, 1	−9.022E − 2
44	3, 4	−2.894	160	4, 18	−0.993	276	10, 13	−8.884E − 2
45	1, 13	−2.843	161	6, 13	−0.993	277	2, 28	−8.715E − 2
46	3, 5	−2.834	162	7, 10	−0.982	278	4, 21	−8.558E − 2
47	0, 16	−2.807	163	8, 6	−0.970	279	13, 2	−8.269E − 2
48	2, 10	−2.804	164	5, 16	−0.949	280	13, 3	−7.176E − 2
49	3, 6	−2.762	165	8, 7	−0.913	281	12, 8	−6.339E − 2
50	1, 14	−2.693	166	7, 11	−0.896	282	11, 11	−6.154E − 2
51	2, 11	−2.681	167	6, 14	−0.886	283	13, 4	−5.785E − 2
52	3, 7	−2.681	168	12, 19	−0.870	284	2, 23	−4.948E − 2
53	0, 17	−2.633	169	1, 21	−0.867	285	13, 5	−4.156E − 2
54	3, 8	−2.590	170	0, 9	−0.866	286	9, 16	−3.828E − 2
55	4, 0	−2.587	171	9, 1	−0.858	287	8, 18	−3.727E − 2
56	4, 1	−2.575	172	4, 19	−0.856	288	12, 9	−3.155E − 2
57	2, 12	−2.552	173	8, 8	−0.850	289	10, 14	−3.063E − 2
58	4, 2	−2.552	174	8, 21	−0.848	290	7, 20	−2.607E − 2
59	1, 15	−2.538	175	9, 2	−0.842	291	13, 6	−2.369E − 2
60	4, 3	−2.517	176	5, 17	−0.825	292	1, 30	−2.240E − 2
61	3, 9	−2.490	177	5, 17	−0.818	293	14, 0	−1.719E − 2
62	4, 4	−2.471	178	5, 23	−0.813	294	11, 12	−1.674E − 2
63	0, 18	−2.457	179	7, 12	−0.806	295	14, 1	−1.507E − 2
64	2, 13	−2.416	180	9, 4	−0.787	296	14, 2	−1.102E − 2
65	4, 5	−2.414	181	8, 9	−0.782	297	14, 3	−5.515E − 3
66	3, 10	−2.382	182	6, 15	−0.777	298	13, 7	−5.331E − 3
67	1, 16	−2.378	183	9, 5	−0.748	299	6, 22	−3.840E − 3
68	4, 6	−2.347	184	3, 22	−0.721	300	0, 25	−9.832E − 4

i	v,j	E(eV)	i	v,j	E(eV)	i	v,j	E(eV)
69	0, 19	−2.278	185	4, 20	−0.719	301	12, 10	−4.649E − 4
70	2, 14	−2.274	186	7, 13	−0.712	302	14, 4	7.228E − 4
71	4, 7	−2.270	187	8, 10	−0.708	303	13, 8	1.186E − 2
72	3, 11	−2.267	188	2, 24	−0.707	304	10, 15	2.454E − 2
73	1, 17	−2.215	189	9, 6	−0.703	305	11, 13	2.528E − 2
74	5, 0	−2.185	190	5, 18	−0.701	306	12, 11	2.765E − 2
75	4, 8	−2.184	191	1, 26	−0.678	307	9, 17	2.936E − 2
76	5, 1	−2.174	192	6, 16	−0.666	308	5, 24	2.994E − 2
77	5, 2	−2.152	193	9, 7	−0.652	309	8, 19	4.211E − 2
78	3, 12	−2.145	194	0, 28	−0.634	310	0, 32	5.467E − 2
79	2, 15	−2.129	195	8, 11	−0.630	311	5, 25	5.978E − 2
80	5, 3	−2.119	196	7, 14	−0.615	312	11, 14	6.103E − 2
81	0, 20	−2.096	197	10, 0	−0.615	313	16, 19	6.428E − 2
82	4, 9	−2.090	198	10, 1	−0.608	314	10, 16	7.388E − 2
83	5, 4	−2.075	199	9, 8	−0.595	315	4, 26	7.546E − 2
84	1, 18	−2.049	200	10, 2	−0.593	316	9, 18	9.101E − 2
85	5, 5	−2.022	201	13, 19	−0.582	317	5, 21	9.681E − 2
86	3, 13	−2.017	202	5, 19	−0.576	318	8, 20	0.115
87	4, 10	−1.989	203	2, 21	−0.573	319	2, 27	0.133
88	2, 16	−1.978	204	10, 3	−0.572	320	3, 28	0.133
89	5, 6	−1.959	205	6, 17	−0.554	321	3, 23	0.140
90	9, 19	−1.913	206	8, 12	−0.549	322	7, 22	0.148
91	5, 7	−1.887	207	0, 23	−0.549	323	17, 19	0.177
92	3, 14	−1.884	208	10, 4	−0.544	324	6, 24	0.190
93	4, 11	−1.881	209	9, 9	−0.533	325	1, 25	0.195
94	1, 19	−1.880	210	7, 15	−0.517	326	2, 30	0.202
95	2, 17	−1.825	211	6, 23	−0.510	327	5, 27	0.217
96	6, 0	−1.811	212	10, 5	−0.510	328	6, 21	0.220
97	5, 8	−1.807	213	10, 6	−0.470	329	5, 26	0.243
98	6, 1	−1.801	214	9, 10	−0.468	330	6, 25	0.261
99	6, 2	−1.780	215	8, 13	−0.465	331	4, 23	0.272
100	4, 12	−1.766	216	3, 25	−0.457	332	1, 32	0.283
101	6, 3	−1.749	217	5, 20	−0.451	333	4, 28	0.307
102	3, 15	−1.747	218	4, 22	−0.446	334	2, 25	0.334

i	v,j	E(eV)	i	v,j	E(eV)	i	v,j	E(eV)
103	0, 22	−1.729	219	6, 18	−0.441	335	3, 27	0.338
104	5, 9	−1.719	220	3, 24	−0.426	336	0, 34	0.375
105	1, 20	−1.709	221	10, 7	−0.425	337	3, 30	0.381
106	6, 4	−1.709	222	7, 16	−0.417	338	0, 27	0.407
107	2, 18	−1.668	223	11, 0	−0.399	339	0, 29	0.427
108	6, 5	−1.659	224	9, 11	−0.399	340	2, 32	0.467
109	4, 13	−1.647	225	11, 1	−0.393	341	4, 27	0.490
110	5, 10	−1.624	226	2, 26	−0.393	342	2, 29	0.528
111	3, 16	−1.606	227	11, 2	−0.381	343	1, 34	0.564
112	6, 6	−1.600	228	8, 14	−0.379	344	1, 29	0.585
113	18, 19	−1.545	229	10, 8	−0.376	345	0, 36	0.673
114	10, 19	−1.537	230	11, 3	−0.362	346	3, 29	0.691
115	6, 7	−1.533	231	1, 28	−0.344	347	4, 29	0.811
116	5, 11	−1.523	232	11, 4	−0.338	348	0, 38	0.934

APPENDIX C

The impact parameters used in the calculation of the collision cross sections are modeled as Gaussians with a defined maximum impact parameter. In the case of the BKMP2 potential, the maximum impact parameter is set at 5 a.u. In chapter 4, calculations for the cross sections using the Mielke potential are done using a varying maximum impact parameter for each energy level. Figure 44 is an example of a few transitions for temperatures 1000K and 10000K. The maximum impact parameter for the 2,1 energy level was chosen to be 4 a.u.

The smaller cross sections, for the most part, are a result of relatively few trajectories for that particular transition. As a result, there are very large error bars associated with these transitions (eg. The transition 1,2 to 0,0 is very sporadic). However, the larger cross sections, which generally correspond to a higher trajectory count, tend to generate smoother lines that flatten out at approximately the selected maximum impact parameter. This implies that there is a limit at which expanding the impact parameter does not increase transitions. This limit was calculated as follows.

Grids of transitions for a variety of initial energy levels was done for 10000K and 1000K courtesy of Stephen Lepp. Based on these, the maximum impact parameter was chosen as the smallest impact parameter that produced no transitions. Then a set of selection rules to describe these results was produced. Table 16 outline these rules.

If $j > 15$ b is increased to 4 if neccessary, and if $j > 25$ b can be increased to 5 if needed. Using these selection rules, grids for the 301 bound energy levels for energies 500 through 30000K were produced.

Figure 44 Maximum Impact Parameter vs Cross Section for Energy Level v $= 1$, j $=$ 2 at 10000 K

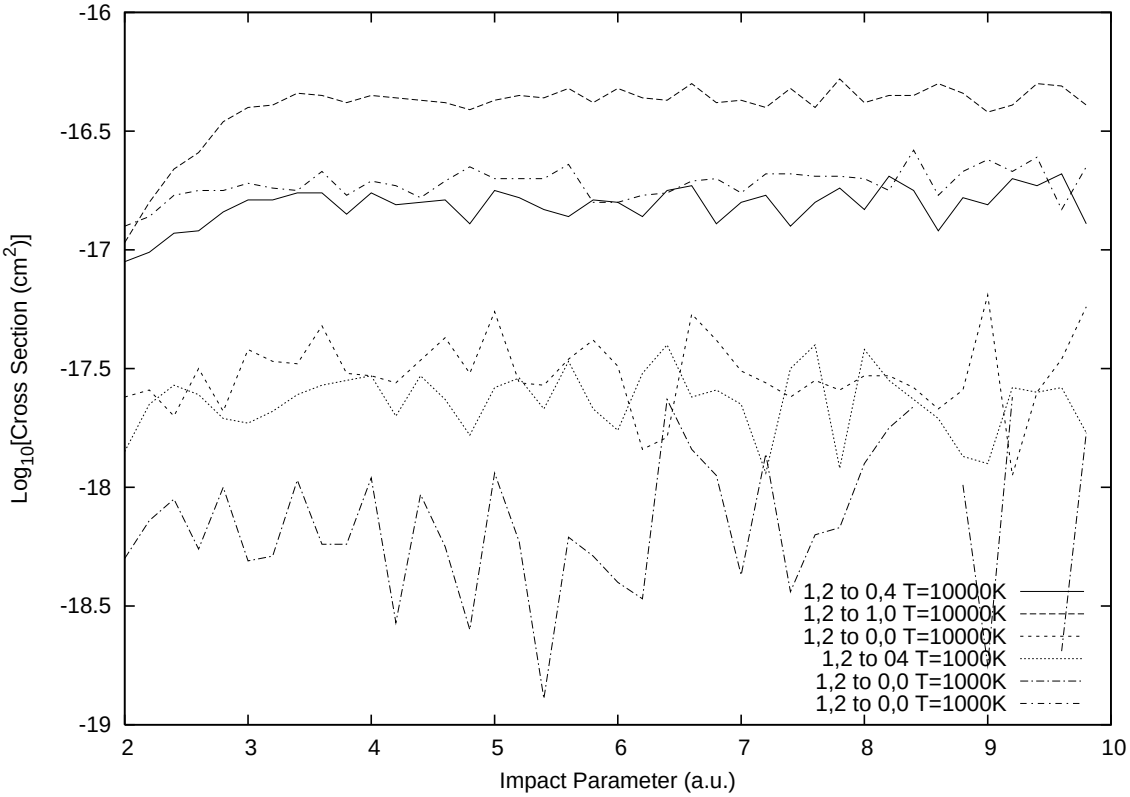

Table 16 b_{max} selection Rules

	For E $\leq$ 7000K	For E $>$ 7000K
v	b_{max} (a.u.)	b_{max}
0-1	3	3
2	3	4
3-7	5	5
> 7	7	7

REFERENCES

[1] Archer, D.M. 2006, PhD thesis, University of Nevada-Las Vegas

[2] Blais, N.C., Truhlar, D.G. 1976, J. Chem. Phys., 65, 5335

[3] Boothroyd, A.I., Keogh, W.J., Martin, P.G., & Peterson, M.R. 1991, J. Chem. Phys., 95, 4343

[4] Boothroyd, A.I., Keogh, W.J., Martin, P.G., & Peterson, M.R. 1996, J. Chem. Phys., 104, 7139

[5] Bougleux, E., & Galli, D. 1997, MNRAS, 288, 638

[6] Dalgarno, A., Allison, A.C., & Browne, J.C. 1969, J. Atm. Sci., 26, 946

[7] Eaton, J.W. 2009, software, GNU Octave version 3.2.3

[8] Eyring, H., & Polanyi, M. 1931, Z. Phys. Chem., B12, 279

[9] Gamow, G. 1949, Rev. Mod. Phys., 21, 367

[10] Galli, D., & Palla, F. 1998, A&A, 335, 403

[11] Gay, C.D., Stancil, P.C., Lepp, S., & Dalgarno, A. 2011, ApJ, 737, 44

[12] Hollenbach, D., & McKee, C.F. 1979, ApJS, 41, 555

[13] Hubble, E. 1928, Proceedings of the National Academy of Sciences, 15, 168

[14] James, H.M., & Coolidge, A.S. 1933, J. Chem. Phys., 1, 825

[15] Karplus, M., Porter, R.N., & Sharma, R.D. 1965, J. Chem. Phys., 43, 3259

[16] Kelley, M.T., & Lepp, S.H. 2012, ApJ, in preparation

[17] Knowles, P.J., & Werner, H.J. 1988, Chem. Phys. Lett., 145, 514

[18] Kolos, W., & Wolniewicz, L. 1965, J. Chem. Phys., 43, 2429

[19] Kolos, W., & Wolniewicz, L. 1968, J. Chem. Phys., 49, 404

[20] LeBourlot, J.Z., Pineau des Forêts, & Flower, D.R. 1999, MNRAS, 305, 802

[21] Lepp, S., & Shull, J.M. 1983, ApJ, 270, 578

[22] Lepp, S., Stancil, P.C., & Dalgarno, A. 1998, Mem. S.A.It., 69, 331

[23] Liu, B. 1973, J. Chem. Phys., 58, 1925

[24] London, F. 1929, Elektrochem. Angew. Phys. Chem., 35, 552

[25] Marshall, R.M., & Purnell, J.H. 1968, J. Chem. Soc. A, 1968, 2301

[26] Mandy, M.E., & Martin, P.G. 1991, J. Phys. Chem., 95, 8726

[27] Mandy, M.E., & Martin, P.G. 1992, J. Phys. Chem., 97, 265

[28] Mandy, M.E., & Martin, P.G. 1993, ApJS, 86, 199

[29] Martin, P.G., & Mandy, M.E. 1995, ApJ, 455, L89

[30] Martin, P.G., Schwarz, D.H., & Mandy, M.E. 1996, ApJ, 461, 265

[31] Martin, P.G. 1996, http://www.cita.utoronto.ca/ pgmartin/h2hdist/

[32] Mielke, S.L., Garrett, B.C., & Peterson, K.A. 2002, J. Chem. Phys., 116, 4142

[33] Oka, T. 2004, J. Mol. Spec. 228, 635

[34] Penzias, A.A., & Wilson, R.W. 1965, ApJ, 142, 1149

[35] Puy, D., Dubrovich, V., Lipovka, A., Talbi, D., & Vonlanthen, P. 2007, A&A, 476, 685

[36] Press, W.H., Teukolsky, S.A., Vetterling, W.T., & Flannery, B.P. 2007, Numerical Recipes: The Art of Scientific Computing, (3rd ed.; New York, New York: Cambridge University Press)

[37] Rutherford, E., The Scattering of α and β Particles by Matter and the Structure of the Atom, Philosophical Magazine. Series 6, vol 21. May 1911

[38] Scott, D. Moss, A. 2009, MNRAS, 397, 445

[39] Shaw, G., Ferland, N.P., Abel, N.P., Stancil, P.C., & van Hoof, P.A.M. 2005, ApJ, 624, 794

[40] Siegbahn, P., & Liu, B. 1978, J. Chem. Phys., 68, 2457

[41] Smith, F.T. 1960, Phys. Rev., 120, 1058

[42] Smith, M.S., Kawano, L.H., & Malaney, R.A. 1993, ApJ, 85, 219

[43] Suyu, S.H., Marshall, P.J., Auger, M.W., Hilbert, S., Blandford, R.D., Koopmans, L.V.E., Fassnacht, C.D., & Treu, T. 2010, ApJ, 711, 201

[44] Tiné, S., Lepp, S., & Dalgarno, A., 1998, Mem. Soc. Astron. Ital., 69, 345

[45] Tolstikhin, O.I., & Nakamura, H. 1998, J. Chem. Phys., 108, 8899

[46] Truhlar, D.G., & Wyatt, R.E. 1976, Ann. Rev. Phys. Chem., 27, 1

[47] Truhlar, D.G., & Horowitz, C.J. 1978, J. Chem. Phys., 68, 2466; erratum 71, 1514E(1979)

[48] Truhlar, D.G. 1981, Potential Energy Surfaces and Dynamics Calculations (New York: Plenum)

[49] Turner, J., Kirby-Docken, K., & Dalgarno, A. 1977, ApJ, 35, 281

[50] Varandas, A.J.C., Brown, F.B., Mead, C.A., Truhlar, D.G., & Blais, N.C. 1987, J. Chem. Phys., 86, 6258

[51] Vodopivec, & A., Lenarcic, Z. 2010, software, wxMaxima version 11.04.0

[52] Vonlanthen, P., Rauscher, T., Winteler, C., Puy, D., Signore, M., & Dubrovich, V. 2009, A&A, 503, 47

[53] Werner, H.J. 1987, Adv. Chem. Phys., 69, 1

[54] Werner, H.J. 1988, J. Chem. Phys., 89, 5803

[55] Williams, T., & Kelley, C. 2004, software, GNUPLOT version 4.0

[56] Wilson, R.W., & Penzias, A.A. 1965, AJ, 70, 697

VITA

Graduate College
University of Nevada, Las Vegas

Matthew T. Kelley

Local Address:
1509 E. Harmon Ave. Apt. 101
Las Vegas, Nevada 89119

Degrees:
Bachelors of Science, Physics, 2007
Marquette University
Milwaukee, Wisconsin

Dissertation Title:
Molecular Processes in Astrophysics: Calculations of $H + H_2$ Excitation, De-excitation, and Cooling

Dissertation Committee:
Committee Chairperson: Dr. Stephen Lepp, Ph.D.
Committee Memeber: Dr. Bing Zhang, Ph.D.
Committee Memeber: Dr. Kentaro Nagamine, Ph.D.
Graduate Faculty Representative: Dr. Balakrishnan Naduvalath, Ph.D.